THE EFFECTS OF WISH/DIP/SPIN90 AND WASP FAMILY PROTEINS

REGULATION OF ARP2/3 COMPLEX ON ACTIN NETWORK

ARCHITECTURE AND DYNAMICS

by

CONNOR JOHN BALZER

A DISSERTATION

Presented to the Department of Chemistry and Biochemistry
and the Graduate School of the University of Oregon
in partial fulfillment of the requirements
for the degree of
Doctor of Philosophy

June 2020

DISSERTATION APPROVAL PAGE

Student: Connor John Balzer

Title: The Effects of WISH/DIP/SPIN90 and WASp Family Proteins Regulation of Arp2/3 Complex on Actin Network Architecture and Dynamics

This dissertation has been accepted and approved in partial fulfillment of the requirements for the Doctor of Philosophy degree in the Department of Chemistry and Biochemistry by:

Mike Harms	Chairperson
Brad Nolen	Advisor
Ken Prehoda	Core Member
Tom Stevens	Core Member
Bruce Bowerman	Institutional Representative

and

Kate Mondloch	Interim Vice Provost and Dean of the Graduate School

Original approval signatures are on file with the University of Oregon Graduate School.

Degree awarded June 2020

DISSERTATION ABSTRACT

Connor John Balzer

Doctor of Philosophy

Department of Chemistry and Biochemistry

June 2020

Title: The Effects of WISH/DIP/SPIN90 and WASp Family Proteins Regulation of Arp2/3 Complex on Actin Network Architecture and Dynamics

Actin-related protein (Arp) 2/3 complex is required to nucleate branched actin networks necessary for numerous cellular processes including cell motility and endocytosis. To nucleate branched actin filaments, Arp2/3 complex must be activated by nucleation promoting factors (NPFs). The best understood NPFs are from the Wiskott-Aldrich Syndrome protein (WASp) family. To activate nucleation, WASp must recruit actin monomers to the complex and the Arp2/3-WASp-actin monomer assembly must bind a preformed actin filament. The requirement for a preformed actin filament ensures that Arp2/3 complex specifically nucleates branched instead of linear actin filaments but creates a paradox. If an actin filament is required for nucleation of new branches, what is the source of the initial filament? We show that a novel family of Arp2/3 complex NPFs, WISH/DIP/SPIN90 (WDS) proteins, allow Arp2/3 complex to bypass the requirement for a preformed actin filament. The Schizosaccharomyces pombe WDS protein, Dip1, binds Arp2/3 complex and co-opts features of branching nucleation to create linear actin filaments that are suitable substrates for WASp-mediated Arp2/3 complex branching nucleation. In vitro, linear filament nucleation by Dip1-bound Arp2/3 complex dominates over WASp-mediated branching activity. This results in formation of disconnected arrays

iv

of actin filaments unlike the highly branched actin architectures observed in vivo. Importantly, unlike WASp, Dip1 remains bound to the end of polymerizing actin filaments, establishing Dip1 as a single-turnover activator of Arp2/3 complex. This mechanistic difference limits the activity of Dip1 relative to WASp, providing a way for cells to ensure that most actin filaments nucleated by Arp2/3 complex are branched, rather than linear, in endocytic actin networks and at other sites where both NPFs are present. Surprisingly, we find that at endocytic sites, WASp plays a role in initiation of actin networks and not just the propagation of networks through branching. In the presence of Dip1, WASp coordinately activates Arp2/3 complex to promote linear filament nucleation. This is accomplished, in part, through the delivery of actin monomers to Dip1-activated Arp2/3 complex. The biochemical properties of Dip1 are conserved in other WDS family proteins suggesting that they are responsible for the initiation of branched actin network assembly in higher eukaryotes.

This dissertation contains previously published and unpublished co-authored material.

CURRICULUM VITAE

NAME OF AUTHOR: Connor John Balzer

GRADUATE AND UNDERGRADUATE SCHOOLS ATTENDED:

University of Oregon, Eugene, OR
Virginia Tech, Blacksburg, VA

DEGREES AWARDED:

Doctor of Philosophy, Chemistry and Biochemistry, 2020, University of Oregon
Bachelor of Science, Biochemistry, 2014, Virginia Tech

AREAS OF SPECIAL INTEREST:

Biochemistry
Cell Biology
Molecular Biology
Microscopy

PROFESSIONAL EXPERIENCE:

Graduate Research Fellow, Department of Chemistry and Biochemistry,
    University of Oregon, Eugene, OR, 2015-2020

Graduate Teaching Fellow, Department of Chemistry and Biochemistry,
    University of Oregon, Eugene, OR, 2014-2015

Laboratory Technician, International Petroleum Products and Additives
    Company, Inc, Richmond, VA, 2011-2014

GRANTS, AWARDS, AND HONORS:

Predoctoral Fellowship, Understanding how the Actin Filament Nucleator Arp2/3
    Complex, is Regulated to Create Exclusively Branched Filaments, American
    Heart Association, 2018-2020

Molecular Biology and Biophysics Training Grant, National Institutes of Health,
    2015-2018

Pete Von Hippel Graduate Scholar Award, University of Oregon, 2017

Borgen Adamson First Year Student Scholarship, University of Oregon, 2015

PUBLICATIONS:

Balzer, C.J., Wagner, A.R., Helgeson, L.A., and Nolen, B.J. (2019). Single-Turnover Activation of Arp2/3 Complex by Dip1 May Balance Nucleation of Linear versus Branched Actin Filaments. Current Biology 29, 3331-3338.e7.

Balzer, C.J., Wagner, A.R., Helgeson, L.A., and Nolen, B.J. (2018). Dip1 Co-opts Features of Branching Nucleation to Create Linear Actin Filaments that Activate WASP-Bound Arp2/3 Complex. Current Biology 28, 3886-3891.e4.

Rodnick-Smith, M., Liu, S.-L., **Balzer, C.J.**, Luan, Q., and Nolen, B.J. (2016). Identification of an ATP-controlled allosteric switch that controls actin filament nucleation by Arp2/3 complex. Nature Communications 7, 12226.

ACKNOWLEDGMENTS

First and foremost, I would like to sincerely thank Dr. Brad Nolen for his mentorship and support throughout my graduate career. Brad, you have always pushed me to be a better scientist and taught me to pay attention to the little details without losing sight of the bigger picture. The skills I have gained in your lab will be instrumental as I take the next steps in my career. I would like to thank my committee members, Dr. Mike Harms, Dr. Ken Prehoda, Dr. Tom Stevens and Dr. Bruce Bowerman, for all of your advice and guidance over the years. To all the Nolen lab members, past and present, thank you for making this work possible. You paved the way and I am grateful for all the mentorship, advice and encouragement you provided. I would like to specifically thank Andrew Wagner for taking me under his wing and answering my many questions. Many of my fondest research memories are from our collaborations during your final years in the lab. To everyone in the IMB, Chemistry and Biology offices, the IMB kitchen staff, Stu Johnson, Adam Fries, Larry Scatena and the University of Oregon, thank you for all of the help and support. To Ryan Holly and Byron Hetrick, thank you for the many discussions over lunch. Your input and ideas helped immensely in moving this project forward.

Thank you to Dr. Jeffrey Crow for giving me the opportunity to work in the lab. The experience solidified my passion for research and was ultimately what led me to pursue my graduate degree. To my friends, thank you for providing me with countless opportunities to get out of the lab and enjoy Oregon. I am going to miss our barbeques, tailgates, river floats, soccer games, camping trips and trivia nights. To my family, thank you all for your unwavering support. Mom and Dad, I cannot thank you enough for the

encouragement, guidance and love you have given me throughout my life. Brennan, Lexi and Jenna, you are the best siblings anyone could ask for and I love you all. To Bebe and Grampa, thank you for always seeing the best in me and encouraging me to do great things. Grampa, I couldn't have picked a better companion to take the first steps of this journey with me. To the Nelson and Manning family, thank you all for supporting Brittany and I throughout our time in Oregon. And most importantly, I would like to thank Brittany. You picked up your life and moved across the country for me to pursue my graduate degree and I would not have made it to this point if you hadn't. Your unconditional love and understanding, no matter how deep I was sucked into my research was heroic. I love you!

I dedicate this work to my family whose love and support made this possible.

TABLE OF CONTENTS

LIST OF FIGURES

CHAPTER I

INTRODUCTION

The Role of the Cytoskeleton in Cells

The cytoskeleton is a highly dynamic network of protein polymers present in every cell that is critical for maintaining cell shape and internal organization while also aiding in numerous cellular processes including cell division and motility (Fletcher and Mullins 2010). The eukaryotic cytoskeleton is composed of three classes of protein filaments: microfilaments, intermediate filaments and microtubules. These filaments are composed of many individual proteins that polymerize into long chains through the aide of numerous regulatory factors. One such protein, actin, is the minimal subunit of microfilaments, or actin filaments, and is the most abundant protein in eukaryotic cells with cytoplasmic concentrations reaching hundreds of micromolar (Thomas D. Pollard, Blanchoin, and Mullins 2000).

Actin monomers self-assemble into filaments that can bundle together and form a scaffold that is critical to maintaining cell shape and provides cellular highways for efficient transport of cargo throughout the cytoplasm (Lodish et al. 2000; Szymanski and Cosgrove 2009). In some areas of the cell, these filaments become branched and crosslinked to form dense actin networks. These networks are critical for generating forces to push and pull on membranes which allows for a diversity of cellular processes (Efimova and Svitkina 2018). These processes include lamellipodial-based cell motility, maintenance of cell-cell junctions, uptake of extracellular components through endocytosis, and excretion of membrane proteins, lipids and neurotransmitters through

endocytosis (T. M. Svitkina et al. 1997; Galletta and Cooper 2009; Efimova and Svitkina 2018; T. Svitkina 2018). Bacterial pathogens also hijack the actin cytoskeleton and utilize branched actin networks to form comet tails driving motility through the cytoplasm and infection of neighboring cells (Lamason and Welch 2017). Elucidating how the cytoskeleton is constructed and regulated is essential to our understanding of the cell processes discussed above.

Construction and Organization of Actin Networks

Polymerization of actin filaments is dependent on the formation of an actin nucleus. It is generally accepted that this nucleus is formed when at least three activated actin monomers collide and bind to one another (Cooper et al. 1983; T. D. Pollard 1990). Activation of actin monomers occurs through the exchange of the divalent cation Ca^{2+} for Mg^{2+} which induces a conformational change in the monomer (Cooper et al. 1983; Thomas D. Pollard 1986). This conformation change increases the rate at which the actin nucleus is formed; however, nucleation of the actin filament is still the rate limiting step in the spontaneous polymerization of actin (Cooper et al. 1983; Thomas D. Pollard and Cooper 1986). Spontaneous nucleation is extremely slow due to thermodynamic instability of actin dimers, which usually dissociate before additional monomers bind to form the stable actin nucleus (T. D. Pollard 1990). While this spontaneous nucleation of actin filaments can be observed *in vitro*, *in vivo*, several actin binding proteins, most notably profilins, further inhibit this process by blocking formation of small actin oligomers through binding at a 1:1 ratio with the actin binding interface on the monomer (Thomas D. Pollard and Cooper 1984; Mullins, Heuser, and Pollard 1998). To overcome

these barriers of spontaneous nucleation, cells utilize a group of proteins referred to as actin nucleators. Actin nucleators bind to and stabilize dimers and timers of actin to promote nucleation, in some cases by mimicking a stable actin dimer (Mullins, Heuser, and Pollard 1998). Cells regulate the localization and concentration of actin filament nucleators to control when and where actin filament networks are formed. This regulation of actin nucleators eliminates the nucleation of ectopic actin networks and ensures that a pool of actin will remain available to the cell at sites where it is required for preforming critical cellular functions.

Actin nucleators can be grouped into three major classes; Arp2/3 complex, formins and tandem-monomer-binding nucleators. Formins and tandem-monomer-binding nucleators like spire proteins, cordon blue (COBL), junction-mediating and regulatory protein (JMY) and adenomatous polyposis coli (APC) all generate linear, unbranched actin filaments (Dominguez 2009; Campellone and Welch 2010). This is accomplished by directly binding multiple actin monomers and positioning them to promote filament-like interactions (Wallar and Alberts 2003; Quinlan et al. 2005). These small actin clusters act as a nucleus for additional monomers to bind, leading to the polymerization of a new filament. Arp2/3 complex is unique in that it nucleates branched actin filaments (Amann and Pollard 2001). The relative contributions of each of these nucleator classes are critical to generating the diversity of actin architectures observed throughout the cell, from bundles of linear filaments to the dendritic, highly branched networks at endocytic sites.

Once nucleated, actin filaments are polarized (Huxley 1963). They contain a fast-growing barbed end and a slower growing pointed end, originally named based on

electron microscopy images of the orientation of myosin "arrowheads" decorating actin filaments (Huxley 1963). Free ATP-bound actin monomers continue to add to these ends while previously incorporated monomers hydrolyze their bound ATP to ADP and release the free phosphate, promoting filament disassembly (T. D. Pollard 1986). This disassembly, which occurs predominantly from the pointed end, leads to a phenomenon referred to as treadmilling; a flux of monomers from the pointed end to the barbed end (Wang 1985; Thomas D. Pollard and Cooper 1986). The rate of treadmilling is dictated by the critical concentration, which is simply the concentration of actin monomers at which filaments are in equilibrium with no net growth or shrinkage (Neuhaus et al. 1983; Stossel et al. 1985). When the cytoplasmic concentration of ATP-bound actin surpasses the critical concertation, polymerization of actin filaments proceeds.

Numerous proteins act on and regulate actin filaments to ensure that appropriate network architectures are achieved. Interactions of actin filament binding proteins with single filaments are critical for controlling their growth and regulating additional binding partners. For example, capping protein binds to the barbed ends of growing actin filaments to prevent the addition of monomers and control the length of actin filaments (Thomas D. Pollard and Cooper 1986). Tropomyosin binds to the sides of actin filaments, primarily in muscles, and promotes interactions with myosin while excluding interactions with other binding partners, including Arp2/3 (Gunning et al. 2015). Actin binding proteins can also promote interactions between multiple filaments. Fascin, villin and other actin bundling proteins tether linear actin filaments to increase their stiffness (Khurana and George 2011). Crosslinking proteins such as α-actinin and fimbrin bind to the sides of multiple filaments promoting connections within actin networks and to other

cellular structures (Matsudalra 1991). Finally, proteins such as actin depolymerizing factor(ADF)/cofilin and gelsolin work to disassemble actin filaments and the networks they make up to replenish the pool of monomers (Ono 2007). The combined efforts of these many actin binding proteins and their regulators determine the properties of the resulting actin network.

The organization of actin filaments and their binding partners determine the architecture of the actin networks that encompass them. This architecture confers properties on the overall network that are critical for preforming cellular functions. A key feature of actin networks is their relative connectivity which is determined by several factors including the branching density, crosslinking and bundling. By altering the number and types of linkages between multiple actin filaments, cells can form a variety of structures from large dendritic actin meshworks to long tightly packed bundles of filaments (Fletcher and Mullins 2010). As the number of linkages increases, there is a proportional increase in the stiffness of the network which is thought to play a role in both force generation and structural integrity of these networks (Esue, Tseng, and Wirtz 2009; Pujol et al. 2012). The combined efforts of the specific pool of actin binding proteins discussed above ensure the formation of actin networks with the necessary properties for the local cellular function. In filopodia, finger-like extensions of the cell membrane, it is important to form stiff actin filament bundles to overcome the membrane tension and stabilize the protrusions (Medalia et al. 2007). As a result, linear filament nucleators and actin bundlers dominate the local pool of proteins. In lamellipodia, large narrow sheets of highly branched actin filaments are generated leading to the formation of a large wave-like structure that allows the cell to crawl along a surface (Schaub,

Meister, and Verkhovsky 2007). This is accomplished by increasing the concentration of Arp2/3 complex and actin cross-linkers at these sites (Ydenberg et al. 2011). Actin networks at endocytic sites are also believed to be composed of short, heavily branched actin filaments (Young, Cooper, and Bridgman 2004; Collins et al. 2011). The branched nature of these networks is thought to be critical to generate the forces to invaginate the membrane (Berro, Sirotkin, and Pollard 2010). Despite the characteristic nature of each of these actin networks, it is also important to note that actin networks are highly dynamic and capable of rapidly changing their architectures and properties to adjust to external stimuli. This is accomplished through the constant disassembly of older actin filaments in networks ensuring an abundant supply of free actin monomers for new filament polymerization at the main point of membrane contact. Understanding how the activities of all the proteins involved in actin network formation are balanced and regulated is critical to understanding how cells build actin networks with architectures suited to perform their local role.

Arp2/3 Complex is a Branched Actin Filament Nucleator

Arp2/3 complex was first identified in Acanthamoeba castellanii a little over 25 years ago and has since been identified in nearly every sequenced eukaryotic genome (L. M. Machesky et al. 1994; Goley and Welch 2006). It is an essential protein complex in eukaryotes. Deletion phenotypes range from defects in cell wall building in *A. thaliana* and ring canal growth in *D. melanogaster* up to embryonic lethality in *C. elegans* and early postnatal lethality in mice (Pratap Sahi et al. 2018; Hudson and Cooley 2002; Sawa et al. 2003; Zhou, Sumigray, and Lechler 2015). In yeast the Arp2/3 complex has been

shown to play a role in actin patch motility (D. Winter et al. 1997; McCollum et al. 1996). In *S. pombe*, Arp2/3 complex is required for viability while in *S. cerevisiae*, only deletion of Arc40 was lethal (Morrell, Morphew, and Gould 1999; D. C. Winter, Choe, and Li 1999). Work from early studies revealed that Arp2/3 complex is made up of seven polypeptides; two actin-related protein subunits, Arp2 and Arp3, along with five others commonly referred to as ARPC1-C5 (Dyche Mullins and Pollard 1999). X-ray crystallography confirmed the predicted structural similarities between the Arp2 and Arp3 subunits of the complex and actin monomers (Robinson et al. 2001). These structures also showed how the other subunits in the complex form a scaffold that control the relative orientation of the actin related protein subunits (Robinson et al. 2001; Nolen and Pollard 2008). A combination of light and electron microscopy revealed that Arp2/3 complex binds to the side of pre-existing actin filaments and forms branches at a characteristic ~70-degree angle, highlighting the unique branching nucleation mechanism of Arp2/3 complex (Amann and Pollard 2001; Egile et al. 2005; Volkmann 2001). Arp2/3 complex branching nucleation has been tied to numerous cellular processes. Lamellipodial leading edge actin networks responsible for directional cell motility, homology-directed repair of DNA double-stranded breaks and cell-to-cell spread of bacterial pathogens are all dependent on Arp2/3 complex branching activity (Suraneni et al. 2012; Schrank et al. 2018; Welch and Way 2013).

Alone, Arp2/3 complex has very little intrinsic nucleation activity. Branching nucleation by Arp2/3 complex requires several additional factors including nucleation promoting factors, ATP, actin monomers and a preformed actin filament (Laura M. Machesky et al. 1999; Dayel and Mullins 2004). Structural studies show that in the

absence of these factors, the Arp2 and Arp3 subunits are positioned in a splayed arrangement that does not allow actin monomers to bind and form the nucleus of the new actin branch (Robinson et al. 2001). Upon binding to nucleation promoting factors (NPFs), the complex undergoes a conformational change to position Arp2 and Arp3 in a conformation that mimics the two adjacent actin subunits in a filament related by the short pitch helical axis (Hetrick et al. 2013). This partially activated complex must interact with the sides of preformed actin filaments to stimulate a further structural rearrangement of the subunits of the complex before nucleation can proceed (Espinoza-Sanchez et al. 2018).

Historically, nucleation promoting factors have been divided into two classes (Welch and Mullins 2002). Nucleation promoting factors in both classes generally contain a conserved C-terminal segment known as the central (C) and acidic (A) region that is responsible for binding directly to Arp2/3 complex (Laura M. Machesky and Insall 1998; Higgs and Pollard 1999). The two NPF classes are distinguished by the presence of either an actin monomer binding site (class I) or an actin filament binding site (class II) adjacent to their Arp2/3 complex activating CA region (Welch and Mullins 2002). Class I NPFs contains several proteins that share a common feature referred to as the verprolin homology or V region. The V region binds directly to actin monomers and delivers them to Arp2/3 complex to help form and stabilize the nucleus for actin branch formation (Miki and Takenawa 1998). While this class of nucleation promoting factors has several members, the canonical and best studied class I NPFs are the members of the Wiskott-Aldrich Syndrome protein (WASp) family. Like Arp2/3 complex, WASp family proteins are found throughout eukaryotes (Kurisu and Takenawa 2009). WASp is characterized by

a single monomer binding V region flanked by a CA region at the C terminal end of the protein (Thomas D Pollard and Borisy 2003). Two WASp proteins simultaneously engage Arp2/3 complex to activate its nucleation activity (Padrick et al. 2011). The mechanism of activation of Arp2/3 complex by WASp proteins is complex. WASp binds Arp2/3 complex through its CA domain which stimulates the activating conformational change described above (Goley et al. 2004; Rodnick-Smith et al. 2016). The tethering of WASp to Arp2/3 complex through the CA region also allows for efficient delivery of actin monomers bound to the V region of WASp (Marchand et al. 2001). Importantly, after delivering monomers to form the stable actin nucleus, WASp proteins are thought to prevent polymerization by blocking the binding of additional monomers to the actin nucleus. This has led to speculation that WASp must be released before the new branch filament can form (Smith, Padrick, et al. 2013; Helgeson and Nolen 2013).

Class II NPFs are believed to stimulate Arp2/3 complex activity by recruiting and tethering Arp2/3 complex to preformed filaments through their actin filament binding domains (Welch and Mullins 2002). In the absence of these NPFs, Arp2/3 binding to the sides of preformed actin filaments is highly inefficient with only ~1% of binding events resulting in the formation of a branch (Smith, Daugherty-Clarke, et al. 2013). By tethering Arp2/3 complex to preformed filaments, class II NPFs may stabilize this interaction and promote more efficient branching. Alone, class II NPFs often only weakly activate Arp2/3 complex nucleation; however, coordination with type I NPFs can lead to higher levels of Arp2/3 complex activity than either alone (Helgeson and Nolen 2013). This finding may explain why multiple NPFs, including members of both class I and class II, are found together at many sites of actin assembly in cells (Weaver et al. 2001;

Sirotkin et al. 2005; Ayala et al. 2008). To understand how Arp2/3 complex is regulated in vivo we need to continue to study how the activities of nucleation promoting factors are coordinated.

The Source of the Actin Seed Filament

As discussed previously, activation of Arp2/3 complex by WASp family proteins requires preformed actin filaments. This requirement ensures that Arp2/3 complex nucleates exclusively branched actin filaments but creates a paradox. If Arp2/3 complex can only nucleate branched actin filaments, where does the first linear preformed filament come from? The origin of the initial seed filament has been discussed in multiple studies in recent years (Wagner et al. 2013; Goode, Eskin, and Wendland 2015; Tyler, Allwood, and Ayscough 2016; Innocenti 2018). From this work, several candidate pathways to address the linear filament generation paradox have been proposed. The most obvious answer was that the linear filament nucleators, formins and tandem-monomer-binding proteins, could create the actin seeds for these branched networks. While this is a reasonable hypothesis, linear filament nucleators and Arp2/3 complex are not always co-localized in cells (Firat-Karalar and Welch 2011; Kovar, Sirotkin, and Lord 2011). In fission yeast, formins For3 and Cdc12 are generally associated with actin cables or rings which are spatially separated from the actin patch structures where Arp2/3 complex activity is required (Kovar, Sirotkin, and Lord 2011). The mammalian formin, mDia2, is localized to lamellipodia and filopodia as well as sites of cytokinesis but not to sites of endocytosis with Arp2/3 complex (Firat-Karalar and Welch 2011). Importantly, formin nucleated filaments are rapidly coated by the stabilizing protein tropomyosin which

inhibits Arp2/3 complex binding (Blanchoin, Pollard, and Hitchcock-DeGregori 2001; Ujfalusi et al. 2009). This suggests that even transport of formin-nucleated actin filaments from their sites of origin to endocytic sites would be insufficient for seeding.

Spire1, a tandem monomer recruitment nucleator, is perhaps a more promising candidate as it has been shown to localize to some early endosomes along with Arp2/3 complex (Morel, Parton, and Gruenberg 2009). However, Spire1 nucleated filaments have not yet been shown to serve as substrates for branching. Additionally, no Spire1 homolog has not been found in yeast. The most comparable proposed *de novo* linear filament generation in yeast is through the polyproline region of the *S. cerevisiae* WASp family homolog, Las17 (Urbanek et al. 2013). It was suggested that the paired basic residues in Las17's polyproline region act as actin monomer binding sites that can increase the local concentration and orientation of monomers to promote binding and nucleation of a new linear filament (Urbanek et al. 2013; Allwood et al. 2016; Tyler, Allwood, and Ayscough 2016). While this activity presents an exciting mechanism of linear filament nucleation, these studies are almost exclusively in vitro, and little evidence exists to support the role of this mechanism in cells. Additionally, there is currently no evidence of this activity in the WASp homologs of other yeast species. Together, these findings suggest that while linear actin filament nucleators may be the source of the initial actin filament for Arp2/3 complex branching activity in some species or in specific cellular contexts, other pathways likely exist.

Another proposed source of the initial preformed actin filaments for Arp2/3 complex branching are pre-existing actin networks. In yeast, internalized, actin-coated vesicles can "touch activate" stalled sites of endocytosis to initiate actin assembly (Basu

11

and Chang 2011). This observation is consistent with the pre-existing actin filaments on the surface of the internalized vesicle serving as the initial filaments for Arp2/3 complex branching at these stalled sites. In this same vein, short filaments generated by cofilin-mediated severing of actin networks have been proposed to provide an initial source of filaments (Chen and Pollard 2013). These filaments could be captured by endocytic patch proteins before disassembly and used as the initial substrate for Arp2/3 complex branching. While these mechanisms may provide a source of linear actin filaments, they do not nucleate filaments *de novo* and would require another seed filament source to initiate the actin networks they arise from.

Recently, the discovery of a novel class of Arp2/3 complex activating proteins, WISH/DIP/SPIN90 (WDS) proteins, has opened the door to another source of actin seed filaments. WDS proteins have been shown to play a role in the initiation of endocytic patches in vivo and in activating Arp2/3 complex nucleation activity in vitro (Basu and Chang 2011; D. J. Kim et al. 2006; Wagner et al. 2013). Additionally, they activate Arp2/3 complex to nucleate linear actin filaments and do not require a preformed actin filament (Wagner et al. 2013). These results support a role for WDS proteins in the creation of initial actin filaments; however, given the absence of monomer binding domains in these proteins the mechanism by which this is accomplished is unclear. Importantly, WDS proteins seem to fit all the cellular requirements necessary to serve as a robust initial filament source. WDS proteins have been identified throughout the eukaryotic tree, they are present at sites of branched actin networks in cells and they provide a *de novo* source of actin filaments through Arp2/3 complex (D. J. Kim et al. 2006; S.-M. Kim et al. 2011; Burston et al. 2009; Basu and Chang 2011; Wagner et al.

2013). It is unlikely that any one of the methods described in this section provides all the actin seed filaments necessary for the diversity of Arp2/3 complex networks in cells. However, WDS proteins currently provide the most viable source of actin seed filaments based on the in vivo evidence connecting them to a role in branched actin network initiation.

WISH/DIP/SPIN90 Proteins Are Unique Arp2/3 Complex Activators

WISH/DIP/SPIN90 (WDS) proteins represent one of the most recently identified Arp2/3 complex activators. Our knowledge of WDS proteins dates back to the discovery of a novel gene, AF3p21, in a patient who had been treated for leukemia (Sano et al. 2000). The gene encoded for an SH3 domain containing protein that was shown to interact with Nck in a yeast two-hybrid screen which gave rise to the name SH3 Protein Interacting with Nck, 90 kDa (SPIN90), although NCK Interacting Protein With SH3 Domain (NCKIPSD), is also used (Lim et al. 2001). Several other groups independently identified SPIN90 at nearly the same time but described it using alternative names including vimentin/VacA-interacting protein (VIP54), diaphanous interacting protein (DIP) and WASP-interacting SH3 protein (WISH) giving rise to the WISH/DIP/SPIN90 moniker (de Bernard et al. 2000; Fukuoka et al. 2001; Satoh and Tominaga 2001). WDS proteins are found throughout the multi-celled animal kingdom as well as in *S. pombe* and *S. cerevisiae* (Matsuyama et al. 2006; Burston et al. 2009; Basu and Chang 2011). The key feature of WDS proteins is the presence of an armadillo repeat motif domain (ARM), a repeating series of three α-helices organized into a right-handed super-helix (Luan et al. 2018). This ARM domain encompasses what was originally described as the

leucine rich domain (LRD) in WDS proteins. Additionally, these proteins typically contain an SH3 domain and a polyproline domain; however, the *S. pombe* and *S. cerevisiae* orthologs, dip1 and Ldb17, respectively, lack the SH3 domain and have shortened or no polyproline regions (Wagner et al. 2013).

WDS proteins are involved in a diversity of cellular processes, specifically those that involve the cytoskeleton. SPIN90 has been implicated in numerous cytoskeletal based cellular processes including maintenance and assembly of myofibrils into sarcomeres, microtubule acetylation, formation of lamellipodia and regulation of dendritic spinogenesis; however, the best studied and most conserved role of WDS proteins is in endocytosis (Lim et al. 2001; You et al. 2017, 201; Teodorof et al. 2009; Lee et al. 2006). Interactions between the SH3 and polyproline domains of SPIN90 with their counterparts in several other proteins including syndaptin, dynamin I and Rab5 were shown to be critical for clathrin-mediated endocytosis (S. H. Kim et al. 2006; Y. Kim et al. 2005; Oh et al. 2013; H. Kim et al. 2019). Additional work showed that Ldb17, the *S. cerevisiae* WDS protein, interacts with Sla1 to ensure proper coat protein assembly and internalization of endocytic patches (Burston et al. 2009). The *S. pombe* homolog, dip1, was determined to play a role in the initiation of actin assembly at endocytic sites (Basu and Chang 2011). While these studies have clearly demonstrated the importance of WDS proteins, our understanding of the mechanistic role these proteins play in cells, both in regulation of the actin cytoskeleton and beyond, remains limited. The work presented in this dissertation takes strides towards broadening our understanding of this activity both in vitro and in vivo.

Endocytosis in Yeast

While several types of endocytosis have been described, clathrin-mediated endocytosis is the predominant pathway by which cells internalize cargo from their external environment (Bitsikas, Corrêa, and Nichols 2014). Clathrin-mediated endocytosis occurs in all eukaryotes and is important for nutrient uptake, signal transduction, recycling membrane receptors, neurotransmission and regulation of the molecular composition and surface area of the plasma membrane (Dergai et al. 2016; Ceresa et al. 1998; Royle and Lagnado 2003; Wei et al. 2018; Kaksonen and Roux 2018). Given its involvement in a diversity of essential processes, clathrin-mediated endocytosis has been studied extensively. This work has demonstrated that many of the steps in this process, as well as the proteins involved, are conserved throughout eukaryotes, despite millions of years of evolutionary separation (Conibear 2010; Sun et al. 2019; Lu, Drubin, and Sun 2016). This conservation allows for findings in simpler model organisms to be extended to more complex systems, and as such, studies of clathrin-mediated endocytosis in yeast are prevalent. Yeast cells such as *S. pombe* and *S. cerevisiae* provide an optimal system to study endocytosis as they can be grown rapidly and in great numbers in the lab. Additionally, their genomes can be readily modified allowing for labeling and mutation of endocytic proteins. This allows us to track proteins spatially and temporally to gain insight into their physiological contributions to endocytosis. Quantitative work from several labs has provided a detailed description of the concentrations, localizations and lifetimes of many of the yeast endocytic patch proteins (Sirotkin et al. 2010; Arasada and Pollard 2011; Galletta, Carlsson, and Cooper 2012; Chen and Pollard 2013; Picco et al. 2015; Manenschijn et al. 2019; Sun et al. 2019). The combination of these studies and

extensive work on the biophysical requirements of invaginating the plasma membrane have built a strong foundation for our understanding of the endocytic process. In general, the endocytic pathway in *S. pombe* and *S. cerevisiae* is fundamentally the same (Arasada et al. 2018). Though more than 60 proteins are involved in yeast clathrin-mediated endocytosis, the process can be divided into three main steps: the recruitment of clathrin and other endocytic coat proteins to the plasma membrane, the invagination of the membrane attached to the external cargo and scission of the invaginated membrane to form an endocytic vesicle that is internalized (Kaksonen and Roux 2018).

A key step in the invagination of the plasma membrane is the assembly of actin. It is widely believed that the actin meshworks at endocytic sites are responsible for generating the forces to deform and internalize the plasma membrane (Goode, Eskin, and Wendland 2015). Determining the mechanism by which actin networks overcome the high turgor pressure and membrane tension of yeast cells has proven difficult. The prevailing theory is that this force is generated through a Brownian rachet like mechanism. Actin monomers are added to the barbed end of actin filaments to fill a gap created by thermal fluctuations in the plasma membrane (Mogilner and Oster 1996). The rigid actin network behind these filaments prevents the membrane from displacing them, leading to a net pushing force on the membrane. To translate this activity into invagination of the plasma membrane, the polymerization of filaments is restricted to a ring around the clathrin coated pit that forms at the cargo binding site on the membrane (Mund et al. 2018). This is accomplished by spatially restricting Arp2/3 complex nucleation promoting factors, specifically WASp, to this ring. Arp2/3 complex is activated only in this region causing polymerization of a donut shaped actin network that

16

pushes on the membrane it encounters. Combined with direct tethering of the actin network to the clathrin coated pit, this leads to plasma membrane invagination (Mund et al. 2018). An alternative theory suggests that two distinct zones of actin polymerization are formed through the activities of spatially separated Arp2/3 complex nucleation promoting factors (Arasada et al. 2018). These two zones of actin polymerization are tethered to the plasma membrane and push against one another as they grow leading to invagination of the membrane. The expansion of the invaginated membrane eventually triggers scission mediated by proteins that pinch the neck of the invaginated membrane creating an endocytic vesicle (Dawson, Legg, and Machesky 2006; Palmer et al. 2015). This vesicle internalizes and the actin network is disassembled to allow for efficient transport of the cargo to its target site in the cell (Chen and Pollard 2013). Work presented in the coming chapters, particularly in chapter III and IV, focuses on understanding the specific roles of Arp2/3 complex and its nucleation promoting factors, Wsp1 and Dip1, in the formation of the branched actin networks at these endocytic sites.

The work presented in Chapter II was co-authored with Andrew Wagner, Luke Helgeson, and Brad Nolen and published in Current Biology. The work presented in Chapter III was co-authored with Andrew Wagner, Luke Helgeson and Brad Nolen and published in Current Biology. The work presented in Chapter IV is unpublished and was co-authored with Andrew Wagner, Luke Helgeson, Michael James, Vladimir Sirotkin and Brad Nolen.

CHAPTER II

DIP1 CO-OPTS FEATURES OF BRANCHING NUCLEATION TO CREATE LINEAR ACTIN FILAMENTS THAT ACTIVATE WASP-BOUND ARP2/3 COMPLEX

*This chapter contains previously published co-authored material.

Author contributions: B.J.N, C.J.B, A.R.W., and L.A.H. conceived the experiments. B.J.N, C.J.B, and A.R.W. wrote the manuscript. C.J.B, A.R.W., and L.A.H. performed experiments.

SUMMARY

When activated by WASP family proteins, Arp2/3 complex nucleates branched actin filaments important for processes like cellular motility and endocytosis [1]. WASP-mediated activation of Arp2/3 complex requires a preformed actin filament, ensuring that activation by WASP creates branched instead of linear filaments. However, this biochemical requirement also means that assembly of branched actin networks must be primed with an initial seed filament [2-4]. We recently described a class of activators called WISH/DIP/SPIN90 (WDS) proteins, that unlike WASP, activate Arp2/3 complex without a preformed filament [4]. While this property may allow WDS proteins to serve

as seed filament generators, it is unknown if actin filaments nucleated by WDS-activated

Arp2/3 complex can activate WASP-bound Arp2/3 complex. Further, despite their

potential importance as branched actin network initiators, little is known about how WDS

proteins turn on Arp2/3 complex. Here we use two color single molecule TIRF

microscopy to show that Dip1, the *S. pombe* WDS protein [5], co-opts features of

branching nucleation to activate Arp2/3 complex. Specifically, it activates Arp2/3

complex to nucleate linear filaments analogous to the branch created by WASP-mediated

activation. The barbed ends of Dip1-Arp2/3 nucleated filaments are free to elongate and

their pointed ends remain anchored to Dip1-bound Arp2/3 complex. The linear filaments

nucleated by Dip1-bound Arp2/3 complex activate WASP-bound Arp2/3 complex as

potently as spontaneously nucleated or branched actin filaments. These observations

provide important insights into the regulation of Arp2/3 complex by its activators and the

molecular basis for initiation of branched actin networks.

RESULTS

Dip1 co-opts features of branching nucleation to create linear filaments.

Unlike WASP, WDS proteins activate Arp2/3 complex without preformed actin

filaments, suggesting they trigger nucleation using a mechanism different from WASP

[4]. Several other observations support this hypothesis. For instance, WDS proteins lack

the canonical Arp2/3 complex interacting region of WASP, the CA (Central, Acidic)

segment, and instead use a C-terminal armadillo repeat motif domain to bind and activate

Arp2/3 complex [4,6]. In addition, WASP uses its conserved V region to recruit

monomers directly to Arp2/3 complex for activation [7,8], while WDS proteins lack V

regions and do not bind to actin monomers [4]. Finally, WASP and WDS proteins bind to different sites on Arp2/3 complex [6,9–13]. However, despite these differences, some experiments indicate potentially overlapping activation mechanisms for these two nucleation promoting factors (NPFs). For instance, both WDS and WASP family proteins stimulate movement of Arp2 and Arp3 into or near a short pitch dimer (filament-like) arrangement, a conformational change required for activation [4,14–17]. How WDS proteins use a set of molecular features both common to and distinct from WASP to switch on Arp2/3 complex is currently unclear, and is critical to understanding this class of actin regulators.

During WASP-mediated activation of Arp2/3 complex, the nucleated filament (daughter filament) elongates from the barbed ends of Arp2 and Arp3, while the pointed end of the Arps bind to the sides of a pre-existing (mother) filament (Figure 1A) [18]. Therefore, we reasoned that like WASP, Dip1 could activate Arp2/3 complex to nucleate filaments that remain anchored by their pointed ends to the complex, with their barbed ends free to elongate (Figure 1A). In this mechanism, linear filaments generated by Dip1-Arp2/3 complex are analogous to branches generated by WASP-activated Arp2/3 complex. To test this model, we fluorescently labeled Dip1 with Alexa Fluor 568 to visualize its influence on actin polymerization in single molecule TIRF microscopy assays. Dip1 labeled with Alexa Fluor 568 on an engineered N-terminal cysteine (568-Dip1) showed decreased activity compared to unlabeled Dip1, but significantly accelerated actin assembly in the presence of Arp2/3 complex, indicating the labeled protein retained activity (Figure 1B). Dip1 at multiple concentrations sedimented as a single peak by analytical ultracentrifugation and lysine biotinylated 568-Dip1 bound to

coverslips photobleached predominantly in single steps (Figure 1C-F and Table S1).

Together these data suggest Dip1 is a monomer at low and high concentrations and 568-Dip1 is suitable for simple single-molecule imaging.
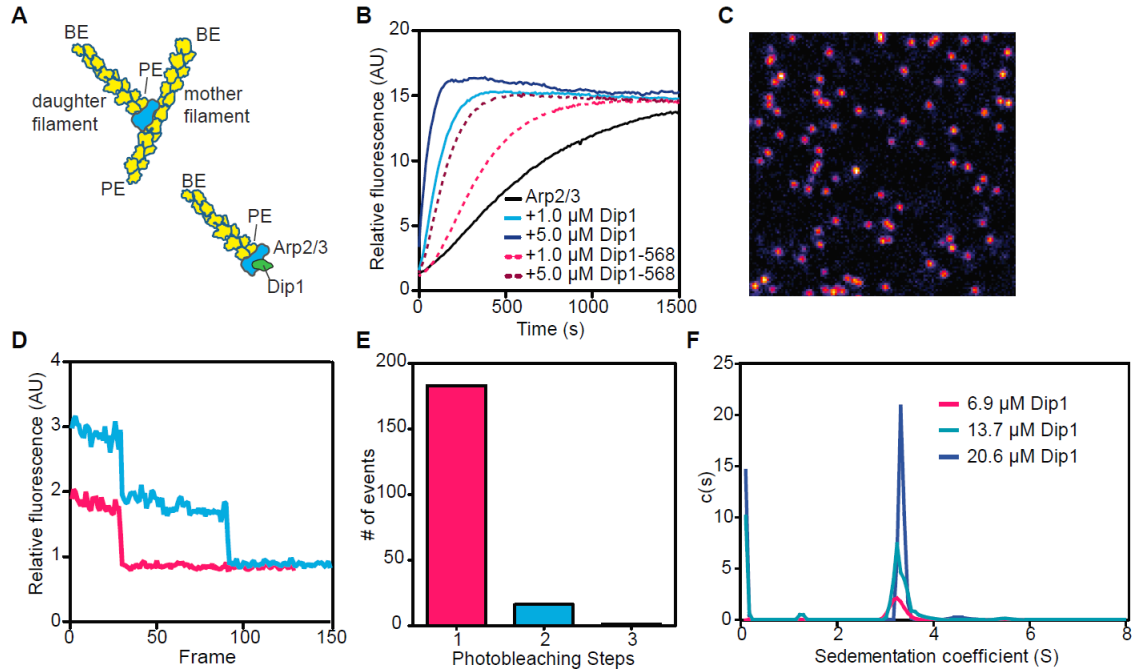
Figure 1: Model of Dip1-mediated Arp2/3 complex activation and characterization of Alexa Fluor 568 labeled Dip1. A. Cartoon of a branched filament nucleated by WASP-activated Arp2/3 complex (top) showing resulting filament polarities (barbed end, BE; pointed end, PE). Bottom half of panel shows a model of Dip1-mediated activation of Arp2/3 complex. In this model, the linear filament nucleated by Dip1-bound Arp2/3 complex is analogous to the daughter filament nucleated during branching nucleation. **B.** Time course of polymerization of 3 µM 15% pyrene-labeled actin in the presence of 50 nM *S. pombe* Arp2/3 complex (SpArp2/3 complex) and either unlabeled or Alexa Fluor 568 labeled Dip1 (568-Dip1). **C.** Representative image of 568-Dip1 molecules bound to a coverslip and visualized by TIRF microscopy. **D.** Examples of fluorescence intensities of single 568-Dip1 puncta over time. **E.** Quantification of events in which 568-Dip1 photobleached in one versus multiple steps. **F.** Plot of c(S) versus (S) for sedimentation velocity analytical ultracentrifugation of three concentrations of unlabeled Dip1. Dip1 sediments predominantly or entirely as a monomer at all three concentrations. See also Table S1.

In actin polymerization reactions containing (non-biotinylated) 568-Dip1, Oregon Green actin and unlabeled Arp2/3 complex, we observed Dip1 molecules bound to one end of actin filaments that adhered to the imaging surface (Figure 2A). The free ends of

Dip1-bound filaments elongated at the rate expected for free barbed ends at 1 µM actin [19], indicating Dip1 molecules bind the pointed end (Figure 2B). Dip1 only bound to filament ends in reactions containing Arp2/3 complex (Figure 2C). Therefore, we conclude that Dip1 binds actin filament pointed ends indirectly through Arp2/3 complex. Together, these data demonstrate that the linear actin filament generated by Dip1-activated Arp2/3 complex is analogous to the branch created by WASP-mediated activation.

Three distinct classes of events produced actin filaments with Dip1 bound at their pointed ends (Figure 2A,D). In class I Dip1 filament binding events (31 out of 141 observations), Dip1 non-specifically adsorbed to the surface and an actin filament appeared to nucleate from the Dip1 punctum (Figure 2A,D, Video S1). While we cannot eliminate the possibility that these events represent capture of a spontaneously nucleated actin filament by surface-adsorbed Dip1, our observations argue against this interpretation (see below). Therefore, we interpret these events as Dip1-Arp2/3 mediated nucleation of linear filaments. In a second, more frequent class of events (class II, 108 of 141), actin filaments "pre-loaded" with Dip1 were observed when they landed on the imaging surface (Figure 2A,D, Video S2). These events could represent surface capture of filaments that were nucleated by Dip1 and Arp2/3 complex in the reaction chamber above the zone of TIRF illumination. Alternatively, they might be spontaneously nucleated actin filaments that bound Dip1 and Arp2/3 complex at their pointed ends before landing on the imaging surface. Two observations argue against the latter explanation. First, association of Dip1 and Arp2/3 complex with pre-existing pointed ends is rare, as we observed very few instances in which Dip1-Arp2/3 bound to free
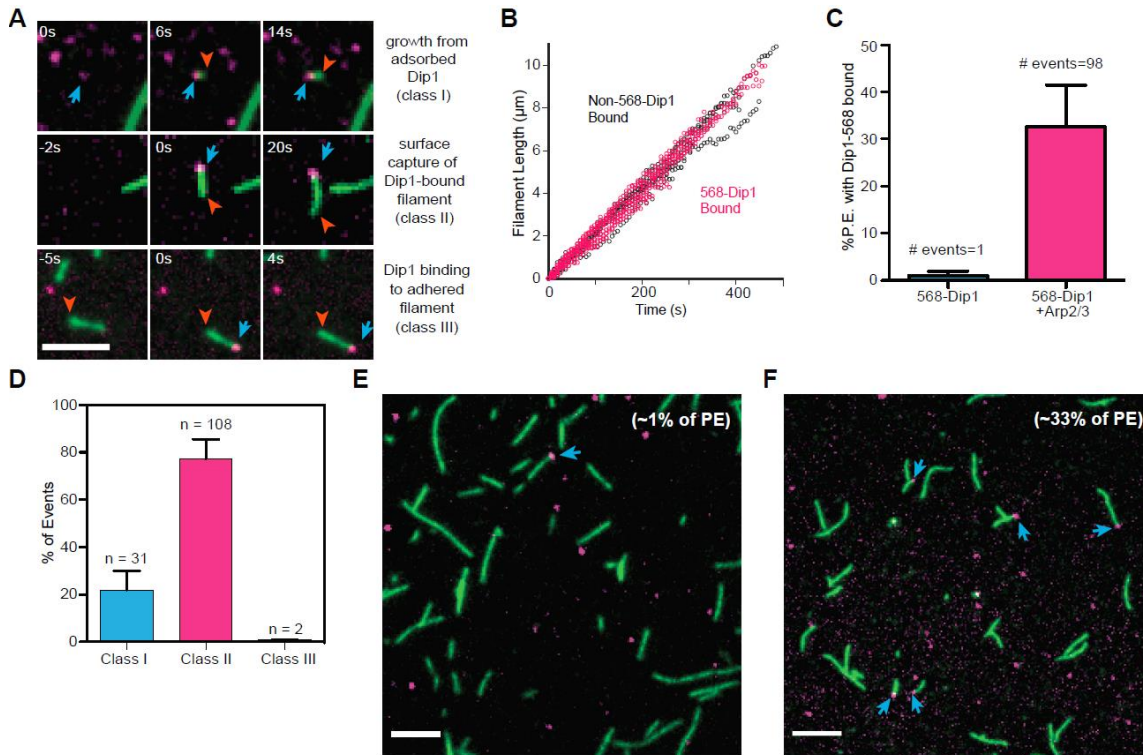
Figure 2: Dip1 co-opts features of branching nucleation to create linear filaments. A. TIRF microscopy images of actin polymerization reactions containing 6 nM 568-Dip1, 1.5 µM 33% Oregon Green labeled actin and 500 nM SpArp2/3 complex. Top, middle and bottom row show three different classes of events. Blue arrows show Dip1 bound to filament ends, red arrow heads mark elongating filament ends. Scale bar: 5 µm. **B.** Plot of filament length versus time for free filaments or filaments with bound Dip1. A total of 3 Non-568-Dip1 bound and 3 568-Dip1 filaments were measured. **C.** Quantification of the percentage of pointed ends with 568-Dip1 bound in actin polymerization reactions containing 6 nM 568-Dip1 and 1.5 µM 33% Oregon Green labeled actin with or without 500 nM SpArp2/3 complex. Error bars: standard error from 4 reactions. We speculate that the single event observed in the absence of Arp2/3 complex is coincident colocalization of a filament end with a surface adsorbed molecule of 568-Dip1. **D.** Quantification of three classes of events in which Dip1 is observed on the ends of filaments for the conditions described in B. Error bars show standard error from 4 reactions. **E.** TIRF microscopy image from a reaction in which 1.5 µM 33 % Oregon Green actin filaments were sheared and flowed into the imaging chamber before adding 6 nM 568-Dip1 and 500 nM SpArp2/3 complex. The total percentage of pointed ends bound to 568-Dip1 is indicated in the upper right corner (of 362 total pointed ends observed). **F.** TIRF microscopy image showing the same sized field of view as F with conditions described in B, in which Dip1 activates Arp2/3 complex to nucleate linear filaments. The total percentage of pointed ends bound to 568-Dip1 is indicated in the upper right corner (of 242 total pointed ends observed). Scale bar: 5 µm. See also Videos S1-S3.

pointed ends of surface-captured filaments (class III events, 2 out of 141 events, Figure

2A,D, Video S3). Second, in a separate experiment, we asked whether Dip1 binds

pointed ends generated by shearing spontaneously nucleated filaments in the presence of

Arp2/3 complex. Dip1 rarely bound pointed ends of spontaneously nucleated and Arp2/3-

capped sheared filaments (<1% of pointed ends) (Figure 2E), but was frequently

observed (33 % of pointed ends) bound in reactions in which the Dip1-Arp2/3 complex

assembly nucleated linear filaments (Figure 2F). Therefore, our data show that Dip1

associates strongly with Arp2/3 complex on a filament pointed end only if it has

cooperated with the complex to nucleate that filament.

Actin filaments nucleated by Dip1 and Arp2/3 complex activate WASP-bound

Arp2/3 complex

Dip1 possesses a key biochemical property that could allow it to seed branched

actin network assembly: it activates Arp2/3 complex without requiring a preformed

filament [4]. In cells, deletion of Dip1 stalls WASP (called Wsp1 in S. pombe) at

endocytic sites and decreases the rate at which new endocytic actin networks are initiated,

leading to a significant decrease in the total number of cortical actin puncta [5]. Together,

these observations led us to propose that that actin filaments nucleated by Dip1-activated

Arp2/3 complex might stimulate WASP-mediated activation of the complex to initiate

branched network assembly. However, it is not clear whether filaments nucleated by

Dip1-activated Arp2/3 complex can trigger activation of WASP-bound Arp2/3 complex.

Importantly, several recent studies show that the mode by which an actin filament is

nucleated can strongly influence its interactions with other actin regulators. For instance,

24

filaments nucleated by the fission yeast formin Cdc12 preferentially bind the fission yeast

tropomyosin Cdc8 [20]. Likewise, actin filaments nucleated by WASP-activated Arp2/3

complex are preferentially excluded from interactions with tropomyosin [21]. These and

other experiments suggest the identity of protein(s) bound to the filament end may

influence the conformation of interior actin filament subunits [22]. While the precise

mechanism of Dip1-mediated activation of the complex is still unclear, a similar

allosteric mechanism could influence the ability of Dip1-Arp2/3 complex nucleated

filaments to activate WASP-bound Arp2/3 complex. Therefore, it is important to directly

test whether filaments generated by Dip1-activated Arp2/3 complex can seed branched

actin network initiation.

The experiments we describe above demonstrate that 568-Dip1 molecules mark

actin filaments nucleated by Dip1-Arp2/3 complex (Figure 2A), allowing us to

distinguish them from spontaneously nucleated filaments. Therefore, our single molecule

TIRF experiments provide an opportunity to directly test whether linear filaments

nucleated by Dip1-activated Arp2/3 complex can activate WASP-bound Arp2/3 complex.

In an assay containing Arp2/3 complex, 568-Dip1, Oregon Green 488 actin and the

Arp2/3 complex-activating fragment of Wsp1, Wsp1-VCA, we observed multiple events

in which new actin filaments appeared to nucleate from 568-Dip1 puncta non-specifically

adsorbed to the surface (Figure 3A). As these linear filaments elongated, we frequently

observed branched filaments growing from their sides (Figure 3A). We also observed

branches growing from Dip1 bound filaments that landed on the imaging surface after

nucleation (Figure 3B, Video S4). Together, these experiments demonstrate that linear

filaments nucleated and bound by Dip1 and Arp2/3 complex stimulate branching

nucleation by WASP-bound Arp2/3 complex. Under the conditions of these reactions, we

observed branching nucleation not only from Dip1-bound filaments, but also from free

unbound filaments and from pre-existing branches (Figure 3A-C, Video S5). Therefore,

we asked if each source of filaments is equally potent in activating WASP-bound Arp2/3

complex. We found that branches nucleated at the same rate from all three filament

sources (Figure 3D).
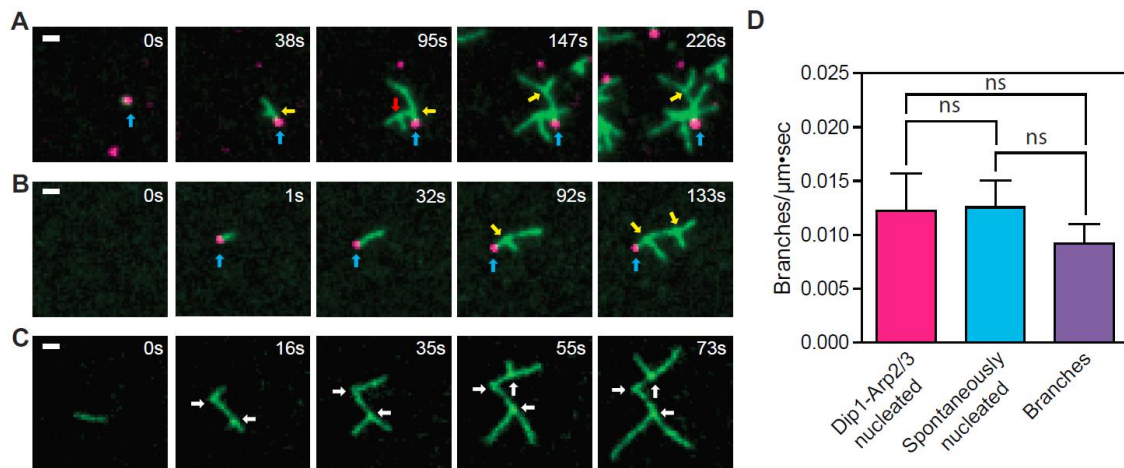
Figure 3: Filaments nucleated by Dip1-bound Arp2/3 complex activate Wsp1-bound Arp2/3 complex to seed branched network assembly. A, B. TIRF microscopy images of Dip1-Arp2/3 nucleated filaments seeding branching nucleation by Wsp1 and Arp2/3 complex. The reaction contained 6 nM 568-Dip1, 250 nM SpArp2/3 complex, 250 nM GST-Wsp1-VCA and 1.5 µM 33% Oregon Green actin. Blue arrows point to Dip1 molecules bound to pointed ends. Yellow arrows point to actin filament branches that grew from Dip1-Arp2/3 nucleated filaments. The red arrow points to a branch that nucleated from another branch. Panels A and B show growth of filaments from surface adsorbed Dip1 (class I event) or from a surface captured Dip1-bound filament (class II event), respectively. **C.** TIRF images of branches growing from spontaneously nucleated filaments used for quantification in D. The reaction contained 250 nM SpArp2/3 complex, 250 nM GST-Wsp1-VCA and 1.5 µM Oregon Green actin. White arrows point to branches. Scale bar is 1 µm in A,B and C. **D.** Quantification of the rate of branching on three sources of filaments: spontaneously nucleated filaments, pre-existing branches and Dip1-Arp2/3 nucleated seed filaments. Error bars: standard error from 3 separate reactions. See also Videos S4 and S5.

DISCUSSION

Our data show that the actin filament nucleated by Dip1 and Arp2/3 complex is analogous to the branched filament created by WASP-mediated activation of the complex (Figure 1A). That Dip1 co-opts features of branching nucleation has implications for understanding multiple aspects of Arp2/3 complex function. For instance, because Arp2/3 complex stays anchored on pointed ends during and after Dip1-mediated activation in this mechanism, the pointed ends of filaments nucleated by Dip1-Arp2/3 complex are protected from depolymerization. Therefore, specific mechanisms may be required to stimulate dissociation of Arp2/3 complex from the pointed ends of filaments nucleated by Dip1-activated Arp2/3 complex. GMF is an ADFH (actin depolymerization factor homology) family protein recently shown to bind directly to Arp2/3 complex to dissociate branches [23–25]. GMF may also have a role in dissociating Arp2/3 complex from the ends of linear filaments nucleated by Dip1-activated Arp2/3 complex. Multiple NPFs or putative NPFs are present at endocytic sites in S. pombe, including, Myo1, Wsp1, Dip1, and Pan1 [5,26,27]. While few experiments address how NPFs coordinately regulate the complex, our results here, together with previous work [4], show that Wsp1 and Dip1 use distinct mechanisms to activate a common mode of nucleation by Arp2/3 complex. If these mechanisms can work in concert, these two classes of NPFs could synergistically activate the complex, potentially influencing the rates of network seeding or propagation of branching, or both. An important future direction will be to investigate the coordinate regulation of Arp2/3 complex by Dip1 and full length Wsp1. While we use only the Arp2/3 complex-activating region (VCA) or Wsp1 in our studies here, full length Wsp1 harbors an N-terminal WH1 domain that

27

likely binds verprolin, an actin monomer binding protein. Further, Quantitative

biochemical studies of the influence of coordinated regulation of Arp2/3 complex by

these two NPFs will be important to understand the kinetics of branched actin initiation

and propagation in cells.

Here we demonstrate that actin filaments nucleated by Dip1-activated Arp2/3

complex stimulate branching nucleation by WASP-bound Arp2/3 complex to seed

assembly of branched actin networks. Several lines of evidence suggest this seeding

function of WDS proteins is broadly conserved. First, diverse WDS proteins activate the

complex with similar biochemical properties and share a conserved Arp2/3 complex

activating domain [4,6]. We anticipate that seeds generated by any WDS family protein

will activate WASP-bound Arp2/3 complexes, as we observed here for Dip1. Second,

previous studies suggest other WDS family proteins are important for actin assembly and

may be involved in initiation of branched actin filament networks. For instance, deletion

of the budding yeast homologue of Dip1, Ldb17, causes endocytosis defects, decreasing

the number of endocytic actin patches and increasing their size [28]. This phenotype is

identical to the dip1Δ phenotype in fission yeast [5], and is consistent with a model in

which Ldb17 initiates new patches by providing preformed filaments to activate WASP-

bound Arp2/3 complex. Less is known about the in vivo function of the mammalian

WDS protein, SPIN90, but experiments suggest that it interacts with endocytic proteins,

and contributes to uptake of at least one endocytic cargo, EGFR [29]. In addition to its

roles in endocytosis, some studies suggest SPIN90 may play a role in assembly of actin in

lamellipodia. Specifically, one group showed that knockdown of SPIN90 in COS-7 cells

prevents PDGF-induced ruffling [30]. Whether SPIN90 provides seed filaments to

initiate branched actin assembly in lamellipodia is an important open question. In addition, it will be important to determine the relative contributions of WDS proteins in seeding compared to other potential mechanisms, which include seeding by formin-nucleated filaments [31], Arp2/3-independent filament nucleation by NPF proteins [32], and capture of filaments generated by cofilin-mediated severing [33].

STAR METHODS

Contact for Reagent and Resource Sharing

Further information and requests for resources and reagents should be directed to and will be fulfilled by the Lead Contact, Brad Nolen (bnolen@uoregon.edu).

Experimental Model and Subject Details

S. pombe strain TP150 was cultured at 30°C in YE5S media until the cells entered the exponential phase, at which point they were harvested for protein purification.

Method Details

Experimental design details

All the data in Figure 1 are single replicates with the exception of panel E, where 200 binding events were counted from 2 separate movies. All puncta within each field of view were analyzed. No statistics were used in any of the analyses in Figure 1. In Figure 2B, three filaments lengths were measured for each condition (568-Dip1 bound vs non-bound) from a single TIRF movie. Filaments were selected for measurement only if their

growth was unobstructed by other filaments in the field and they remained adhered to the surface. For the 568-Dip1 bound filaments that were tracked, 568-Dip1 remained bound to the end of the filament for the duration of measurement, which was greater than 400 seconds in all cases. In Figure 2C, 106 total filaments were counted in the absence of Arp2/3 and 242 were counted in the presence of Arp2/3 complex. In both cases, counts were made from a total of four replicate movies. All filaments in each selected frame of a movie were counted. In panel 2D, 242 total filaments were counted from a total of four replicate movies to determine the percentage of each class of 568-Dip1 binding events. All filaments in a selected frame of the movie were counted. The bars represent the average 568-Dip1 binding percentage for each binding class from the four replicates with standard error for each class. In Figure 3D, to determine the branching density of the three sources of seed filaments, all the filaments in three replicate movies were measured and counted. The bars represent the average branching rate from the three replicates with standard error for each seed filament source. A two-tailed T test assuming unequal variances was used to determine if the branching rates were significantly different. No other statistical methods, sample size estimations, strategies for randomization, stratification, or blinding were used in the experiments or their analyses in this study.

Protein Expression, Purification, and Labeling

To generate a Dip1 construct for site specific labeling with a cysteine reactive fluorescent dye, the six endogenous cysteines were mutated to alanine by amplifying pGV67-SpDip1 [4] with non-overlapping 5'-phosphoryated primers encoding the mutation. The N-terminal Not1 restriction site, used to generate the GST-TEV-Dip1

expression vector, codes for a cysteine that was exploited for labeling. For expression and labeling of mutant protein, BL21-CodonPlus(DE3)RIL E. coli transformed with the pGV67 Dip1 expression vector was grown in 5 mL of LB plus 100 µg/mL ampicillin and 35 µg/mL chloramphenicol overnight at 37 °C. One milliliter of this culture was used to inoculate 50 mL of LB plus ampicillin and chloramphenicol that was grown until turbid at 37 °C with shaking at 180 rpm. Ten milliliters of this culture were used to inoculate 1 L of LB plus ampicillin and chloramphenicol. These cultures were grown to an O.D.600 of 0.6-0.7, induced with 0.4 mM isopropyl 1-thio-β-D-galactopyranoside (IPTG), and grown overnight at 22 °C for 12-14 hours. To each 1 L culture ethylenediaminetetraacetic acid (EDTA) and phenylmethanesulfonyl fluoride (PMSF) were added to 2 mM and 0.5 mM, respectively. The cultures were pelleted at 4000 rpm for 20 minutes in the Fiberlite F8B rotor at 4 °C. Cells were resuspended in 100 mL of lysis buffer; 20 mM Tris pH 8.0, 140 mM NaCl, 2 mM EDTA, 1 mM dithiothreitol, 0.5 mM phenylmethylsulfonyl fluoride, plus 2 protease inhibitor tablets (Roche). The resuspended cells were lysed by sonication on ice with intermittent pulses to keep the temperature below 10 °C. The lysate was clarified by centrifugation in a JA-20 rotor at 18,000 rpm for 30 minutes, and the soluble fraction was loaded on a 10mL glutathione sepharose column equilibrated in GST-binding buffer (20 mM Tris pH 8, 140 mM NaCl, 2 mM EDTA, 1 mM DTT). Protein was eluted with 30 mL of elution buffer (20 mM Tris pH 8.0, 140 mM NaCl and 50 mM glutathione adjusted to pH 8.0). Peak fractions were pooled and TEV protease was added at a 25:1 ratio (by mass). The reaction mix was dialyzed overnight at 4 °C against 20 mM Tris pH 8.0, 50 mM NaCl and 1 mM dithiothreitol. The sample was loaded onto a 6 ml Resource Q column at pH 8.0 and eluted with a gradient of 50 mM to

500 mM NaCl. Protein was then concentrated in an Amicon-Ultra concentration device before loading on a Superdex 200 HiLoad 16/60 gel filtration column and eluted in a buffer containing 20 mM HEPES pH 7.0 and 50 mM NaCl. Peak fractions were pooled and concentrated to ~ 40 µM for labeling. A 10 mM solution of Alexa Fluor 568 C5 Maleimide was prepared by dissolving in DMSO according to manufacturer's protocol. Protein was labeled by the dropwise addition of a 10-40 molar ratio of dye:protein while stirring at 4 °C. After 12-16 hours, the reaction was dialyzed against 20 mM Tris pH 8.0, 50 mM NaCl, and 1 mM dithiothreitol for 24 hours at 4 °C with buffer exchanges after 4hr and 8hrs. Labeled protein sample was loaded on a 5mL Hi-Trap desalting column and peak fractions were pooled and flash frozen in liquid nitrogen. The concentration of 568-Dip1 and the percentage labeled was calculated by measuring the absorbance at 575 nm and 280 nm. The concentration of Alexa Fluor 568 was calculated using the extinction coefficient, ε, 91,900 M^{-1} cm^{-1}. The concentration of Dip1 was calculated using Beer's law with the following correction factor for contribution from Alexa Fluor 568: [Dip1] = (Abs280 – (Abs575 * 0.403))/ε, where, ε, the extinction coefficient of Dip1 was estimated based on amino acid content at 36,330 M^{-1} cm^{-1}. Biotinylated 568-Dip1 was prepared by incubating a 15-fold molar excess of EZ-Link-NHS-PEG12-biotin (Thermofisher) for 9 hours in labeling buffer (20 mM Imidazole pH 7.5, 50 mM NaCl) at 4 ºC. The reaction was quenched by dialysis overnight in 20 mM Tris pH 8.0 and 50 mM NaCl.

To prepare lysates for S. pombe Arp2/3 complex purification, 10 mL of a turbid culture of S. pombe (TP150 strain) cells was added to each 1 L of YE5S in a 2.8 L flask. These cultures were grown for ~12 hrs at 30 °C with shaking. All subsequent steps were

carried out at 4 °C. EDTA and PMSF were added to 2mM and 0.5 mM, respectively, and the cells were harvested by centrifugation. The pellet was resuspended in 2 mL of lysis buffer (20mM Tris pH 8.0, 50 mM NaCl, 1 mM EDTA, 1mM DTT) per gram of wet cell pellet, plus 6 protease inhibitor tablets per liter of lysis buffer. Cells were lysed in a microfluidizer (Microfluidics Model M-110EH-30 Microfluidizer Processor) at 23 kPSI for 5 to 6 passes. After lysis 0.5 mM PMSF was added and the lysate was spun down in a JA-10 (Beckman) rotor at 9,000 rpm for 25 minutes. The supernatant was transferred to prechilled 70 mL polycarbonate centrifuge tubes (Beckman Coulter # 355655) and spun at 34,000 rpm for 75 minutes at 4 °C in a Fiberlite F37L rotor (Thermo-Scientific). The supernatant was filtered through cheesecloth into a graduated cylinder and the volume was measured. Under heavy stirring, 0.243 g of ammonium sulfate per mL of supernatant was added over approximately 30 minutes. The solution stirred for an additional 30 minutes, then pelleted in the Fiberlite F37L rotor at 34,000 rpm for 90 minutes. The pellet was resuspended in 50 mL of PKME (25 mM PIPES, 50 mM KCl, 1 mM EGTA, 3 mM MgCl2, 1 mM DTT and 0.1 mM ATP) and dialyzed against 8 L PKME overnight in 50,000 MWCO dialysis tubing. The dialysate was spun down at 34,000 rpm for 90 minutes in the Fiberlite F37L rotor. Ten milliliters of GS4B beads equilibrated in GST binding buffer (20 mM Tris pH 8, 140 mM NaCl, 1 mM EDTA, and 1 mM DTT) were charged with 15 mg of GST-N-WASP-VCA to make a GST-VCA affinity column. Additional binding buffer was added until no protein was detectable in the flow through by Bradford assay. The column was then equilibrated in PKME pH 7.0 and then supernatant was loaded at 1 mL per min before washing the column with additional PKME (~45 mL). The column was washed with PKME +150 mM KCl until no protein

33

was detected in the flow through by Bradford assay (~30 mL). Protein was eluted with PKME + 1 M NaCl into ~2 mL fractions until no protein was detected by a Bradford assay (~30mL). Fractions containing Arp2/3 complex were pooled and dialyzed against 2 L of QA buffer (10 mM PIPES, 25 mM NaCl, 0.25 mM EGTA, 0.25 mM MgCl2, pH 6.8 w/ KOH) in 50,000 MWCO dialysis tubing overnight. The complex was then purified by ion exchange chromatography on an FPLC using a 1mL MonoQ column with a linear gradient of QA buffer to 100% QB buffer (10 mM PIPES, 500 nM NaCl, 0.25 mM EGTA, 0.25 mM MgCl2, pH 6.8 w/ KOH) over 40 column volumes with a flow rate of 0.5 mL per minute. Fractions containing Arp2/3 complex were pooled and dialyzed against Tris pH 8.0, 50 mM NaCl and 1 mM DTT in 50,000 MWCO dialysis tubing overnight. The dialysate was concentrated to 1.5 mL in a 30,000 MWCO concentrator tube (Sartorius Vivaspin Turbo 15 #VS15T21) using the Fiberlite F13B rotor at 2,500 rpm for 5 to 10 minute cycles. Between each cycle the solution was mixed by gentle pipetting. The concentrated sample was loaded on a Superdex 200 size exclusion column in Tris pH 8.0, 50mM NaCl, and 1mM DTT. Eluted fractions with pure Arp2/3 complex were concentrated as described above and the final concentration determined by measuring the absorbance at 290 nm ($E290=139,030$ $M^{-1}cm^{-1}$) before flash freezing.

To purify GST-Wsp1-VCA, 5 mL of LB plus 100 µg/mL ampicillin and 35 µg/mL chloramphenicol was inoculated with BL21(DE3)-RIL cells transformed with a pGv67-GST-Wsp1-VCA plasmid and grown overnight at 37 °C. One milliliter of this culture was used to inoculate 50 mL of LB plus ampicillin and chloramphenicol and was grown until turbid at 37 °C with shaking at 180 rpm. Ten mL of this culture was used to inoculate each 1 L of LB plus ampicillin and chloramphenicol. These cultures were

34

grown at 37 °C to an OD600 of 0.4 to 0.6 and induced with 400 µL of 1 M IPTG per liter

of culture. The cultures were grown at 22 °C for 12-14 hrs. To each 1 L culture, EDTA

and PMSF were added to 2 mM and 0.5 mM, respectively, before pelleting at 4000 rpm

for 20 minutes at 4 °C in the Fiberlite F8B rotor. The pellet was resuspended in 100 mL

of lysis buffer (20 mM Tris pH 8, 140 mM NaCl, 1 mM DTT, 0.5 mM PMSF) plus 2

protease inhibitor tablets. The cells were lysed by sonication on ice with intermittent

pulses to keep the temperature below 10 °C. The lysate was then spun down for 45 min at

18,000 rpm in a JA-20 rotor at 4 °C. The clarified lysate was loaded onto a column

containing 10 mL of GS4B beads equilibrated in GST-binding buffer (20 mM Tris pH 8,

140 mM NaCl, 2 mM EDTA, 1 mM DTT) and washed with 7 column volumes of GST-

binding buffer. Protein was eluted from the column with 30 mL of GST-elution buffer pH

adjusted to 8.0 with NaOH (20 mM Tris pH 8.0, 100 mM NaCl, 1 mM DTT, 50 mM

reduced L-glutathione). The elution was dialyzed overnight at 4 °C in 2 L of 20 mM Tris

pH 8.0, 50 mM NaCl, and 1 mM DTT in 3500 MWCO dialysis tubing. The dialysate was

then loaded onto a Source30Q column on an FPLC equilibrated in QA buffer (20 mM

Tris pH 8.0, 100 mM NaCl, 1 mM DTT). GST-Wsp1-VCA was eluted from the column

over a 20 column volume gradient to 100% QB buffer (20 mM Tris pH 8.0, 500 mM

NaCl, 1 mM DTT). Fractions containing GST-Wsp1-VCA were concentrated to 1.5 mL

and flowed over a Superdex 75 size exclusion column equilibrated in 20 mM Tris pH 8.0,

150 mM NaCl, and 1 mM DTT. Pure fractions of GST-Wsp1-VCA were pooled and

concentrated to desired volume using a 3500 MWCO spin concentrator tube (Sartorius

Vivaspin Turbo 15 #VS15T91) in the Fiberlite F13B rotor at 2,500 rpm for 5 to 10

minute cycles at 4 °C. An extinction coefficient of 5,500 $M^{-1}cm^{-1}$ was used to determine protein concentration.

Biotin-inactivated myosin was prepared by reacting 2 mg of myosin with 5 µL of 250 mM EZ-Link-Maleimide-PEG11-Biotin dissolved in DMSO. The labeling reaction was carried out in 500 µL reaction buffer (20 mM HEPES, 500 mM KCl, 5 mM EDTA pH 8.0, 1 µM ATP and 1 mM MgCl2) on ice for 6 hours. The Biotin-myosin was then dialyzed into 0.5 L of storage buffer (20 mM Imidazole pH 7.0, 500 mM KCl, 5 mM EDTA pH 8.0, 1 mM DTT and 50% glycerol) using a 3500 MWCO dialysis thimble (Thermofisher Slide-A-Lyzer MINI dialysis unit 0069550).

Analytical Ultracentrifugation

Dip1 was diluted to 6.9, 13.7, and 20.6 µM to a final buffer concentration of 20 mM Tris pH 8.0, 50 mM NaCl, and 1 mM TCEP. Cells were inserted into a Beckman An50 Ti rotor and spun at 50,000 rpm at 20 °C in a Beckman XL-I analytical ultracentrifuge. Sedimentation was monitored using interference optics and the resulting radial interference scans were fit using a non-interacting continuous c(S) distribution model in SEDFIT [34]. The frictional ratio was set to 1.2 for the initial fit of the data without using the nonlinear regression method and was then optimized using nonlinear regression algorithms to improve the fit. The fits were regularized using a confidence level of 0.95 and were considered satisfactory if the root mean squared deviation was less than 0.01 and the residuals were random and less than 2% of the signal. The final parameters, including the fitted values the sedimentation coefficient and the frictional ratios are shown in Table S1.

TIRF microscopy slide preparation

TIRF flow chambers were constructed and reactions setup as previously described with slight modifications [19]. Coverslips (24 x 60 # 1.5) were cleaned in Coplin jars by sonicating in acetone followed by 1 M KOH for 25 min each, with a deionized water rinse between each sonication step. Coverslips were then rinsed twice with methanol and aminosilanized by incubating in 1% APTES (Sigma), 5 % acetic acid in methanol solution for 10 min before sonicating for 5 min, and then incubating for an additional 15 min. Coverslips were then rinsed with 2 volumes of methanol followed by thorough flushing with deionized water. After air drying, TIRF chambers were created by sandwiching cleaned coverslips and a glass microscope slide using double-sided tape to create an ~14 μL, 0.5 cm wide chamber. Chambers were passivated by incubating chambers for 4-5 hours in 300 mg/mL methoxy PEG succinimidyl succinate, MW5000 (JenKem) containing 1-3% biotin-PEG NHS ester, MW5000 (JenKem) dissolved in 0.1 M NaHCO3 pH 8.3. Excess PEG was washed away with 0.1 M NaHCO3 pH 8.3 and chambers were stored in deionized water for less than 1 week. All cleaning steps were carried out at room temperature. Immediately prior to imaging, chambers were incubated for 8 minutes with 1 μM NeutrAvidin (ThermoFisher) followed by 8 minutes with 50-150 nM biotin inactivated myosin (Cytoskeleton, Inc), both prepared in 50 mM Tris pH 7.5, 600 mM NaCl. Chambers were washed 2 times with 20 mg/mL BSA in 50 mM Tris pH 7.5, 600 mM NaCl followed by 2 washes with 20 mg/mL BSA in 50 mM Tris pH 7.5, 150 mM NaCl. Chambers were finally pre-incubated with TIRF buffer (10 mM Imidazole pH 7.0, 1 mM MgCl2, 1 mM EGTA, 50 mM KCl, 100 mM DTT, 0.2 mM

37

ATP, 25 mM Glucose, 0.5 % Metylcellulose (400 cP at 2%), 0.02 mg/mL Catalase

(Sigma) and 0.1 mg/mL Glucose Oxidase (MP Biomedicals)).

Actin Polymerization Reactions in TIRF chambers

       In a typical reaction, 1 µL of 2.5 mM MgCl2 and 10 mM EGTA was mixed with

5 µL of 9 µM 33% Oregon Green actin and incubated for 2 minutes. Four microliters of

the actin solution were then added to 16 µL of a solution containing 1.25x TIRF buffer

and any other proteins. Reactions were imaged on a Nikon TE2000 inverted microscope

equipped with 100x 1.49 numerical aperture TIRF objective, 50 mW 488 nm and 561 nm

Sapphire continuous wave solid state laser lines (Coherent), a dual band TIRF

(zt488/561rpc) filter cube (Chroma C143315), and a 1x -1.5x intermediate magnification

module. Images were collected using an 512x512 pixel EM-CCD camera (iXon3,

Andor). For two color reactions, typical imaging conditions were 50 ms exposures with

the 488 nm laser and 50 to 100 ms exposures with the 561 nm laser at 1 s intervals. For

photobleaching measurements of 568-Dip1, 150 ms exposures with the 561 nm laser and

500 ms intervals were used. The concentration of 568-Dip1 was kept in the low

nanomolar range in all assays to prevent high backgrounds of non-specifically adsorbed

568-Dip1 from obscuring Dip1 filament binding events.

Pyrene Actin Polymerization Assay

       In a typical reaction, 2 µL of 10X ME buffer (5 mM MgCl2, 20 mM EGTA) was

added to 20 µL of 15% pyrene labeled actin and allowed to incubate for 2 minutes in 96

well flat bottom black polystyrene assay plates (Corning 3686). To initiate the reaction,

78 µL of buffer containing all other proteins was added to the actin, bringing the final

buffer concentration in the reaction to 10 mM Imidazole pH 7.0, 50 mM KCL, 1 mM

EGTA, 1 mM MgCl2, 200 µM ATP and 1 mM DTT. Polymerization of actin was

monitored using a TECAN Safire 2 plate reader by exciting the pyrene actin at 365 nm

and monitoring the emission at 407 nm.

Pointed End Binding Assay

A solution of 7.5 µM 33% Oregon Green actin was pre-incubated for 2 minutes

with 0.5 mM MgCl2 and 2 mM EGTA to exchange the calcium in G-actin storage buffer

for magnesium. The actin was then diluted in TIRF buffer and reacted for 20 minutes.

Filaments were sheared by drawing solution two times through a 30-gauge needle on a 3

mL syringe. The reaction was diluted 10-fold in TIRF buffer containing 6 nM 568-Dip1,

500 nM S. pombe Arp2/3 complex, and 0.1 µM 33% Oregon Green actin. Control

reactions did not contain Arp2/3 complex. Binding to pointed ends was assayed by

equilibrating the final mixture for 2 minutes and then imaging by TIRF microscopy in

flow chambers as described above.

TIRF Microscopy Image Analysis

Images were prepared in Image J. Background was subtracted with a 10-pixel

rolling ball radius for the 561 channel and a 15-pixel rolling ball radius for the 488

channel. The total actin polymer was calculated using a custom image processing script

run in Matlab (Mathworks), described as follows. For each frame, pixels corresponding

to filament fluorescence were identified using image segmentation followed by

morphological area opening to remove non-filament small fluorescent objects. The final

pixel number value was converted to micrometers (1px = 106.7 nm) to yield the total

length of actin filaments in the image frame. To measure the number of Dip1 pointed end

binding events (Figure 3) and calculate the branching rates from different filament

sources (Figure 3), reactions were analyzed up to 120 seconds after imaging was

initiated. A custom ImageJ plugin was used to measure the lengths of actin filaments over

time (Figure 3, plugin was a gift from Jeff Kuhn).

Quantification and Statistical Analysis

The number of replicates and meaning of error bars can be found in the figure

legends. The significance of data in Figure 3D was calculated using a two-tailed T test

assuming unequal variances.

BRIDGE TO CHAPTER III

In this chapter, we showed that Dip1 co-opts aspects of actin branching nucleation

to activate Arp2/3 complex to nucleate linear actin filaments. Dip1 remains bound to the

pointed end of these new linear filaments indirectly through Arp2/3 complex. We went

on to show that these linear filaments act as substrates for WASP-bound Arp2/3 complex

and have the biochemical properties to serve as the seed filaments for actin network

initiation in cells. In Chapter III we will investigate the implications of the long lifetime

of Dip1-bound Arp2/3 complex on the pointed end of filaments on the architecture of

actin networks in vivo.

CHAPTER III

SINGLE TURNOVER ACTIVATION OF ARP2/3 COMPLEX BY DIP1 MAY BALANCE NUCLEATION OF LINEAR VERSUS BRANCHED ACTIN FILAMENTS

*This chapter contains previously published co-authored material.

SUMMARY

Arp2/3 complex nucleates branched actin filaments important for cellular motility, endocytosis, meiosis, and cellular differentiation [1–4]. WASP proteins, the prototypical Arp2/3 complex activators, activate Arp2/3 complex only once it is bound to the side of an actin filament [5,6]. This ensures WASP-activated Arp2/3 complex only nucleates branched actin filaments but means branched actin networks must be seeded with an initial preformed filament. Dip1 and other WISH/DIP/SPIN family proteins activate Arp2/3 complex without preformed filaments [7], creating seed filaments that activate WASP-bound Arp2/3 complex [8]. Importantly, Dip1-mediated activation of

Arp2/3 complex creates linear filaments instead of branches [7], so cells may need to limit Dip1 activity relative to WASP to preserve the dendritic nature of actin networks. However, how the simultaneous action of Dip1 and WASP influences the architectures of Arp2/3-assembled networks is unclear, so it is unknown if such regulatory mechanisms are required, and if so, what they are. We use TIRF microscopy to show that Dip1 causes actin assembled with WASP and Arp2/3 complex to form disconnected networks with many linear filaments rather than highly branched arrays. We discover a key biochemical difference between Dip1 and WASP that may limit linear filament nucleation in cells; while WASP must be released for nucleation, Dip1 stays associated with Arp2/3 complex on the pointed ends of nucleated actin filaments, so Dip1 is consumed in the reaction. Using live cell imaging of fission yeast, we provide evidence that Dip1 is a single turnover activator of Arp2/3 complex in vivo, revealing a mechanism by which Dip1 can initiate branched actin networks at endocytic sites without disrupting their branched architectures.

RESULTS

Dip1 induces disconnected linear actin network architectures, even in the presence of Wsp1

The branching nucleation activity of Arp2/3 complex allows it to assemble networks of short, crosslinked actin filaments that are thought to be optimal for pushing against broad surfaces [9,10]. However, unlike Wsp1, the S. pombe Wiskott-Aldrich Syndrome (WASP) family protein, the S. pombe WISH/DIP/SPIN90 family protein, Dip1, activates Arp2/3 complex to nucleate linear actin filaments instead of branches

[7,11]. Both Dip1 and Wsp1 are present at sites of endocytosis [11,12], so we wondered how their simultaneous activity on Arp2/3 complex influences actin network assembly. To address this, we used TIRF microscopy to visualize in vitro actin assembly mediated by Wsp1 and Arp2/3 complex with increasing concentrations of Dip1 (Figure 1A). In reactions lacking Dip1, many branches grew from a few spontaneously nucleated filaments, generating networks with high branching densities (Figure 1B). Adding Dip1 to the reactions caused network architectures to become less dendritic and more disconnected when comparing networks with the same amount of total polymer (Figure 1A). At 75 nM Dip1, the branch density decreased ~ 4-fold compared to reactions without Dip1, even though 150 nM Wsp1-VCA was present (Figure 1B). These data show that Dip1 induces Arp2/3 complex to produce poorly connected filament networks with greater proportions of linear filaments, even in the presence of Wsp1. For technical reasons (see below, and Figure S1), we could not measure the branch density at equivalent timepoints across the range of Dip1 concentrations we tested. However, the influence of Dip1 on actin network architectures is not due to the fact that we compared actin networks with equal total polymer length rather than at equivalent reaction time points, since reactions containing low (3.75 nM) versus high (75 nM) Dip1 showed that adding Dip1 decreased the branching density and the branch to linear filament ratio at a single timepoint (80 s) (Figure S2).

The influence of Dip1 on actin network assembly by Arp2/3 complex and Wsp1 initially led us to hypothesize that Dip1 competes with Wsp1 for activation of Arp2/3 complex. While structural and biochemical studies demonstrate that WASP and WDS family proteins bind to distinct sites on Arp2/3 complex [13–20], eliminating the

43

possibility of direct competition, the two NPFs could potentially allosterically reduce

each other's binding, causing negative cooperativity. Therefore, we asked if increasing

the concentration of Wsp1 would counteract the effect of Dip1, increasing the proportion

of branched filaments, presumably by decreasing the amount of Dip1-bound Arp2/3

complex. Unexpectedly, increasing the Wsp1 concentration from 150 nM to 600 nM in

presence of 15 nM Dip1 did not increase the branching density when comparing

---

Figure 1: Arp2/3 complex preferentially nucleates linear actin filaments in the presence of both Dip1 and Wsp1. A. TIRF microscopy images of actin polymerization assays containing 150 nM GST-Wsp1-VCA, 1.5 µM 33% Oregon Green-labeled actin, 50 nM SpArp2/3 complex and the indicated concentrations of Dip1. The reaction time is indicated in the upper right corner of each panel. Panels are aligned by total filament length in the full uncropped frame from which each panel is derived. The corresponding total filament length for each panel from left to right is 250, 500, 1000, 1500, and 2000 µm. Scale bar: 5 µm. **B.** Plot of the branch density versus Dip1 concentration for reactions as shown in Panel A. Branches were counted when the total filament length was 1500 µm (panels boxed in magenta in A). Error bars: SE from 4 to 6 regions of interest containing at least 130 filaments from 2-3 separate TIRF reactions. **C.** TIRF microscopy images of actin polymerization assays containing 15 nM Dip1, 1.5 µM 33% Oregon Green-labeled actin, 50 nM SpArp2/3 complex and indicated concentrations of GST-Wsp1-VCA. The reaction time is indicated in the upper right corner of each panel. Panels are aligned by total filament length as described in panel (A). Scale Bar: 5 µm. **D.** Plot of the branch density versus the concentration of GST-Wsp1-VCA as shown in panel C. Branches were counted when the total filament length was 1500 µm (panels boxed in magenta in C). Error Bars: SE from 4 to 6 regions of interest containing at least 340 total filaments from 2-3 separate TIRF reactions. **E.** Plot of total actin filament length in the field of view versus time for reactions described in panel (A) with the indicated concentration of Dip1. The standard error is calculated from the measurements of the full field of view from 2 or 3 reactions and is shown in a lighter shade around the means at each time point (dark lines). The increased polymer accumulation rate is due to faster nucleation in the Dip1-containing reactions, since Dip1 does not influence filament barbed end elongation rates [7,8]. **F.** Plot of the branch rate versus the concentration of Dip1 added to reactions as shown in panel (A). Measurements were made when the reaction reached a total filament length of 1500 µm. The time component of the rate is based on an extrapolation of the lifetime of the filament determined from filament lengths and the barbed elongation rate (see methods). Each point represents the average branching rate within a region of interest containing between 19 and 230 filaments. See also Figures S1-S2.
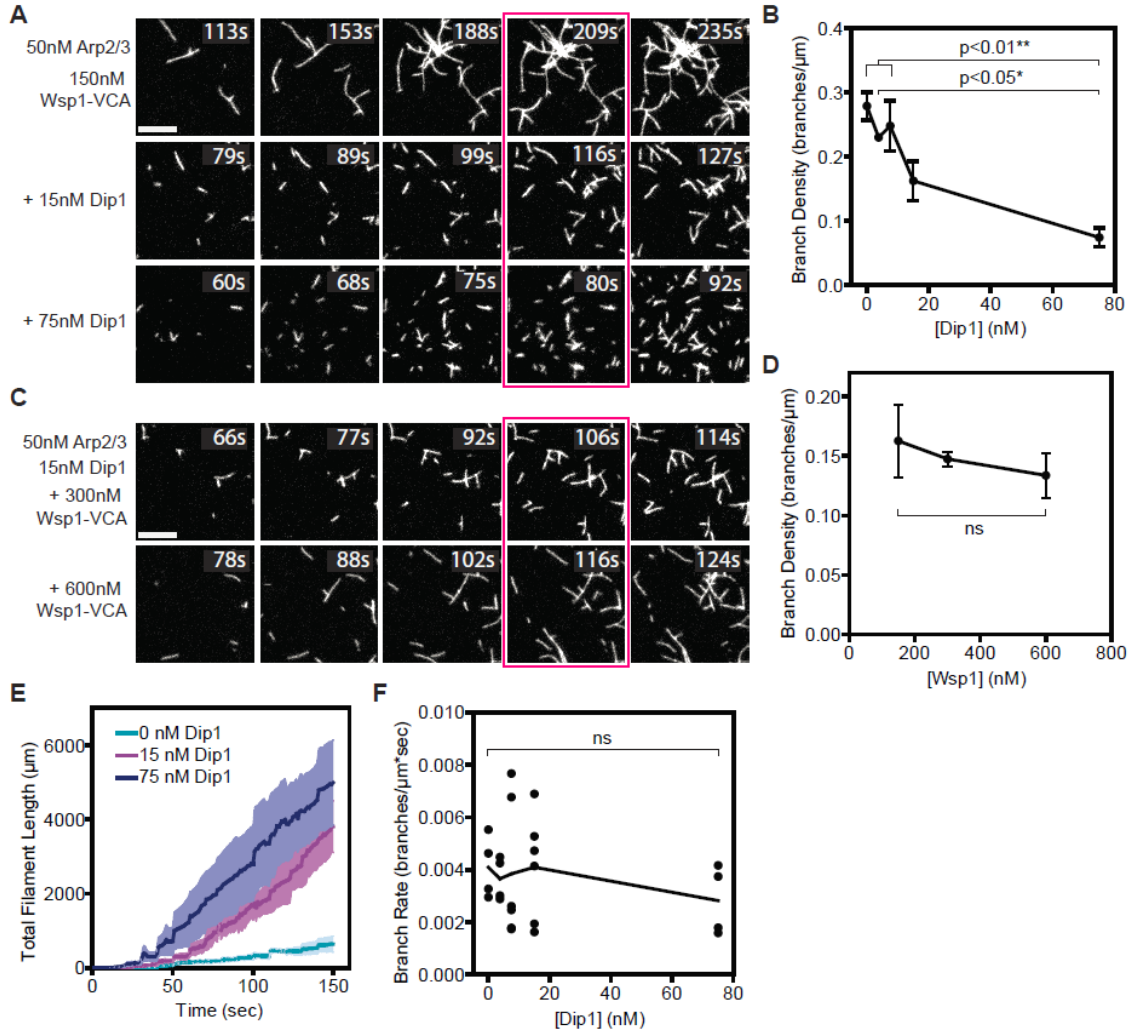
networks with the same amount of total polymer (Figures 1C and 1D). These data argue against a simple negative cooperativity model in which allosteric competition between WASP and Dip1 for binding Arp2/3 complex controls flux though linear versus branched filament pathways.

We previously showed that Dip1 activates Arp2/3 complex with a reduced lag phase because it can trigger nucleation by Arp2/3 complex without waiting for slow spontaneous nucleation of actin filaments, unlike WASP [7]. Therefore, we wondered if the disconnected architectures observed in the presence of both NPFs result from rapid

activation of Arp2/3 complex by Dip1 and accumulation of many linear filaments before a significant fraction of WASP-bound complexes can be activated by pre-existing filaments. Consistent with this hypothesis, we found that actin polymer accumulates more rapidly in the presence of Dip1, with linear filaments appearing much more rapidly than branches (Figures 1A and 1E). However, because previous data showed that WDS proteins compete with actin filaments for binding to Arp2/3 complex [16], it is also possible that linear filament generation by Dip1 is faster than branching because Dip1 blocks Arp2/3 complex from binding pre-existing filaments, thereby inhibiting WASP-mediated activation [16]. Importantly, the branching rate was not decreased by adding up to 75 nM Dip1, indicating that this concentration of Dip1 does not effectively prevent Wsp1-bound Arp2/3 complex from binding to actin filaments (Figures 1F and S2).

Dip1 remains bound to the pointed ends of actin filaments for hundreds of seconds after activating Arp2/3 complex

Programmed release of WASP allows it to catalyze multiple rounds of Arp2/3 complex activation at the attachment zone between a polymerizing network and a membrane [21,22]. This multi-turnover capability allows prolonged motility of WASP-coated beads in reconstituted motility assays and may also be important for continuous assembly of actin networks in cells [23,24]. Whether release of Dip1 from Arp2/3 complex is programmed into its activation mechanism, like WASP, or if it instead stays bound to the complex after triggering nucleation is unclear. This distinction dictates how fast a Dip1 molecule can be turned over to catalyze additional rounds of nucleation, so is

46

critical in understanding the balance between linear and branched filament generating NPFs at endocytic sites.

To determine if "programmed" Dip1 release is a feature of its activation mechanism, we labeled it with Alexa568 (Alexa568-Dip1) and visualized its action on Arp2/3 complex in reactions containing Oregon Green-labeled actin using TIRF microcopy. As we reported previously, these reactions produced multiple events in which a new linear actin filament grew from an Alexa568-Dip1 molecule non-specifically adsorbed to the surface [8](Figure 2A). Dip1 does not nucleate filaments on its own and does not bind actin filaments in the absence of Arp2/3 complex, so we interpret these events as Dip1 and Arp2/3 complex nucleating a linear filament [7,8]. Importantly, Dip1 did not release from filament ends upon nucleation, and the Alexa568 signal was visible at the filament end for many seconds as the filament elongated (Figure 2A). To determine how long Dip1 stays bound to Arp2/3 complex after nucleation, we measured the average length of Dip1 binding events. Under our initial imaging conditions, the average lifetime of the Alexa568-Dip1 signal on filament ends was ~195 seconds. To determine if this lifetime was controlled by photobleaching or dissociation, we decreased the laser exposure by increasing the time interval between frames during the acquisition (Figure 2B). At the lowest exposure levels we tested, the majority of filament-bound Dip1 molecules failed to release (or photobleach) before the end of the experiment (Figures 2B, 2C and Video S1), so we could not determine the rate constant for dissociation of Dip1 from Arp2/3 complex on filament ends. However, these measurements set a lower limit on the average Dip1 lifetime on the filament end at 325 seconds (Figure 2C). Together, these data show that Dip1-mediated activation of the

47

complex does not require Dip1 release, and that Dip1 stays bound to Arp2/3 complex after nucleation and throughout elongation of the filament.

Dip1 binds to treadmilling actin networks in S. pombe while most Wsp1 remains cortical

Our in vitro data show that Dip1 stays bound to actin filament ends for hundreds of seconds after nucleation of the linear filament, demonstrating that - unlike WASP - release of Dip1 is not programmed into the nucleation mechanism. We wondered if Dip1 also remains bound to Arp2/3 complex after it activates nucleation of actin filaments at endocytic sites in S. pombe. Arp2/3 complex becomes incorporated into the actin networks it nucleates [24–27], so if Dip1 fails to release from the complex after triggering nucleation, it will also become incorporated into the network. In wild type S. pombe, it can be difficult to distinguish between proteins that stay bound to the cortex or incorporate into the actin network because of the small size of endocytic actin patches (~200 nm) [28,29]. To circumvent this issue, we labeled Dip1 and the S. pombe actin patch marker, Fim1, in the context of an end4Δ strain and imaged the equatorial plane of the cells using spinning disk confocal microscopy (Figure 3A). END4 deletion converts punctate and transient endocytic actin networks into semi-continuously polymerizing actin comet tails that treadmill away from endocytic adaptors on the cortex and into the cytoplasm [12,30] (Figure 3A).

In an end4 deleted strain expressing Dip1-mNeonGreen and Fim1-mCherry, Dip1 colocalized with Fim1-marked actin networks (Figure 3A), consistent with a previous report showing that slightly overexpressed Dip1 shows a comet tail-like localization
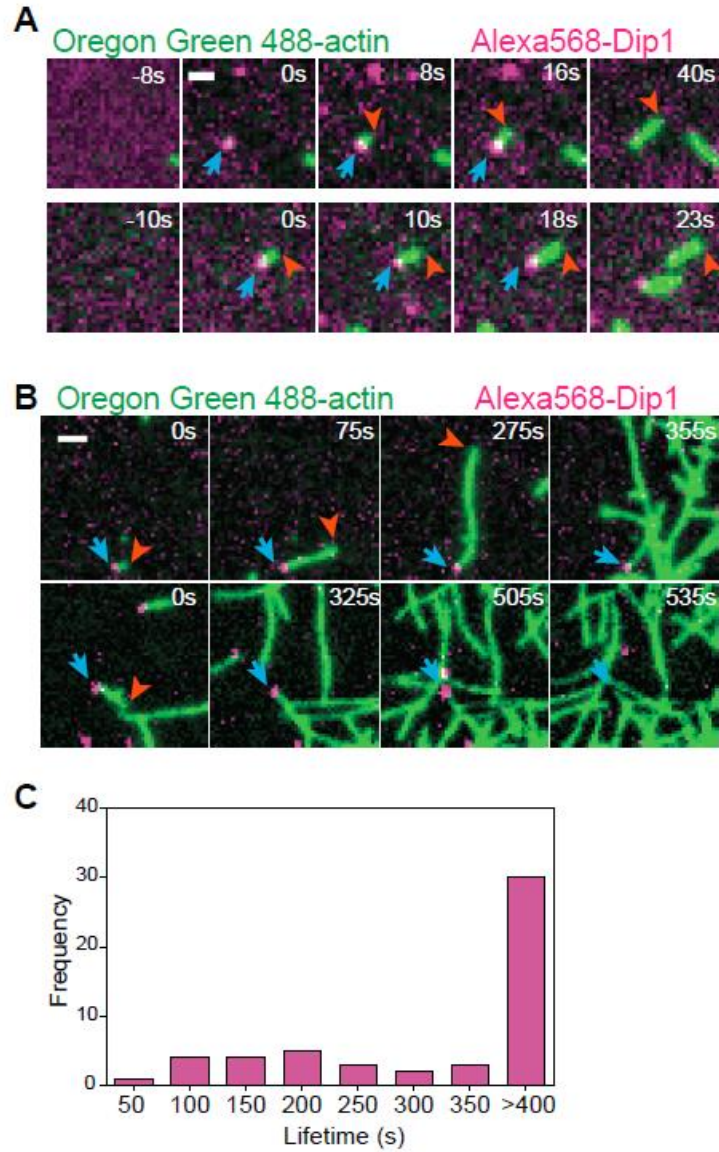
Figure 2: Dip1 remains bound to actin filaments for hundreds of seconds after nucleation. A. TIRF microscopy images of the polymerization of 1.5 μM 33% Oregon Green-labeled actin in the presence of 6 nM Alexa568-Dip1, 250 nM GST-Wsp1-VCA, and 500 nM SpArp2/3 complex collected with 50 ms exposure times at 200 ms intervals. Top row shows an event in which Dip1 non-specifically adsorbed to the surface activates Arp2/3 complex to nucleate a linear filament. Bottom row shows an event in which a Dip1-bound actin filament landed on the imaging surface. Blue arrows indicate the position of Dip1 and orange arrows mark the barbed end of the growing filament. **B.** Same as A, except that the interval for data collection was changed to 5s. The laser power was kept constant. The times indicated in the upper right corner of panels (A) and (B) correspond to the time since the appearance of the Alexa568-Dip1 molecule. **C.** Histogram of single molecule lifetimes on actin filament ends for videos collected as described in (B). See also Video S1.

49

pattern in an end4Δ strain [12]. Monitoring the dynamics of Dip1 at comet tail sites

revealed that Dip1 treadmills inward from the cortex at the same rate as Fim1-marked

actin (Figure 3B). We previously showed that Dip1 does not bind actin filaments directly,

and only binds strongly to Arp2/3 complex on an actin filament pointed end if it has

---

Figure 3: Localization of Dip1 and Wsp1 at wild type endocytic actin networks and treadmilling actin networks induced by deletion of END4. A. Spinning disk confocal images of Dip1-mNeonGreen (green) and Fim1-mCherry (magenta) in end4Δ S. pombe cells. The white arrows indicate representative treadmilling actin networks. Scale bar: 2 µm. **B.** Kymographs showing Dip1-mNeonGreen (green) and Fim1-mCherry (magenta) signal in treadmilling actin networks in end4Δ cells. The kymographs were made from a one pixel-wide line drawn from the exterior of the cell into the cytoplasm as depicted in the cartoon. The top of each panel is the cortex and the white arrow shows the direction of internalization into the cytoplasm. Scale bar: 0.5 µm. **C.** Montage of Dip1-mNeonGreen (green) and Fim1-mCherry (magenta) signals in a treadmilling actin network in end4Δ cells. The interval between each tile is 1 second. Scale bar: 0.5 µm. **D.** Spinning disk confocal images of Dip1-mNeonGreen (green) and mCherry-Wsp1 (magenta) in wildtype S. pombe cells. The white arrows indicate representative endocytic patch sites. The large structures in the Dip1-mNeonGreen channel are autofluorescence (Figure S4). Scale bar: 2 µm. **E.** Kymographs of Dip1-mNeonGreen (green) and mCherry-Wsp1 (magenta) dynamics in wild type cells. The kymographs are generated as described in panel C. Scale Bar: 0.5 µm. **F.** Plot showing the average normalized pixel intensity of mCherry-Wsp1 and Dip1-mNeonGreen along a line drawn through an endocytic patch from the exterior of the cell into the cytoplasm as depicted in the cartoon in panel B. Measurements were made when the total Wsp1 was at its peak intensity. The peak pixel intensity was aligned to 0.21 µm, the average distance of the peak pixel intensity of Wsp1 from the cortex at this timepoint. Traces represent the average of 15 endocytic patches selected proportionally from the histogram in panel G. **G.** Histogram of the distance between the peak signals of mCherry-Wsp1 and Dip1-mNeonGreen, as depicted by the black arrow in panel F. Positive numbers correspond to patches in which Dip1 is further from the cortex than Wsp1. On average, Dip1-mNeonGreen peak signal is 120 nm further from the cortex than mCherry-Wsp1 peak signal. See Materials and Methods for additional details (n = 56 patches, one sample t-test p < 0.0001). **H.** Kymographs of Dip1-mNeonGreen (green) and Fim1-mCherry (magenta) at cortical sites with multiple actin treadmilling events in end4Δ cells. Scale Bar: 1 µm. **I.** Spinning disk confocal images of GFP-Wsp1 (green) and Fim1-mCherry (magenta) in end4Δ S. pombe cells. The white arrows indicate representative treadmills. Scale bar: 2 µm. **J.** Kymographs of GFP-Wsp1 (green) and Fim1-mCherry (magenta) at repetitively treadmilling comet tails in end4Δ cells. Scale bar: 1 µm. See also Figures S3-S4 and Videos S2-S4.
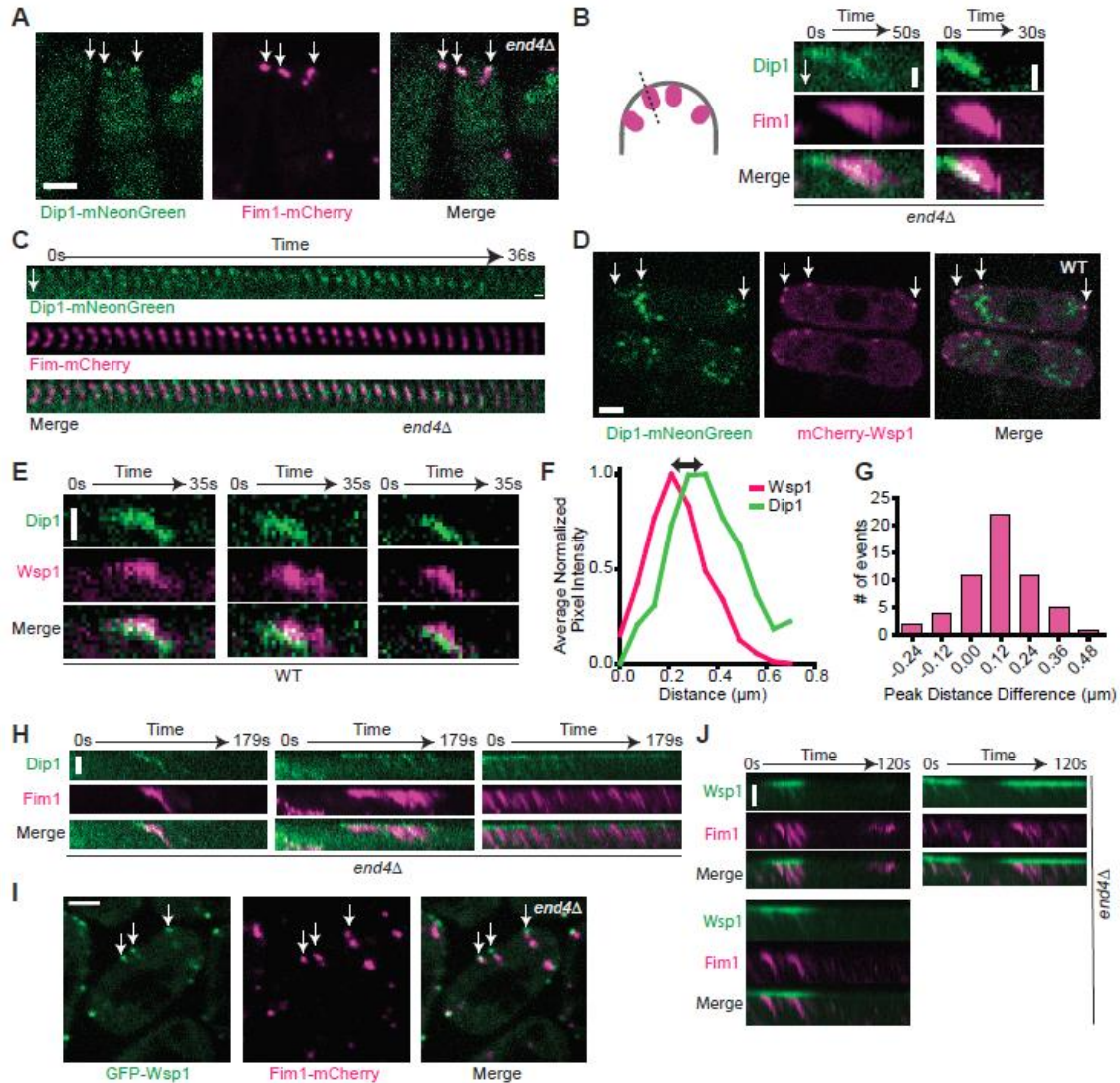
cooperated with the complex to nucleate that filament [8]. Therefore, our observation that Dip1 treadmills is consistent with a model in which it remains bound to Arp2/3 complex after triggering nucleation. Interestingly, Dip1 tended to incorporate in punctate patterns rather than spreading evenly throughout the entire treadmill, suggesting that bursts of Dip1 activity may occur at the cortex (Figure 3C and Video S2).

We next examined Dip1 localization in endocytic actin patches from wild type cells. During endocytosis, Wsp1 remains cortical as the actin network assembles, and

then moves inward slightly when the vesicle internalizes [11,29]. To determine whether Dip1 localization is distinct from Wsp1 in a wild type background, we labeled Wsp1 with mCherry and Dip1 with mNeonGreen. In most endocytic patches, Dip1 and Wsp1 partially colocalized, but Dip1 was further from the cortex than Wsp1 (Figures 3D, 3E and Video S3). Analysis of endocytic events from several cells revealed that the peak Dip1 signal is on average ~120 nm further from the cortex than the Wsp1 peak signal when the Wsp1 intensity is maximal (Figures 3F and 3G).

To more clearly visualize differences between Wsp1 and Dip1, we compared the behavior of each NPF in the context of an end4 deletion strain. Actin comet tails that formed in the end4 deletion strain treadmilled for variable lengths of time before releasing from the membrane and moving into the cytoplasm (VideoS2 and S4). In many instances, multiple comet tails grew from a single site at the cortex, with the actin network reinitiating after each instance of comet tail release (VideoS2 and S4). The peak Dip1 signal frequently moved inward with the treadmilling actin network, in some cases leaving little or no signal behind at the cortex (Figures 3H, S3, Video S2). In contrast, most Wsp1 remained at the cortex, with only a small portion of GFP-Wsp1 fluorescence evenly distributed within the comet tail (Figures 3I, 3J and Video S4). This observation is consistent with a model in which cortical Wsp1 molecules can catalyze multiple rounds of nucleation by Arp2/3 complex. This mechanism may help cells control the balance between branching and linear filament nucleation at endocytic sites (see discussion).

DISCUSSION

Our data reveal a critical mechanistic difference between WASP and WDS family NPFs. While WASP release is programmed into the nucleation mechanism, Dip1 release is not. Instead, Dip1 stays bound to Arp2/3 complex on the pointed ends of actin filaments for an average of over 5 minutes, more than 15 times longer than the average lifetime of an endocytic actin patch [31]. This suggests that Dip1 is a single turnover activator of Arp2/3 complex at endocytic sites. Our in vivo data support this model, showing that Dip1 incorporates into treadmilling actin networks, presumably because it is bound to Arp2/3 complex and thus unable to stimulate additional rounds of nucleation. The single turnover mechanism of Dip1-mediated activation of Arp2/3 complex may be important in limiting the linear filament nucleation activity of Dip1, since the catalytic activity of an NPF is proportional to its turnover rate. Endocytic actin patches contain at peak ~20 Dip1 molecules, ~150-230 Wsp1 molecules and ~320 Arp2/3 complexes [12,31]. Because Dip1 is consumed in the reaction, 20 likely represents the upper limit on the number of Dip1-Arp2/3 nucleated linear filaments per patch (Figure 4A).

In contrast to Dip1, our data here and several other studies have shown that most WASP remains cortically localized rather than incorporating into treadmilling actin networks [24,30]. Therefore, it is possible that single WASP molecules catalyze multiple rounds of branching nucleation in treadmilling networks in vivo to allow continued branched actin assembly at the cortex, as occurs in reconstituted systems in which WASP is attached to polystyrene beads or glass surfaces [23,32,33]. While it is still unclear how actin filaments are organized to generate force at endocytic sites [34,35], some experiments support a model in which WASP nucleates a network that assembles at the base of the

endocytic invagination, pushing inward on a disk of adaptor proteins attached to the tip of the invagination [36,37]. This model is consistent with our observation that Dip1 is more cytoplasmic than Wsp1 in wild type yeast, as Dip1 molecules bound to the initial filaments that seeded the network would move inward as the actin network grows away from the cortex (Figure 4A).

Here we show that in vitro, linear filament nucleation by Dip1-activated Arp2/3 complex is dominant over Wsp1-mediated branching. This suggests that cells must employ mechanisms to limit linear filament generation by Dip1-activated Arp2/3 complex. Under the conditions we tested, the dominance of Dip1 is due to the fast kinetics of Arp2/3 complex activation by Dip1 relative to activation by Wsp1 (Figure 4B, model 1). Given that the mammalian WDS protein, SPIN90, blocks Arp2/3 complex from interacting with actin filaments [16], we expected competition between Dip1 and actin filaments for Arp2/3 complex binding would provide another mechanism (Figure 4B, model 2) by which linear filament generation could dominate in vitro. However, our data indicate that this mechanism contributes little to the dominance of Dip1 under the conditions here, since increasing the concentration of Dip1 up to 75 nM did not decrease branching rates. We suspect that the inability of Dip1 to block branching at these concentrations is due to its relatively weak affinity for the isolated Arp2/3 complex [7]; it is likely that only a small percentage of the complex binds Dip1 at this concentration. Our data also indicate that Dip1 and Wsp1 do not compete for binding and activation of the complex, either directly or allosterically (Figure 4B, model 3). This observation indicates that increasing the local concentration of activated Wsp1 is not an effective way to limit the linear filament nucleation activity of Dip1. Therefore, the ~8 fold higher
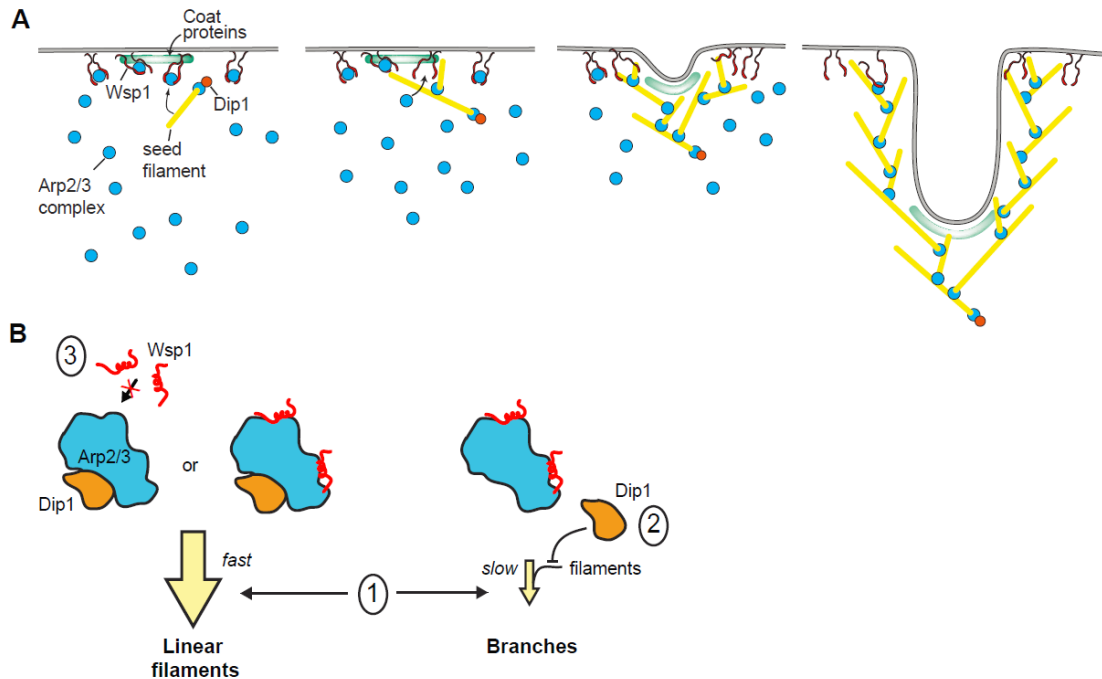
Figure 4: Proposed models of Dip1 activity and dynamics in vitro and at endocytic patches. A. Cartoon model showing activity of Dip1 (orange circle), Wsp1 (paired red lines), Arp2/3 complex (cyan circles), coat proteins (green zone) and actin (yellow lines) during membrane invagination of an endocytic patch. The number of molecules depicted is roughly proportional to the measured concentrations of these proteins at endocytic sites [12,31]. Dip1 activates Arp2/3 complex to create a linear filament that initiates assembly of the actin network. Dip1 remains bound to Arp2/3 complex so it can only activate a single Arp2/3 complex during assembly of the network. Most Wsp1 molecules remain bound to the cortex allowing them to catalyze multiple rounds of branching. The Dip1-bound linear filament that primed network assembly moves inward as Wsp1-mediated activation of the complex nucleates branches at the cortex. **B.** Cartoon model showing potential mechanisms of coordinate Arp2/3 complex regulation by Dip1 and Wsp1. The three Arp2/3 complexes represent the different possible binding states of the complex in the presence of both NPFs. Given that WDS proteins have been shown to block actin filament binding, we assume that Arp2/3 complex bound to both activators would create a linear actin filament [16]. Model 1: faster kinetics of activation of the Arp2/3 complex by Dip1 compared to Wsp1-bound Arp2/3 complex. Model 1 explains the dominance of Dip1 over Wsp1 in vitro. Model 2: competition between Dip1 and actin filaments for binding to Arp2/3 complex. Our data indicate that model 2 does not contribute to the dominance of Dip1 over Wsp1 in vitro, though this competition may be important in vivo. Model 3: competition between Dip1 and Wsp1 for binding to Arp2/3 complex. Our data argue against a role for model 3 either in vitro or in vivo.

concentration of Wsp1 at endocytic sites likely does little to drive endocytic networks

toward highly branched topologies [12,31]. However, because actin filaments trigger

Wsp1-mediated activation of the complex but likely block Dip1 from activating, the relative flux between the linear verses branched filament nucleation pathways likely depends on the local concentration of actin filaments (Figure 4B, model 1). We speculate that when a branched network assembles on a membrane, the high local concertation of actin filaments may allow WASP proteins to better compete with WDS family proteins, providing a mechanism by which Dip1 activity could be limited to the initiation phase of branched actin network assembly. This effect of actin filaments, combined with the consumption of Dip1 after a single round of Arp2/3 complex activation, may sufficiently limit linear filament generation at endocytic sites. We note that it was not possible under the conditions of our TIRF assays to deplete the pool of Dip1, so Dip1 activity dominated over Wsp1 despite the single turnover nature of the activity of Dip1.

An important future direction will be to investigate the coordinate regulation of Arp2/3 complex by Dip1 and full length Wsp1. While we use only the Arp2/3 complex-activating region (VCA) of Wsp1 in our studies here, the N-terminal region of Wsp1 harbors a WH1 domain that likely binds verprolin (an actin monomer binding protein [11]), and polyproline segments that have a variety of potential binding partners [38]. Understanding how these potential interaction partners influence network propagation will be important for understanding how Wsp1 controls actin network assembly in the presence of Dip1 in cells.

STAR METHODS

Lead Contact and Materials Availability

Further information and requests for resources and reagents should be directed to

and will be fulfilled by the Lead Contact, Brad Nolen (bnolen@uoregon.edu).

Schizosaccharomyces pombe strains generated in this study are available upon request.

Experimental Model and Subject Details

This study uses *Schizosaccharomyces pombe* cells which were grown at 30°C in

YE5S media with shaking at 180 rpm unless otherwise noted. S. pombe cells were

maintained in exponential phase for 24-48 hours before harvesting for imaging. A list of

all strains used in this manuscript can be found in the Key Resources Table.

Method Details

Protein Expression, Purification, and Fluorescent Labeling

To generate a Dip1 construct for site specific labeling with a cysteine-reactive

fluorescent dye, the six endogenous cysteines were mutated to alanine by amplifying

pGV67-Dip1 (described previously [8]) with non-overlapping 5'phosphoryated primers

encoding the mutation. The final expressed protein after TEV cleavage included the full

coding sequence for Dip1 along with a short N-terminal polypeptide sequence left after

TEV cleavage (GSMEFELRRQACGR). The cysteine in this N-terminal polypeptide was

exploited for tagging with the fluorescent dye. For expression and labeling,

BL21(DE3)RIL E. coli transformed with the pGV67 Dip1 expression vector was grown

to an O.D.595 of 0.6-0.7, induced with 0.4 mM isopropyl 1-thio-β-D-galactopyranoside, and grown overnight at 22 °C. Cells were lysed by sonication in lysis buffer: 20 mM Tris pH 8.0, 140 mM NaCl, 2 mM EDTA, 1 mM dithiothreitol, 0.5 mM phenylmethylsulfonyl fluoride, and protease inhibitor tablets (Roche). The lysate was clarified by centrifugation, and the soluble fraction was loaded on a glutathione sepharose column and eluted with 20 mM Tris pH 8.0, 140 mM NaCl and 50 mM glutathione. Peak fractions were pooled and a 25:1 ratio (by mass) of TEV protease to recombinant proteins was added. The reaction mix was dialyzed overnight against 20 mM Tris pH 8.0, 50 mM NaCl and 1 mM dithiothreitol at 4°C. The sample was loaded onto a 6ml Resource Q column at pH 8.0 and eluted with a gradient of 50 mM to 500 mM NaCl. Protein was then concentrated in an Amicon-Ultra concentration device and loaded onto a Superdex 200 HiLoad 16/60 gel filtration column equilibrated in 20 mM HEPES pH 7.0, 50 mM NaCl. Peak fractions were pooled and concentrated to ~40 µM for labeling. A 10 mM solution of Alexa568 C5 Maleimide (Thermo Fisher) was prepared by dissolving in water according to the manufacturer's protocol. Protein was labeled by the dropwise addition of a 10-40 molar ratio of dye:protein while stirring at 4°C. The reaction was quenched after 12-16 hours by dialyzing against 20 mM Tris pH 8.0, 50 mM NaCl, and 1 mM dithiothreitol for 24 hours with buffer exchanges after 4 and 8 hours. Labeled protein sample was loaded on a 5mL Hi-Trap desalting column and peak fractions were pooled and flash frozen in liquid nitrogen. The concentration of Alexa568 dye was determined by measuring the absorbance at 575 nm and dividing this by the dye extinction coefficient of 92,009 $M^{-1}cm^{-1}$. The concentration of 568-Dip1 was determined by subtracting the absorbance at 575 nm multiplied by the correction factor of 0.403 from

the absorbance at 280 nm and then dividing this number by the Dip1 extinction coefficient of 36,330 $M^{-1}cm^{-1}$.

To purify S. pombe Arp2/3 complex, 10 mL of a turbid culture of S. pombe (TP150 strain) was added to 1 L of YE5S media in a 2.8 L Fernbach flask. The cultures we grown at 30°C for ~12 hours with shaking at 180 rpm. Additional YE5S media (35 g/L) was added and the cells were grown for an additional 4 hours. Following growth, all steps were carried out at 4°C. Cultures were brought to 2 mM EDTA and 0.5 mM PMSF before harvesting the cells by centrifugation. The cell pellet was resuspended in 2 mL of lysis buffer (20mM Tris pH 8.0, 50 mM NaCl, 1 mM EDTA, 1mM DTT) per gram of wet cell pellet, plus 6 protease inhibitor tablets per liter of lysis buffer. Lysis was carried out in a microfluidizer (Microfluidics Model M-110EH-30 Microfluidizer Processor) by passing cells through the interaction chamber 5 to 6 times at 25 kPSI. The lysate was spun down at 9000 rpm for 25 minutes in a JA-10 (Beckman) rotor after adding 0.5 mM PMSF. The supernatant was decanted into prechilled 70 mL polycarbonate centrifuge tubes (Beckman Coulter #355655) and spun in a Fiberlite F37L rotor (Thermo-Scientific) at 34,000 rpm for 75 minutes. The supernatant was filtered through cheesecloth into a prechilled graduated cylinder. Ammonium sulfate was added to the supernatant (0.243 g/mL) over ~30 minutes with heavy stirring. The solution was allowed to stir for an additional 30 minutes before it was pelleted at 34,000 rpm for 90 minutes in a Fiberlite F37L rotor. The pellet was resuspended in 50 mL PKME (25 mM PIPES, 50 mM KCl, 1 mM EGTA, 3 mM MgCl2, 1 mM DTT and 0.1 mM ATP), added to 50,000 MWCO dialysis tubing and dialyzed overnight against 8 L of PKME. The dialysate was centrifuged in the Fiberlite F37L rotor for 90 minutes at 34,000 rpm. The supernatant was

59

added to a GST-VCA affinity column. The column contained 10 mL of GS4B beads pre-equilibrated in GST-binding buffer (20 mM Tris pH 8.0, 140 mM NaCl, 1 mM EDTA, and 1 mM DTT) and then charged with 15 mg of GST-N-WASP-VCA. Prior to addition of the supernatant, GST-binding buffer was added to the column until no protein was detectable by Bradford assay and the column was then equilibrated in PKME pH 7.0. The supernatant was loaded at 1 mL per minute and washed with ~45 mL of additional PKME. The column was then washed with ~30 mL of PKME + 150 mM KCl at which point no protein was detected in the flow through by Bradford assay. Protein was eluted from the column with PKME + 1 M NaCl into approximately 2 mL fractions until no further protein was detected by Bradford assay (~30 mL). All fractions containing Arp2/3 complex were pooled, added to 50,000 MWCO dialysis tubing and dialyzed against 2 L of QA buffer (10 mM PIPES, 25 mM NaCl, 0.25 mM EGTA, 0.25 mM MgCl2, pH 6.8 w/ KOH) overnight. The complex was then loaded onto a 1 mL MonoQ column attached to an FPLC and was eluted using a linear gradient of QA buffer to 100% QB buffer (10 mM PIPES, 500 nM NaCl, 0.25 mM EGTA, 0.25 mM MgCl2, pH 6.8 w/ KOH) over 40 column volumes at a flow rate of 0.5 mL/minute. Any fractions with Arp2/3 complex were pooled, added to 50,000 MWCO dialysis tubing and dialyzed against Tris pH 8.0, 50 mM NaCl and 1 mM DTT overnight. The dialysate was concentrated to ~1.5 mL in a 30,000 MWCO concentrator tube (Sartorius Vivaspin Turbo 15 #VS15T21) in a Fiberlite F13B rotor spinning at 2,500 rpm for 5 to 10 minute cycles. Between each cycle, the solution was gently pipetted to mix. The concentrated Arp2/3 complex was loaded on a Superdex 200 size exclusion column pre-equilibrated in Tris pH 8.0, 50 mM NaCl and 1 mM DTT. The complex was eluted into 1.25 mL fractions with the same buffer at 1

mL/minute. Fractions containing Arp2/3 complex were pooled and concentrated as described above before determining the final concentration. The final concentration was determined by measuring the absorbance at 290 nm (E290 = 139,030 $M^{-1}cm^{-1}$) and then the protein was aliquoted and flash frozen.

To express GST-Wsp1-VCA, BL21(DE3)-RIL cells were transformed with a pGV67-GST-Wsp1-VCA plasmid. A single colony was picked and used to inoculate 5 mL of LB plus 100 µg/mL ampicillin and 35 µg/mL chloramphenicol which was grown overnight with shaking at 37°C. A milliliter of this overnight culture was added to 50 mL of LB plus ampicillin and chloramphenicol and grown at 37°C with shaking at 180 rpm until the culture was turbid. From this starter culture, 10 mL was used to inoculate each liter of LB plus ampicillin and chloramphenicol. The 1 L cultures were grown at 37°C to an OD600 of between 0.4 and 0.6 and induced by adding 400 µL of 1 M IPTG per liter. The cultures were grown for 12 to 14 hours at 22°C before adding 2 mM EDTA and 0.5 mM PMSF. Cultures were centrifuged at 4°C for 20 minutes at 4000 rpm in the Fiberlite F8B rotor to pellet cells. The pellet was resuspended in 100 mL of lysis buffer (20 mM Tris pH 8.0, 140 mM NaCl, 1 mM DTT, 0.5 mM PMSF) plus 2 protease inhibitor pellets per 4 L of starting culture. Lysis was carried out by sonication on ice with intermittent pulses to ensure the temperature of the lysate remained below 10°C. The lysate was then centrifuged at 4°C for 45 minutes at 18,000 rpm in a JA-20 rotor (Beckman). The supernatant was loaded onto a column containing 10 mL of GS4B beads pre-equilibrated in GST-binding buffer (20 mM Tris pH 8.0, 140 mM NaCl, 2 mM EDTA, 1 mM DTT). The column was washed with ~70 mL of GST-binding buffer and protein was eluted with 30 mL of GST-elution buffer pH 8.0 (20 mM Tris pH 8.0, 100 mM NaCl, 1 mM DTT, 50

61

mM reduced L-glutathione). The elution was loaded into 3500 MWCO dialysis tubing and dialyzed overnight in 2 liters of 20 mM Tris pH 8.0, 50 mM NaCl and 1 mM DTT at 4°C. The dialysate was loaded onto a Source30Q column pre-equilibrated in QA buffer (20 mM Tris pH 8.0, 100 mM NaCl, 1 mM DTT) and GST-Wsp1-VCA was eluted from the column over a 20 column volume gradient to 100% QB buffer (20 mM Tris pH 8.0, 500 mM NaCl, 1 mM DTT). All fractions containing GST-Wsp1-VCA were pooled and concentrated to ~1.5 mL in a 3500 MWCO spin concentrator tube (Sartorius Vivaspin Turbo 15 #VS15T91) in the Fiberlite F13B rotor at 2,500 rpm for 5 to 10 minute cycles at 4°C. The GST-Wsp1-VCA was loaded onto a Superdex 75 size exclusion column pre-equilibrated in 20 mM Tris pH 8.0, 150 mM NaCl and 1 mM DTT and eluted from the column at 1 mL/minute into 1.25 mL fractions. Fractions containing pure GST-Wsp1-VCA were concentrated as described above before determining the final concentration. The final concentration was determined by measuring the absorbance at 280 nm (E280 =5,500 $M^{-1}cm^{-1}$) and then the protein was aliquoted and flash frozen.

Fission Yeast Strains and Molecular Biology

The Key Resources Table lists all *Schizosaccharomyces pombe* strains used in this study. To make *S. pombe* strain SpBN157-6, we crossed two strains provided by Volodia Sirotkin, VS1124a (kanMX6-Pwsp1-GFP-wsp1, fim1-mCherry-clonNAT) and VS872 (end4Δ::ura4+). Crossing and random spore analysis were carried out as previously described with some modifications [39]. A droplet of sterile water was pipetted onto an SPA5 mating plate and sterile wooden sticks were used to mix equal amounts of each strain being crossed into the droplet. The plate was incubated at 25°C

for 2 to 4 days and tetrad formation was confirmed using a microscope. Tetrads were treated in Zymolyase solution (to 5 mL of sterile water add 0.5 mL of 1 mg/mL Zymolyase (20T) in Zymolyase buffer (1 M sorbitol, 50 mM potassium phosphate pH 7.5, and 5 mM EDTA pH 8.0)). A pinhead of mated cells were added into the 15 mL conical tube containing the Zymolyase solution and vortexed briefly to mix. The tetrads were incubated at 30 °C for 12 to 16 hours on a Labquake tube rotator. The spore concentration was measured with a hemocytometer and ~500 spores were plated on YE5S plates to germinate at 25°C for 3 to 5 days. Single colonies were isolated and checked for the appropriate genotype using a combination of growth on antibiotic plates, microscopy and genomic PCR and sequencing.

Using InFusion cloning (Takara), we constructed a plasmid containing 351 bp of the genomic DIP1 5' UTR followed by the DIP1 ORF, mNeonGreen, the ADH1 terminator, the hphMX6 resistance cassette and 610 bp of the genomic DIP1 3' UTR. To construct S. pombe strain SpBN278-3, this region of the plasmid was linearized and transformed into S. pombe cells with an end4 deletion and Fim1-mCherry background. To make S. pombe strain SpBN280-1, the region of the plasmid described above was transformed into another strain provided by Volodia Sirotkin, VS1025-7 (kanMX6-Pwsp1-mCherry-wsp1). Transformations were carried out as previously described with some modifications [40]. Briefly, 20 to 50 mL of S. pombe cells were grown to a density of around 1 x 107 cells/mL before pelleting by centrifugation at 1300 x g for 5 minutes. The cells were washed by resuspending in 5 mL of sterile deionized water and pelleted by centrifugation as described above. Cells were again resuspended in 1 mL of sterile deionized water and transferred to a sterile microcentrifuge tube before pelleting at

16,000 x g for 1 min. The cells were then resuspended in 100 µL of sterile TE/LiAc solution (10 mM Tris-HCl, 1 mM EDTA, and 0.1 M lithium acetate, pH 7.5) and mixed with 2 µL of 10 mg/mL salmon sperm (carrier) DNA (Invitrogen) and 2 to 5 µg of the expression plasmid. This mixture was incubated at room temperature for 10 minutes, after which 260 µL of freshly prepared 40% TE/LiAc/PEG solution (40% w/v PEG4000 in sterile TE/LiAc) was added and allowed to incubate for an additional 1 hour at 30°C. After incubation, 43 µL of DMSO was added to the solution and mixed by gentle inversion before heat shock for 5 minutes at 42°C. The cells were then pelleted by centrifugation at 6000 x g for 1 minute, resuspended in 1 mL of sterile water, pelleted again, and then resuspended in 500 µL of sterile water. Finally, 250 µL of cells were spread onto EMM(4S)-uracil plates to select for successful transformants. Transformants typically appeared within 3 days to 1 week after growth at 30°C.

Preparation of S. pombe for Imaging

S. pombe cells were grown in YE5S media at 30°C with shaking at 180 rpm. Cells were back diluted to an optical density (600 nm) of ~0.2 in EMM(5S) and maintained in the exponential phase for 24 to 48 hours before imaging. Just before imaging, cells were collected by centrifuging at 900 x g for 3 minutes, washed once with EMM5S, and finally resuspended in 20-100□L EMM5S. Cells were mounted on 0.25% gelatin pads containing 10 mM propyl gallate and imaged within 30 minutes.

Confocal Microscopy Imaging of Fission Yeast

S. pombe cells on gelatin pads were imaged on a Nikon TE2000-U inverted

microscope equipped with a 100x/1.49 numerical aperture TIRF objective, a 1x - 1.5 x

intermediate magnification module, a Coherent OBIS 488 nm LS 60 mW laser, a

Coherent Sapphire 50 mW 561 nm continuous wave solid state laser, an acousto-optic

tunable filter (AOTF), a filter wheel (Applied Scientific Instrumentation) containing

ET525/50, ET605/52 and ZET488/561m-TRF 25 mm Dia Mounted filters and a

Yokogawa spinning disk scan head (CSU10). Images were collected on an EMCCD

camera (iXon Ultra-897, Andor). For imaging of the mCherry-Wsp1 and Fim1-mCherry

signal, images were typically taken using 200 to 300 ms exposures of 15 to 20 mW 561

nm laser at 1 second intervals with the ET605/52 filter. Dip1-mNeonGreen and GFP-

Wsp1 were typically imaged using 300 to 400 ms exposures of 25 mW 488 nm laser at 1

second intervals with the ET525/50 filter. All images were collected at a single focal

plane taken at the center of the cell.

Analysis of S. pombe Confocal Microscopy Images

Images were processed and analyzed using the FIJI distribution of Image J [41].

For spinning disk confocal images, the brightness and contrast were adjusted and then

images were cropped. Videos were made using the Multi Stack Montage (BIOP) FIJI

plugin and arrows were added with the Image, Stack and Timelapse Arrow Labelling

Tool for ImageJ. Montages were made using the Make Montage plugin. Kymographs

were created by drawing a single pixel wide line through an endocytic patch from the

outside of the cell into the cytoplasm and then using the Reslice tool.

To determine if Dip1 has a different localization pattern in endocytic patches than Wsp1, the relative position of their peak intensities was measured. Any patch that was present in the cell between 20 and 40 seconds after the start of the video was measured. A straight line was drawn through the center of each measured patch from outside of the cell towards the cell center following the direction of the internalizing patch. The pixel intensity along this line was measured using the Plot Profile tool to determine the intensity of both mCherry-Wsp1 and Dip1-mNeonGreen at each position along the line. The distance between the peak signals of Wsp1 and Dip1 were measured when the average Wsp1 signal across the line was at its maximum. A total of 56 patches across 8 cells were measured. To determine if the position of Dip1 and Wsp1 in these patches was statistically different, a one-sample t test with a hypothetical mean of 0 was used. The result showed a p-value of < 0.0001 with a 95% confidence interval of 0.076 to 0.153 and a t-value of 5.98.

In Figure 3, panel F, the Dip1-mNeonGreen and mCherry-Wsp1 signals across 15 patches were normalized, averaged and plotted. The average pixel intensities were normalized to a range of 0 to 1 by first subtracting the lowest value across the line from each measurement and then dividing by the peak intensity. The 15 patches were selected proportionally from each bin of the histogram in panel G. The peak signal of Wsp1 was set to 0.21 µm and the signal of Dip1 was plotted based on its relative position to Wsp1 in that endocytic patch.

To determine the position of the peak signal of Dip1-mNeonGreen or GFP-Wsp1 in actin comet tails the ImageJ macro, StackProfileData (Michael Schmid), was used to plot the intensity of each pixel along a single pixel wide line through the center of the

comet tail in each frame of the video. The peak signals of Dip1 and Wsp1 were analyzed from the initial appearance of Fim1-mCherry until the actin comet tail released from the membrane. The highest intensity pixel along the line in each frame was determined using the profile plot. If a higher intensity pixel was present within 2 pixels of either side of the profile line, this value was used as the peak intensity pixel. The position of the cortex was set by the location of the Dip1 or Wsp1 peak signal in the first analyzed frame for that comet tail. If the position of the peak signal was within 2 pixels (~0.32 µm) of the cortex, it was considered to be cortically localized.

Total Internal Reflection Fluorescence (TIRF) Microscopy Imaging of Actin Polymerization

TIRF flow chambers were constructed and reactions setup as previously described with slight modifications [42]. The coverslips were cleaned by sonicating for 25 minutes in acetone, rinsed with water, and sonicated for 25 minutes in 1 M KOH in Coplin jars. The coverslips were then rinsed twice with methanol before being aminosilanized by incubating in a 1% APTES (Sigma) and 5% acetic acid in methanol solution for 10 minutes, sonicating for 5 minutes, and then incubating for an additional 15 minutes at room temperature. Coverslips were then rinsed twice with methanol followed by deionized water and left to air dry. TIRF chambers were created by sandwiching double-sided tape (Scotch) between a glass microscope slide and a clean and dry coverslip (24 x 60 #1.5) to create a ~14 μL, 0.5 cm wide chamber. TIRF chambers were passivated by incubating for 4-5 hours in 300 mg/mL methoxy PEG succinimidyl succinate, MW5000 (JenKem) containing 1-3% biotin-PEG NHS ester, MW5000 (JenKem) dissolved in 0.1

M NaHCO3 pH 8.3. After incubation, 0.1 M NaHCO3 pH 8.3 was flowed into chambers to wash away excess PEG. TIRF chambers were stored in deionized water at 4°C for no more than 1 week. Just before use, TIRF chambers were incubated for 8 minutes with 1 µM NeutrAvidin (ThermoFisher) followed by 100 nM biotin inactivated myosin (Cytoskeleton, Inc.), both prepared in high-salt (HS) TBS (50 mM Tris pH 7.5, 600 mM NaCl). Chambers were then washed 2 times with 20 mg/mL BSA in HS-TBS followed by 2 washes with 20 mg/mL BSA in low-salt (LS) TBS (50 mM Tris pH 7.5, 150 mM NaCl). Finally, TIRF chambers were pre-incubated with TIRF buffer (10 mM Imidazole pH 7.0, 1 mM $MgCl_2$, 1 mM EGTA, 50 mM KCl, 100 mM DTT, 0.2 mM ATP, 25 mM Glucose, 0.5% Methylcellulose (400 cP at 2%), 0.02 mg/mL Catalase (Sigma) and 0.1 mg/mL Glucose Oxidase (MP Biomedicals).

TIRF Microscopy Actin Polymerization Reactions

To initiate the reaction, 1 µL of 2.5 mM $MgCl_2$ and 10 mM EGTA was mixed with 5 µL of 9 µM 33% Oregon Green-labeled actin and incubated for 2 min before adding 4 µL of this actin solution to 16 µL of 1.25 x TIRF buffer and any other proteins. Reactions were imaged on a Nikon TE2000-E inverted microscope equipped with a 100x 1.49 NA TIRF objective, 50 mW 488 nm and 561 nm Sapphire continuous wave solid state lase lines (Coherent), an acousto-optic tunable filter (AOTF), a dual band TIRF (zt488/561rpc) filter cube (Chroma C143315), a filter wheel (Finger Lakes Instrumentation) containing ET525/50 and ET605/52 filters, and a 1x to 1.5x intermediate magnification module. Images were taken using a 512x512 pixel EM-CCD camera (iXon3, Andor). For single color reactions, 50 ms exposures with the 488 nm

laser at 10 mW were taken at 1 second intervals, and a typical polymerization reaction was imaged for 10-15 minutes. For two color reactions, typical imaging conditions were 50 ms exposures with the 488 nm laser at 10 mW and 50 ms exposures with the 561 nm laser at 35 mW with 200 ms intervals. For low exposure imaging conditions, the exposure times and laser powers remained the same; however, a 5 second interval between frames was used to decrease the overall exposure time of Alexa568-Dip1. The concentration of Alexa568-Dip1 was kept at 6 nM to minimize the background signal in the 561 channel from non-specifically adsorbed Alexa568-Dip1.

TIRF Microscopy Image Analysis

Images were prepared using the FIJI distribution of Image J [41]. For actin polymerization experiments, the backgrounds of image sequences were subtracted using a 10-pixel rolling ball radius. The total actin polymer length, as shown in Figure 1E, was calculated using a custom image processing script run in Matlab (Mathworks), described as follows. For each frame, pixels corresponding to filament fluorescence were identified using image segmentation followed by morphological area opening to remove non-filament small fluorescent objects. The final pixel number value was converted to micrometers (1px = 106.7 nm) to yield the total length of actin filaments in the image frame. To calculate the reported branch densities (Figures 1B,D), the number of branches were counted manually and divided by the length of the seed filament when the total polymer length in each video was approximately 1500 µm. The branching rate in Figure 1F was calculated as the number of primary branches divided by one half the seed filament length multiplied by the lifetime of the seed. The lifetime of the seed filament

was calculated as the length of the seed multiplied by 370 actin monomers/µm divided by the barbed end elongation rate of 11.8 actin monomers/second [43]. To determine the branch to linear filament ratio, in each region of interest, the total number of branches was divided by the total number of seeds. To determine how long Dip1 stayed bound to Arp2/3 complex after nucleation, we measured the average length of Dip1 binding events from both filaments that grew from a Dip1 puncta already on the surface and also from filaments that landed on the surface after nucleation, extrapolating the birth time of the Dip1-Arp2/3 nucleated filaments in the latter based on the filament length and elongation rate of the filaments.

Quantification and Statistical Analysis

The numbers of replicates and description of error bars can be found in the figure legends. To determine if there were significant differences in the data in Figures 1B, D and F, a one-way analysis of variance (ANOVA) with a Tukey's Multiple Comparison test was used. Data points with significant differences are indicated on each plot with the respective p-values. All other data points were not significantly different from one another. For Supplemental Figures, two-tailed t-tests assuming unequal variances were used to determine if the average values were significantly different. The respective p-values are reported in the figure panels above data points that were determined to be statistically different.

Data and Code Availability

This study did not generate any datasets or code.

BRIDGE TO CHAPTER IV

In this chapter, we showed that, in vitro, Dip1 activation of Arp2/3 complex to nucleate linear actin filaments occurs more rapidly than Wsp1-mediated branching activity, leading to disconnected arrays of linear filaments. We also identified an important mechanistic difference between Dip1 and Wsp1 activation of Arp2/3 complex. While Wsp1 is released after nucleation, allowing activation of multiple Arp2/3 complexes, Dip1 is a single turnover activator of the complex. The in vivo consequence of this difference is that, unlike Wsp1, Dip1 is consumed by its interaction with Arp2/3 complex and is incorporated into the growing actin network. We speculate that this feature might play a key role in regulating linear filament nucleation to allow for the formation of the highly branched networks observed at endocytic sites. In Chapter IV, we will further investigate the in vivo contributions of both Dip1 and Wsp1 to actin assembly as well as look at how these two proteins Arp2/3 complex activation activities might be coordinated.

WSP1 SYNERGISTICALLY COACTIVATES ARP2/3 COMPLEX WITH DIP1 TO NUCLEATE LINEAR ACTIN FILAMENTS

*This chapter contains unpublished co-authored material.

Author contributions: Connor Balzer, Brad Nolen, Andrew Wagner, Luke Helgeson, Vladimir Sirotkin and Michael James conceived the experiments. Connor Balzer and Brad Nolen wrote the manuscript. Connor Balzer, Luke Helgeson and Michael James generated reagents and performed experiments.

INTRODUCTION

Arp2/3 complex is an important cytoskeletal regulator that nucleates actin filament networks important in a broad range of cellular processes, including cell motility, differentiation, endocytosis, meiotic spindle positioning, and DNA repair (Goley and Welch, 2006; Hurst et al., 2019; Rotty et al., 2013; Yi et al., 2011). Multiple classes of nucleation promoting factors (NPFs), including WASP family proteins (Type I NPFs), cortactin and related proteins (Type II NPFs) and WISH/DIP/SPIN90 (WDS) family proteins, activate the nucleation activity of Arp2/3 complex in response to cellular signals (Goley and Welch 2006; Wagner et al. 2013). *In vitro*, activated NPFs can function

independently to efficiently stimulate actin filament nucleation by Arp2/3 complex, but in cells, actin networks assembled by Arp2/3 complex frequently contain multiple classes of NPFs with non-redundant roles in actin assembly (Galletta et al., 2008; Murphy and Courtneidge, 2011; Sirotkin et al., 2005). Understanding how distinct NPFs coordinately control Arp2/3 complex to assemble cellular actin networks is critical to understanding actin regulation.

At sites of endocytosis in *S. pombe*, Arp2/3 complex nucleates the assembly of branched actin networks that drive invagination of the plasma membrane (Sun et al., 2019). The activity of Arp2/3 complex at endocytic sites can be controlled by at least three distinct NPFs: Wsp1, Dip1, and Myo1 (Sirotkin et al., 2005; Wagner et al., 2013). Each of these NPFs is relatively potent in activating Arp2/3 complex *in vitro*, and analysis of Wsp1 mutant or Dip1 knockout strains suggests that activation of Arp2/3 complex by both NPFs is required for normal endocytic actin assembly (Basu and Chang, 2011; Sirotkin et al., 2005; Wagner et al., 2013). On the other hand, while multiple experiments suggest the motor activity of Myo1 is important for normal actin dynamics, mutations in the Myo1 Arp2/3-activating segment do not influence endocytic internalization or coat protein dynamics, indicating the NPF activity of Myo1 may not by important for actin assembly in *S. pombe* (MacQuarrie et al., 2019; Sun et al., 2019).

It is currently unknown how Wsp1 and Dip1 cooperate to assemble functional endocytic actin networks in *S. pombe*, but key biochemical differences between these NPFs have led to a model for their coordinate activity. Wsp1, the *S. pombe* member of the WASP family NPFs, has a characteristic VCA motif at its C-terminus that is sufficient for activation of Arp2/3 complex (Higgs and Pollard, 2001; Sirotkin et al.,

73

2005). The CA segment within this motif binds Arp2/3 complex at two sites

(Boczkowska et al., 2014; Luan et al., 2018b; Padrick et al., 2011; Ti et al., 2011), while

the V segment binds actin monomers, which Wsp1 must recruit to the complex to trigger

nucleation (Marchand et al., 2001; Rohatgi et al., 1999). Importantly, the Wsp1-bound

Arp2/3 complex must also bind to a pre-existing actin filament to stimulate nucleation

(Achard et al., 2010; Machesky et al., 1999; Smith et al., 2013a; Wagner et al., 2013).

This requirement ensures that Wsp1 creates branched actin filaments when it activates the

complex, but also means a preformed filament must be provided to seed assembly of the

network. Dip1, like the other members of the WISH/DIP/SPIN90 (WDS) family proteins,

uses an armadillo repeat domain to bind and activate the complex (Luan et al., 2018a).

Unlike Wsp1, Dip1 does not require a pre-existing actin filament to trigger nucleation

(Wagner et al., 2013). Therefore, Dip1-medaited activation of Arp2/3 complex creates

linear filaments instead of branches (Wagner et al., 2013). Importantly, the linear

filaments nucleated by Dip1-activated Arp2/3 complex can activate Wsp1-bound Arp2/3

complex, which creates new branched actin filaments that activate subsequent rounds of

Wsp1-Arp2/3 mediated branching nucleation (Balzer et al., 2018). Therefore, by

activating Arp2/3 complex without a preformed actin filament, Dip1 kickstarts the

assembly of branched actin networks. These biochemical observations have led to a

model of how Dip1 and Wsp1 coordinate actin assembly at endocytic sites in yeast. In

this model, Dip1's role as an NPF is solely to generate seed filaments that kickstart the

assembly of the endocytic actin network, whereas Wsp1 exclusively functions as a

propagator of branched networks once they have been initiated.

Recent live cell imaging data support distinct seeding and propagating roles for Dip1 and Wsp1, respectively. For instance, in *dip1Δ* strains, the rate of initiation of new patches is markedly decreased, but once an endocytic actin network is initiated, it assembles rapidly, suggesting Dip1 is important for seeding but not propagation of the network (Basu and Chang, 2011). Further, deletion of the Wsp1 CA segment motif causes failure of endocytic actin patches to internalize, a process thought to be dependent on the propagation of branches (Sun et al., 2019). However, some data suggests that the seeding and propagating roles of Wsp1 and Dip1 might not be distinct. Specifically, biochemical and structural data suggested that the two NPFs might simultaneously bind Arp2/3 complex, so could potentially synergize to activate nucleation (Luan et al., 2018a, 2018b; Wagner et al., 2013).

Here we show that contrary to the previous model, Wsp1 cooperates with Dip1 to generate seed filaments. We provide evidence that this cooperation is important for initiation of endocytic actin networks in cells. By imaging endocytic actin patch dynamics in *S. pombe*, we find that despite the fact that Wsp1 is a key biochemical propagator of branched actin networks, it also has a significant influence on the rate at which new endocytic actin patches are created in *S. pombe*, indicating it plays a role in initiation. Through single molecule TIRF microscopy and other biochemical assays, we find that the role of Wsp1 in initiation is likely due to its ability to synergize with Dip1 to activate Arp2/3 complex. Specifically, we show that Dip1 and Wsp1 coactivate actin filament nucleation by Arp2/3 complex *in vitro*. Unexpectedly, in coactivating the complex with Wsp1, Dip1 converts Wsp1 from a branched to linear filament generating NPF. Coactivation by Wsp1 and Dip1 requires actin monomer recruitment by Wsp1 but

does not require a preformed actin filament. As a result, the two NPFs together can more potently create seed filaments for branched network initiation than Dip1 alone. This explains the decreased rate of patch initiation in Wsp1 mutations that block its activation of Arp2/3 complex in cells.

RESULTS

Deletion of the WASP CA segment causes a decrease in the patch initiation rate

To test their relative importance in the initiation versus propagation of endocytic actin networks, we measured the influence of Dip1 and Wsp1 mutations on actin dynamics in fission yeast using the endocytic actin patch marker Fim1 labeled with GFP (Berro and Pollard, 2014a). In wild type cells, Fim1-marked actin patches accumulate in cortical puncta over ~6 sec before moving inward and simultaneously disassembling (Fig. 1A-C) (Berro and Pollard, 2014b; Sirotkin et al., 2010)). To quantify actin patch initiation defects, we measured the rate at which new Fim1-marked puncta appeared in the cell (Fig. 1D). As expected based on previous results, the Dip1 deletion strain showed a significant reduction in the patch initiation rate compared to the wild type strain (0.030 versus 0.008 patches/sec/μM^2) and a corresponding decrease in the number of actin patches in the cell (Fig. 1D,E) (Basu and Chang, 2011). However, once actin assembly was initiated, Fim1-GFP accumulated at the same rate or more rapidly than in the wild type strain (Fig. 1B,C). These observations are consistent with previously reported measurements (Basu and Chang, 2011), and suggest that Dip1 contributes to the initiation but not the propagation of branched endocytic actin networks.
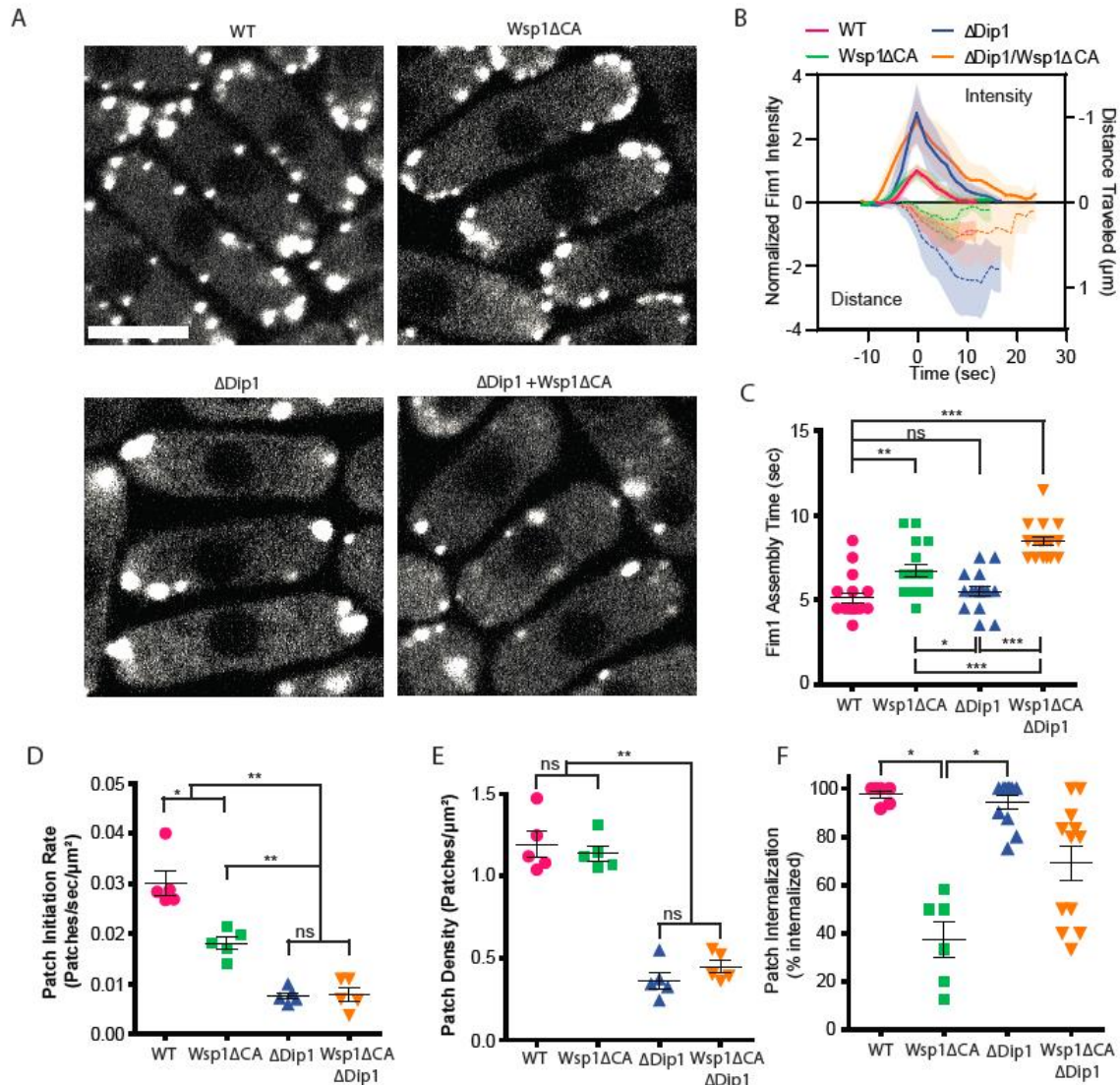
Figure 1. Wsp1 plays a role in the initiation of endocytic actin patches. A. Equatorial plane images of Fim1-GFP in *S. pombe* cells taken using spinning disk confocal microscopy. Scale Bar: 5 µm. **B.** Plot showing the relative Fim1-GFP intensity in *S. pombe* mutant endocytic patches over their lifetimes. Traces represent the average of 10 endocytic patches. Standard error shown as shaded region around each trace.   **C.** Plot comparing the assembly time of Fim1-GFP in endocytic patches in wildtype cells to Wsp1ΔCA and Dip1Δ mutants. Error bars: standard error from 10 cells. **D.** Plot comparing the endocytic patch initiation rate in wildtype cells to Wsp1ΔCA and Dip1Δ mutants. Error bars: standard error from 5 cells. * represents p < 0.003, ** represents p < 0.0004. **E.** Plot comparing the endocytic actin patch density in wildtype cells to Wsp1ΔCA and Dip1Δ mutants as determined based on the number of Fim1-GFP-marked cortical puncta. Error bars: standard error from 5 cells. ** represents p < 0.00009. **F.** Plot showing the percentage of endocytic patches internalized in *S. pombe* mutant cells. Error bars: standard error from 6 to 12 cells. * represents p < 0.001.

To investigate the contribution of Wsp1 toward initiation and propagation of the actin networks, we deleted the CA segment from *WSP1* at its endogenous locus and measured the influence of this mutation on actin dynamics. This mutation (Wsp1ΔCA) prevents Wsp1 from binding or activating Arp2/3 complex (Marchand et al., 2001), but leaves intact its WASP-homology 1 domain, proline-rich segment, and actin binding Verprolin-homology motif (V). In the *wsp1ΔCA* mutant the average time between the first appearance of Fim1-GFP and when it reaches peak concentration, which we refer to here as the patch assembly time, increases from ~5 to ~7 seconds, consistent with another recent study (Fig. 1B,C) (Sun et al., 2019; Lacy et al., 2019). In addition, the *wsp1ΔCA* mutation decreased the percentage of actin patches that internalized (Fig 1F). These observations are consistent with a role for Wsp1 in the propagation of branched actin during endocytosis. However, to our surprise, we also found that *wsp1ΔCA* strains also showed a 40 percent decrease in rate of initiation of new actin patches compared to wild type cells (Fig. 1D). While this defect is less than observed for deletion of Dip1, it suggests – contrary to our initial prediction – that Wsp1 may play a role in initiating new endocytic actin patches. Deletion of both the CA segment of Wsp1 and Dip1 (*dip1Δ, wsp1ΔCA*) did not decrease the actin patch initiation rate more than deletion of Dip1 alone (Fig. 1D). This suggests that Wsp1 may contribute to the Dip1-mediated actin patch initiation pathway rather than acting in a separate parallel pathway for initiation of actin assembly.

Dip1 and Wsp1 synergize during Arp2/3-mediated actin filament assembly

Previous biochemical and structural data suggested that Dip1 and Wsp1 might simultaneously bind Arp2/3 complex, so could potentially cooperate to activate nucleation (Luan et al., 2018a, 2018b; Wagner et al., 2013). Therefore, we reasoned that by directly synergizing with Dip1 to activate the complex, Wsp1 could contribute to actin network initiation. However, how the two NPFs together influence the activity of Arp2/3 complex is uncertain. Previous data showed that mixing both Wsp1 and Dip1 in a bulk actin polymerization assay increased the actin polymerization rate, but the reason for the increase was unknown (Wagner et al., 2013). Specifically, because those experiments were carried out at sub-saturating conditions, it was unclear whether Wsp1 and Dip1 activate in independent but additive pathways or alternatively, if the two NPFs synergize in activation of Arp2/3 complex. To test this, we titrated Dip1 into actin polymerization reactions containing Arp2/3 complex and the minimal Arp2/3-activating region of Wsp1, Wsp1-VCA. Dip1 was saturating at ~40 µM, and at this concentration the addition of Wsp1-VCA increased the maximum polymerization rate in the pyrene actin assembly assays ~1.6 fold (Fig 2A,B, Supplementary Table 1). These results suggest that the increased actin polymerization rates in the presence of both NPFs cannot be explained by an additive effect in activating Arp2/3 complex, but instead the NPFs are synergistic.

Wsp1 synergizes with Dip1 and Arp2/3 complex to produce linear actin filaments

Our bulk actin polymerization assays demonstrate that Wsp1 and Dip1 synergize to activate Arp2/3 complex, but it is unclear whether synergetic activation requires that the complex bind a preformed actin filament, as occurs when Wsp1 activates Arp2/3

complex on its own. Therefore, it is unclear whether the synergistic activation mechanism

could explain how Wsp1 contributes to initiation of new endocytic actin patches. To

better understand how the two NPFs synergize, we used single molecule TIRF

microscopy to monitor the assembly of Oregon Green 488-labeled actin in the presence

of Arp2/3 complex and Wsp1, Dip1, or both NPFs. We previously showed that Dip1

remains bound to Arp2/3 complex on the pointed end of filaments after nucleation and

---

Figure 2: Wsp1-VCA increases the number of linear filaments nucleated by Dip1-bound Arp2/3 complex. A. Time courses of polymerization of 3 µM 15% pyrene-labeled actin in the presence of 10 nM *S. pombe* Arp2/3 complex (SpArp2/3 complex) and 0 to 30 µM *S. pombe* Dip1 (Dip1) with or without 1 µM *S. pombe* Wsp1-VCA (Wsp1-VCA). **B.** Plot of the maximum polymerization rates in pyrene-labeled actin polymerization assays as described in A. Data points were fit to the following equation: Max poly rate = (max poly rate$_{max}$ x [Dip1])/($K_{1/2}$ + [Dip1]) + y-intercept where $K_{1/2}$ represents the [Dip1] needed to get half-maximum max polymerization rate and the y-intercept represents the maximum polymerization rate in the absence of Dip1. Note that A shows only a subset of the assays while the maximum polymerization rates of the entire data set are shown in B. See Supplementary Table 1 for details on fits. **C.** TIRF microscopy images of actin polymerization assays containing 100 nM SpArp2/3, 6 nM Alexa Fluor 568-labeled SpDip1 (568-Dip1)(magenta) and 1.5 µM 33% Oregon Green labeled actin (green) with or without 1 µM SpWsp1-VCA or 1 µM GST-SpWsp1-VCA. The panels are aligned by the reaction times noted above each column. White arrows indicate actin filament pointed ends bound by 568-Dip1. Scale bar: 2 µm. **D.** Quantification of the percentage of pointed ends bound by 568-Dip1 two minutes and thirty seconds into actin polymerization assays in C. Error bars represent the mean with standard error. P-values *** = < 0.0001. **E.** TIRF microscopy images of actin polymerization assays containing 250 nM SpArp2/3, 6 nM 568-Dip1 (magenta) and 1.5 µM 33% Oregon Green labeled actin (green) in the presence or absence of 250 nM GST-SpWsp1-VCA. The panels are aligned by the reaction times noted above each column. White arrows indicate actin filament pointed ends bound by 568-Dip1. Scale bar: 3 µm. **F.** Quantification of the percentage of pointed ends bound by 568-Dip1 two minutes and thirty seconds into actin polymerization assays in E. Error bars represent the mean with standard error. P-values *** = < 0.0001. **G.** Time courses of polymerization of 3 µM 15% pyrene-labeled actin in the presence of 10 nM SpArp2/3 complex and 0 to 20 µM Dip1 with or without 200 nM GST-SpWsp1-VCA. **H.** Plot of the maximum polymerization rate in pyrene-labeled actin polymerization assays containing GST-Wsp1-VCA and Dip1 as described in G. The fits for reactions without Wsp1 or with Wsp1-VCA (panel B) are shown for comparison. See Supplementary Table 1 for details on parameters of fits.
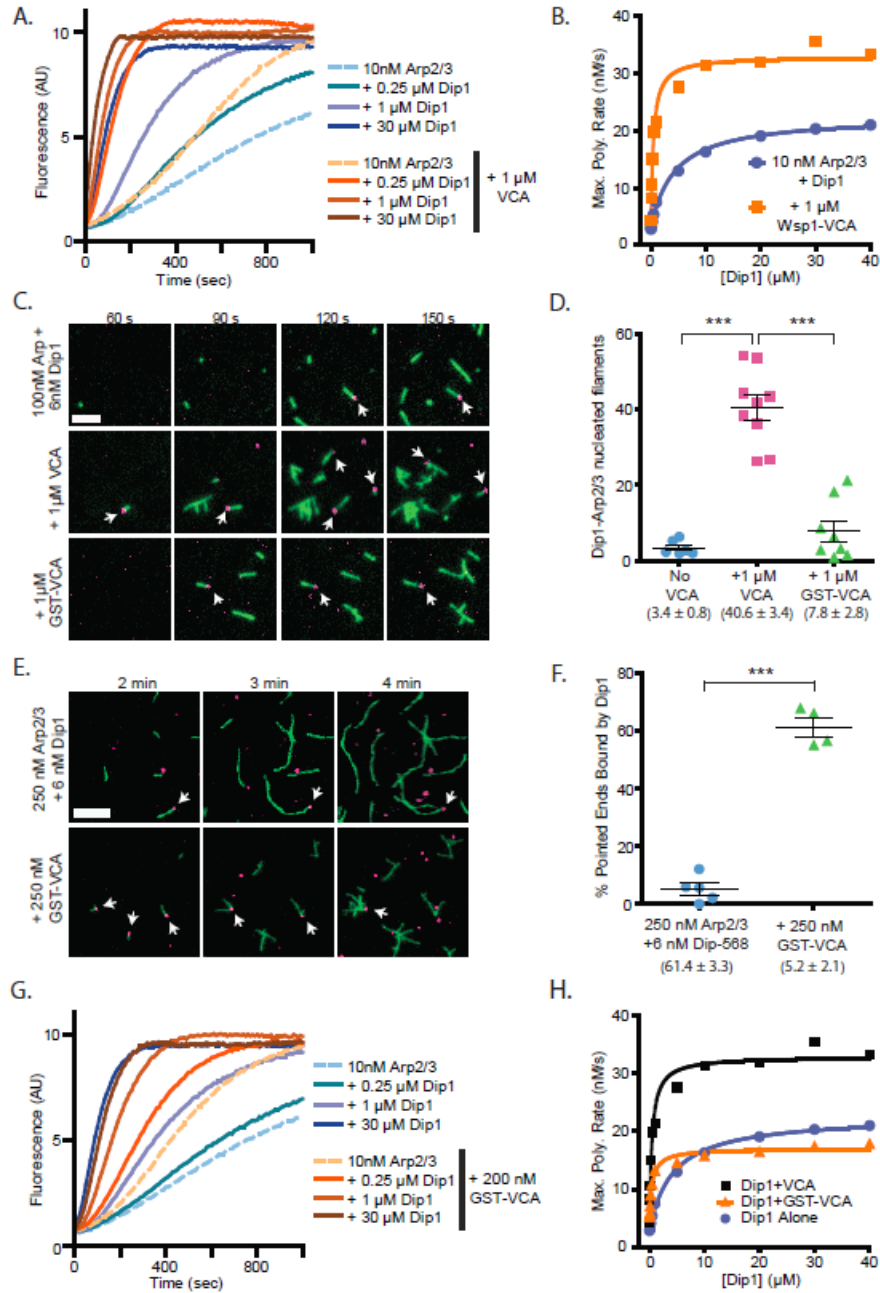
throughout elongation (Balzer et al., 2019). Furthermore, Dip1 binds very weakly to actin

filaments capped with Arp2/3 complex on their pointed ends (Balzer et al., 2018).

Therefore, we labeled Dip1 with Alexa Fluor 568 (568-Dip1) to mark actin filaments

nucleated by Arp2/3 complex and Dip1. In the presence of Arp2/3 complex and 568-

Dip1, we observed assembly of linear filaments, a subset of which had Dip1 bound at one end (Fig. 2C). These filaments, which largely represent Dip1-Arp2/3 nucleated filaments (Balzer et al., 2018), account for 3.4% of the total number for filament pointed ends present in the reaction after two and a half minutes (Fig. 2C,D). Adding Wsp1-VCA to the reaction significantly increased the number of linear actin filaments with bound Dip1. At 1 μM Wsp1-VCA, the number of Dip1-bound filaments increased 12-fold over reactions without Wsp1 (Fig. 2C,D). These data demonstrate that synergistic activation of Arp2/3 complex by the two NPFs results in the nucleation of linear rather than branched actin filaments. Therefore, we conclude that like Dip1-mediated activation (Wagner et al., 2013), synergistic co-activation by both NPFs does not require a pre-existing actin filament.

Because Wsp1 may function as an oligomer when clustered at endocytic sites (Padrick et al., 2008), we also tested if Wsp1-VCA dimerized with GST synergizes with Dip1 to activate Arp2/3 complex. Under our initial reaction conditions (100 nM Arp2/3 complex and 1 μM GST-VCA), we did not detect synergistic coactivation of the complex by Dip1 and GST-VCA (Fig. 2D). However, in reactions in which the concentration of Arp2/3 complex was increased 2.5-fold, the number of pointed ends with bound Dip1 increased significantly in the presence of GST-VCA, indicating dimeric (GST) Wsp1-VCA synergizes with Dip1 (Fig. 2E,F). To further investigate the influence of Wsp1 dimerization on synergy, we compared the influence of monomeric and dimeric Wsp1-VCAs on the maximum polymerization rate in bulk pyrene actin polymerization assays containing Arp2/3 complex and a range of Dip1 concentrations (Fig. 2G). These data showed both dimeric and monomeric Wsp1-VCA significantly decrease the

concentration of Dip1 required to saturate the reaction (Fig. 2H). However, unlike monomeric Wsp1-VCA, dimeric Wsp1-VCA did not increase the maximum polymerization rate at saturating Dip1. These data demonstrate that monomeric Wsp1 is more potent in its synergy with Dip1 than dimeric Wsp1, and point to differences in the mechanism of synergistic activation between monomeric and dimeric Wsp1-VCA (see discussion).

Actin monomers stimulate activation of Arp2/3 complex by Dip1

To determine the mechanism of co-activation by Dip1 and Wsp1, we first examined the kinetics of activation by Dip1 alone to identify steps in the activation pathway that might be accelerated by Wsp1. We measured time courses of actin polymerization in reactions containing actin, S. pombe Arp2/3 complex and a range of concentrations of Dip1 (0-15 μM) and asked whether various kinetic models were consistent with the polymerization time courses (Fig. 3A). In the simplest model we considered (Fig. 3B (i)), Dip1 binds to Arp2/3 complex and initiates an irreversible activation step to create a filament barbed end. This step could represent an activating conformational change, such as subunit flattening of the two actin-related proteins in the complex, Arp2 and Arp3, or their movement into the short pitch helical arrangement (Fig. 3B) (Rodnick-Smith et al., 2016; Wagner et al., 2013)). The value of the irreversible activation step was floated in the simulations, and the other rate constants were fixed or restrained as described in the supplementary materials. The simple model produced simulated time polymerization courses that fit the data poorly compared to the measured time courses (Fig. 3A, Supplementary Fig. 1). Specifically, the simulations predicted

83

faster polymerization than observed at time points near steady state when the

concentration of free actin monomers is low. Therefore, we wondered whether collision
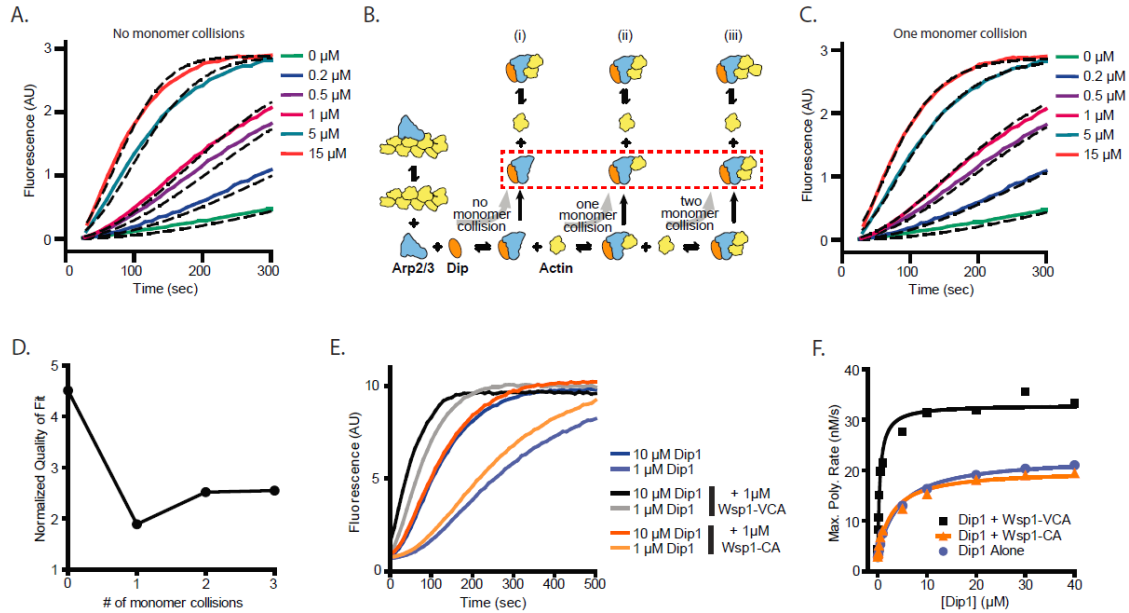
Figure 3: Monomer recruitment by Wsp1-VCA is required for maximal coactivation of Arp2/3 complex with Dip1. A. Plot of time courses of polymerization of 3 µM 15% pyrene-labeled actin in the presence of 50 nM SpArp2/3 complex and 0 to 15 µM Dip1 (solid colored lines). Dashed lines over each trace show the best fits from the no monomer collision model in B. Only a subset of the reactions and fits used in the simulation are shown. For the complete data set see Supplementary Figure 1. **B.** Cartoon diagram showing kinetic pathways used to fit the experimental polymerization time courses. Dashed red lines indicate the nucleus in each of the three pathways tested. For additional details see Supplementary Figure 2 and Supplementary Table 2. **C.** Plot of time courses of pyrene actin polymerization (solid lines) as in A, with dashed lines over each trace indicating the best fits from the one monomer collision model in B. **D.** Plot of the objective value obtained from the fits of the pyrene-labeled actin polymerization data in A and C with models containing 0 to 3 monomer collisions. The objective value represents the normalized mean square weighted sum of squares. **E.** Time courses of polymerization of 3 µM 15% pyrene-labeled actin containing 10 nM SpArp2/3 complex and 1 µM or 10 µM Dip1 with or without 1 µM SpWsp1-CA or 1 µM SpWsp1-VCA. **F.** Plot of the maximum polymerization rates of the pyrene-labeled actin polymerization assays as in E. The fits for reactions without Wsp1 or with Wsp1-VCA (Figure 2B) are shown for comparison. Data points were fit as described in the methods. See Supplementary Table 1 for details on parameters of fits.

with and binding of one or more actin monomers to the Dip1-Arp2/3 assembly might be required to complete the activation process and create a nucleus. To test this, we altered the kinetic model to include one or more actin monomer binding steps before creation of the nucleus (Fig. 3B, (models ii-iii), Supplementary Fig. 2). These models produced simulated polymerization time courses that fit the data significantly better than the reaction pathway without actin monomer collisions (Fig. 3C,D). The pathway with one actin monomer binding step fit the data most closely, but the fits with two or three monomer binding steps also improved the fit over the reaction pathway without actin monomer binding (Fig. 3D). These data suggest that actin monomer binding to the Dip1-bound Arp2/3 complex stimulates activation.

Actin monomer recruitment by Wsp1 is required for co-activation of Arp2/3 complex by Wsp1 and Dip1

Our data suggest that slow binding of actin monomers to Dip1-bound Arp2/3 complex limits the nucleation rate. Importantly, unlike Dip1, Wsp1 binds both Arp2/3 complex and actin monomers, so can directly recruit actin monomers to nascent nucleation sites (Beltzner and Pollard, 2008; Marchand et al., 2001). Therefore, we wondered if Wsp1 synergizes with Dip1 by recruiting actin monomers to the Dip1-Arp2/3 complex assembly. To test this, we asked whether the actin monomer-recruiting V region of Wsp1 is required for synergistic coactivation of Arp2/3 complex by Dip1 and Wsp1. We found that while adding Wsp1-VCA to actin polymerization reactions containing saturating Dip1 increased the maximal polymerization rate ~1.6-fold compared to reactions without Wsp1, addition of Wsp1-CA had little or no effect on the

maximum polymerization rate (Fig. 3E,F). Therefore, we conclude that actin monomer recruitment by Wsp1 is required for potent synergy with Dip1. Wsp1-CA decreased slightly the concentration of Dip1 required for half maximal saturation ($K_{1/2}$), suggesting it influences one or more of the activation steps (Supplementary Table 1). However, this influence was small compared to the reduction in the $K_{1/2}$ of Dip1 caused by Wsp1 with a V region (Supplementary Table 1).

Increased monomer affinity for the nascent nucleus cannot explain synergy on its own

Our data show that Wsp1 must recruit actin monomers to Arp2/3 complex to potently synergize with Dip1 in activation. To better understand how actin monomer recruitment contributes to synergy we sought to kinetically model synergistic activation of the complex by the two NPFs. To decrease the number of unknown rate constants inherent in an explicit model of all the reactions in a mixture containing Dip1, Wsp1, Arp2/3 complex, we used a simplified model based on the activation by Dip1 alone (Fig, 4A,B). We asked if this simplified model could fit time courses of actin polymerization for reactions containing both Dip1 and Wsp1 if the rate constants of key steps were increased. We limited the fitting to reactions with Dip1 concentrations greater than 0.5 µM, as higher concentrations of Dip1 limit the contribution of branching nucleation to actin assembly (Balzer et al., 2019). This allowed us to ignore the action of Wsp1 alone on Arp2/3 complex in the simulated reactions. Given that Wsp1 directly tethers actin monomers to the complex, we first asked whether increasing the monomer affinity for the Dip1-Arp2/3 assembly could explain the increased rate of filament nucleation. To test

this, we simulated polymerization using the Dip1 alone activation model and allowed the

off rate (k_{-10}) for the actin monomer bound to the Dip1-Arp2/3 assembly to float. All

other rate constants were fixed at the values determined for reactions without Wsp1.
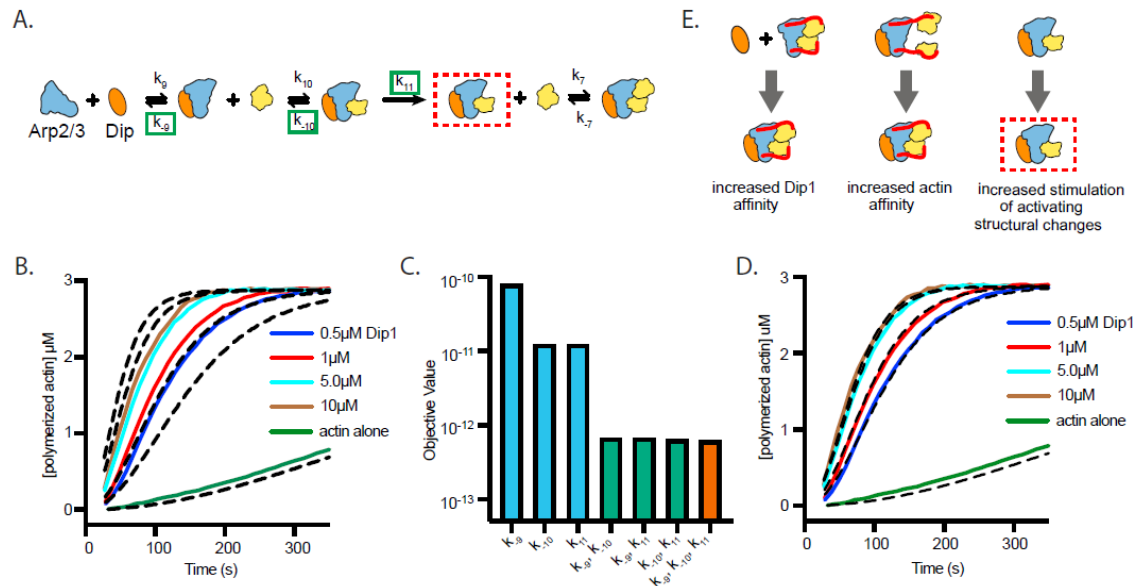
Figure 4. Wsp1-bound monomer recruitment accelerates multiple steps of the Dip1-mediated activation pathway. A. Simplified kinetic model of synergistic activation of Arp2/3 complex by Dip1 and Wsp1 based on the Dip1 alone "single monomer collision" activation pathway from Fig. 3B. Note that Wsp1-VCA is not explicitly included in the model. Rate constants boxed in green were floated to fit time courses of reactions that contained both Dip1 and monomeric Wsp1-VCA. The purpose of this simplified model is to test the potential influence of Wsp1-mediated actin monomer recruitment on the steps of Dip1-mediated activation of Arp2/3 complex highlighted in E. **B.** Plot of time courses of polymerization of 3 µM 15% pyrene-labeled actin in the presence of 50 nM SpArp2/3 complex and a range of Dip1 from 0 to 15 µM (solid colored lines). Dashed lines over each trace indicate the best fits from the model where only the off rate of the actin monomer bound to Dip1-Arp2/3 complex (k_{-10}) was floated. Only a subset of the time courses used for the simulation are shown. **C.** Objective values obtained from models floating the noted parameters. The objective value represents the normalized mean square weighted sum of squares. **D.** Plot of time courses of shown in B. Dashed lines over each trace indicate the best fits from the model where k_{-9}, k_{-10} and k_{11} were floated. Only a subset of the traces fit by the model are shown. **E.** Depiction of the steps in Dip1-mediated activation of Arp2/3 complex that may be influenced by monomer recruitment. Dashed red lines in A and E indicate the nucleation competent state.

These simulations fit the data poorly, indicating the synergy between Wsp1 and Dip1

cannot be explained by increased affinity of actin monomers for the Dip1-Arp2/3

assembly alone (Fig. 4C,D). However, when we floated the dissociation constant for actin monomers (k_{-10}) and either the k_{off} of Dip1 for Arp2/3 complex (k_{-9}) or the rate constant for the activation step (k_{11}) (or all three), the simulations closely matched the measured polymerization time courses (Fig. 4D,E). These observations suggest that multiple steps in the Dip1-mediated activation pathway are accelerated when Wsp1-bound actin monomers are recruited to the complex.

DISCUSSION

Here we propose a model in which Wsp1 synergizes with Dip1 to activate Arp2/3 complex and initiate the assembly of endocytic actin networks. Previous measurements of the dynamics of fluorescently labeled NPFs support this model, because they show that the two NPFs colocalize at endocytic sites and arrive with nearly identical timing, ~2 seconds before actin filaments begin to polymerize (Basu and Chang, 2011; Sirotkin et al., 2010). Given that Dip1 is biochemically specialized to initiate branched actin network assembly, it might be expected to peak in concentration before actin begins to polymerize. However, the accumulation kinetics of Dip1 are nearly identical to Wsp1; both accumulate over ~6 seconds as actin assembles, reach a peak concentration just before (~2s) the actin filament concentration peaks, and then dissociate as the patch begins to internalize and actin disassembles (Basu and Chang, 2011). The gradual accumulation of Dip1 suggests that it might coactivate Arp2/3 complex with Wsp1 well after actin polymerization has been initiated and throughout the assembly/propagation of the actin patch. This activity would have implications for determining the architecture of actin filament networks at the endocytic sites (see below).

Relatively little is known about how the NPFs that control actin assembly at endocytic sites are regulated, despite their importance in driving endocytosis. In *S. cerevisiae*, both inhibitors and activators of the WASP family protein Las17 have been
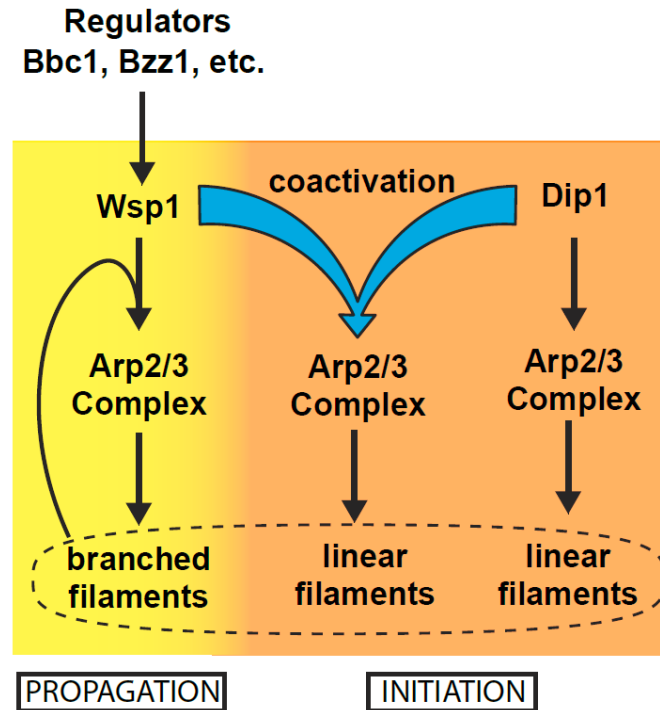
Figure 5. Proposed Model for Coordination of Initiation and Propagation of Endocytic Actin Patch Assembly. Diagram depicting how the regulation of Wsp1 may indirectly activate Dip1 through coactivation of Arp2/3 complex to nucleate linear actin filaments. Joint regulation of Wsp1 and Dip1 provides a mechanism to coordinate the initiation and propagation of endocytic patch actin networks.

identified (Goode et al., 2015), and recent experiments suggest that clustering Las17 at high concentrations at endocytic sites might trigger its activity (Sun et al., 2017). Building evidence suggests homologues of the proteins that regulate Las17 in *S. cerevisiae* may control Wsp1 activity in *S. pombe* (Arasada and Pollard, 2011; MacQuarrie et al., 2019), perhaps at least partially by clustering it at endocytic sites. Almost nothing is known about the regulation of Dip1, but we show here that Wsp1 synergizes with Dip1, so activators that turn on Wsp1 could also indirectly stimulate

Dip1 (Fig. 5). Therefore, an attractive hypothesis is that the activation pathway for Wsp1 stimulates both Wsp1 and Dip1, thereby coordinating the initiation and propagation phases of endocytic actin assembly (Fig. 5). However, some evidence supports the existence of a distinct activation pathway for Dip1. For instance, the N-terminal ~160 amino acids of Dip1 are not required for activity (Wagner et al., 2013), but this segment is relatively well conserved among yeast, so may play a role in localizing or regulating Dip1 independent of Wsp1. Given that initiation is a key step in regulating the assembly of branched actin networks, elucidating how cells control the activity of Dip1 will be an important future goal.

Electron microscopy studies indicate that endocytic actin networks are branched (Young et al., 2004), and the highly dendritic nature of these filamentous networks is thought to allow them to drive invagination of the plasma membrane (Lacy et al., 2018). Wsp1 creates a branched actin filament when it activates Arp2/3 complex on its own, but we show here that when Wsp1 activates the complex with Dip1 it creates a linear actin filament. This observation suggests that cells may need to limit synergistic activation of the complex by Dip1 and Wsp1 to preserve the dendritic nature of endocytic actin networks. We anticipate that synergistic activation by Wsp1 and Dip1 is limited using the same mechanisms that prevent Dip1 alone from activating too many Arp2/3 complexes at endocytic sites. For instance, we showed previously that when Dip1 activates on its own, it remains bound to Arp2/3 complex long after nucleation, unlike Wsp1, so each Dip1 molecule likely only activates one Arp2/3 complex (Balzer et al., 2019). We found here that even when it activates with Wsp1, Dip1 stays bound to Arp2/3 complex on the ends of filaments long after nucleation, so Dip1 is also likely single turnover in the context of

90

synergistic activation (Fig. 2). Combined with the low concentration of Dip1 at endocytic actin patches, this single turnover mechanism may help limit the number of linear filaments created at endocytic sites (Balzer et al., 2019; Basu and Chang, 2011). Competition with actin filaments may provide a second mechanism for limiting linear filaments generated through synergy between Wsp1 and Dip1. We showed previously that actin filaments compete with WDS proteins for binding to Arp2/3 complex (Luan et al., 2018a). Therefore, even if both NPFs are present, activation by Wsp1 alone may dominate once actin filaments begin to accumulate at endocytic sites.

Our simulations of actin polymerization kinetics indicate that when Dip1 activates Arp2/3 complex on its own, actin monomers collide with and bind to the Dip1-Arp2/3 complex assembly to help create the nucleation-competent state. While the function of bound actin monomers is uncertain, multiple lines of evidence suggest that actin monomer binding may stimulate activating conformational changes in the Dip1-Arp2/3 complex assembly. For instance, we previously showed that both Dip1 alone and actin monomers recruited by WASP proteins stimulate movement of Arp2 and Arp3, the two actin-related proteins in the complex, into a filament-like arrangement called the short pitch conformation (Hetrick et al., 2013; Rodnick-Smith et al., 2016; Wagner et al., 2013). Therefore, one possibility is that actin monomers stimulate Dip1-mediated activation by helping the Dip1-bound complex adopt the short pitch conformation. Furthermore, a recent cryoEM structure of Dip1 bound to activated Arp2/3 complex and its nucleated actin filament shows that in addition to moving into the short pitch conformation, Arp2 and Arp3 undergo an intrasubunit conformational change called flattening (in review). This structural change, which brings the Arps closer to the

conformation that actin subunits adopt in filaments, may also be stimulated by binding of actin monomers to the Dip1-Arp2/3 complex assembly.

We show here that direct tethering of actin monomers by monomeric Wsp1 potently accelerates activation of Arp2/3 complex by Dip1, allowing the two NPFs to synergize. Direct tethering of actin monomers to the Dip1-Arp2/3 complex assembly increases their effective concentration, which could potentially explain synergy between Dip1 and Wsp1. However, a kinetic model that accounted for the increased effective concentration (by decreasing the off rate of actin monomers for the Dip1-Arp2/3 assembly) could not fully explain the acceleration of actin polymerization in reactions containing both NPFs (Fig. 4). To accurately simulate synergistic activation, our models also had to allow Wsp1-recruited actin to either increase the affinity of Dip1 for Arp2/3 complex or to accelerate the final activation step (Fig. 4). While it is unclear whether one or both of these additional steps are influenced during synergistic activation, we previously showed that Dip1 does not influence the binding affinity of monomeric Wsp1 in a fluorescence anisotropy binding assay (Wagner et al., 2013), arguing against cooperative binding to Arp2/3 complex by the two NPFs. Therefore, we speculate that Wsp1-recuited actin monomers may stimulate the activating step (modeled as k_{11} in our simulations) more rapidly than randomly colliding and binding actin monomers. Understanding the molecular basis for the acceleration of this step will be important for understanding how Dip1 and Wsp1 activate Arp2/3 complex synergistically and on their own.

A surprising result of this work is that Wsp1 dimerized by GST showed significantly less synergy with Dip1 than monomeric Wsp1. While dimerized Wsp1

moderately decreased the amount of Dip1 required to reach half maximal saturation ($K_{1/2}$, see Supplementary Table 1), at saturating Dip1, the maximum polymerization rate was less with GST-Wsp1 than without it. Given that dimeric WASP proteins can recruit two actin monomers and typically bind ~100-150 fold more tightly to the complex than monomeric WASP proteins (Padrick et al., 2011, 2008), we initially expected that dimeric Wsp1 would have greater synergy with Dip1. However, previous biochemical and structural data indicate WASP proteins - when activating on their own - must be released from nascent branch junctions before nucleation (Helgeson and Nolen, 2013; Smith et al., 2013b). Because they likely bind the branch junction more tightly (Helgeson and Nolen, 2013), dimeric WASP proteins are thought to release more slowly, thereby decreasing how fast nucleation occurs once WASP is bound compared to monomeric WASP constructs. Therefore, tight binding by dimeric Wsp1 to the nascent linear filament nucleus could slow its release, thereby decreasing the nucleation rate and diminishing synergy between Dip1 and Wsp1. The significant differences we observed between dimeric and monomeric Wsp1 in synergizing with Dip1 highlight the need to better understand how Wsp1 activates Arp2/3 complex in cells. Recent experiments in budding yeast showed that Las17 is recruited to endocytic sites through a set of multivalent interactions similar to the types of interactions that incorporate WASP proteins into phase separated droplets *in vitro* (Banjade and Rosen, 2014; Li et al., 2012; Sun et al., 2017). Whether or not Wsp1 accumulates in similar phase separated droplets, it will be important to understand if Wsp1 engages Arp2/3 complex as a monomer or oligomer, as this will significantly influence the kinetics of its activation of the complex alone or with Dip1.

93

METHODS

Protein Expression, Purification and Fluorescent Labeling

To purify *S. pombe* Dip1, an N-terminally glutathione S-transferase (GST) tagged Dip1 plasmid was generated by cloning the full length Dip1 sequence into the pGV67 vector as described previously (Balzer et al. 2018). The restriction sites chosen for cloning resulted in the presence of a short N-terminal polypeptide sequence (GSMEFELRRQACGR) on the end of the coding sequence for Dip1 after cleavage with tobacco etch virus (TEV). To purify Dip1, BL21(DE3) RIL E. coli cells transformed with this pGV67-Dip1 plasmid were grown to an O. D. 595 of 0.6-0.7, induced with 0.4 mM isopropyl 1-thio-β-D-galactopyranoside (IPTG), and allowed to express overnight at 22°C. Cells were lysed by sonication in lysis buffer (20 mM Tris pH 8.0, 140 mM NaCl, 2 mM EDTA, 1 mM dithiothreitol (DTT), 0.5 mM phenylmethylsulfonyl fluoride (PMSF), and protease inhibitor tablets (Roche)) and then clarified by centrifugation (JA-20 rotor (Beckman), 18,000 rpm, 25 minutes, 4°C). The supernatant was pooled and loaded onto a 10 mL glutathione sepharose 4B (GS4B) column equilibrated in GST-binding buffer (20 mM Tris pH 8.0, 140 mM NaCl, 2 mM EDTA, 1 mM DTT). After binding of protein, the column was washed with GST-binding buffer until no protein was detected in the flow through (~10 CV) and then protein was eluted with elution buffer (20 mM Tris pH 8.0, 140 mM NaCl and 50 mM glutathione). Fractions containing GST-Dip1 were pooled and dialyzed overnight against 20 mM Tris pH 8.0, 50 mM NaCl and 1 mM DTT at 4°C in the presence of a 25:1 ratio (by mass) of TEV protease to recombinant protein. The dialysate was loaded onto a 6 mL Resource Q column equilibrated in QA buffer (20 mM Tris pH 8.0, 50 mM NaCl, 1 mM DTT) and eluted over a 20 column

volume gradient to 100 % QB buffer (20 mM Tris pH 8.0, 500 mM NaCl, 1 mM DTT). The protein was concentrated in a 10k MWCO Amicon-Ultra centrifugal filter (Millipore Sigma) and loaded onto a Superdex 200 HiLoad 16/60 gel filtration column equilibrated in 20 mM Tris pH 8.0, 100 mM NaCl and 1 mM DTT. Fractions containing pure Dip1 were pooled and flash frozen in liquid nitrogen. The final concentration of S. pombe Dip1 was determined by measuring the absorbance at 280 nm and dividing this by the Dip1 extinction coefficient of 36,330 $M^{-1}cm^{-1}$.

The Dip1 construct used for site specific labeling with the cysteine-reactive Alexa Fluor 568 C5 maleimide (Thermo Fisher) had the six endogenous cysteine residues in Dip1 mutated to alanine by amplifying the pGV67-Dip1 plasmid with non-overlapping 5' phosphorylated primers encoding the mutations. The single cysteine in the short N-terminal polypeptide sequence of the end of the coding sequence for Dip1 was used for tagging with the Alexa Fluor 568 C5 maleimide. Expression and purification of this Dip1 mutant was identical to the wild type purification until the protein was loaded onto the Superdex 200 HiLoad 16/60 gel filtration column. In order to promote efficient labeling, the size exclusion column was equilibrated in 20 mM HEPES pH 7.0 and 50 mM NaCl before loading and eluting the concentrated protein. Peak fractions containing Dip1 were pooled and concentrated to 40 µM for labeling. A 10 mM solution of Alexa Fluor 568 C5 maleimide dye in water was added dropwise to the protein while stirring at 4 °C until the solution reached a 10 to 40 molar ratio of dye to protein. The reaction was quenched after 12-16 hours by dialyzing against 20 mM Tris pH 8.0, 50 mM NaCl, and 1 mM DTT for 24 hours with buffer exchanges after 4 and 8 hours. Labeled Dip1 was loaded onto a Hi-Trap desalting column and the peak fractions were pooled and flash frozen using liquid

nitrogen. The final concentration of Alexa Fluor 568 dye was determined by measuring the absorbance at 575 nm and dividing this by 92,009 $M^{-1}cm^{-1}$, the extinction coefficient if the dye. The final concentration of 568-Dip1 was determined by the following equation: $\frac{A_{280}-(A_{575}\times 0.403)}{36,330 M^{-1}cm^{-1}}$

To purify *S. pombe* Wsp1-VCA, residues 497-574 were cloned into the pGV67 vector containing an N-terminal GST tag followed by a TEV cleavage site. A 5 mL culture of BL21(DE3)-RIL E. coli cells transformed with the pGV67-Wsp1-VCA vector in LB plus 100 μg/mL ampicillin and 35 μg/mL chloramphenicol was grown overnight at 37 °C. One milliliter of this culture was used to inoculate 50 mL of LB plus ampicillin and chloramphenicol which was allowed to grow at 37°C with shaking at until turbid. Ten milliliters of this turbid culture were added to a 2.8 L flask containing 1 L of LB plus ampicillin and chloramphenicol and grown to an O. D. 600 of 0.4-0.6 before inducing by adding IPTG to 0.4 mM. Cells were allowed to express for 12 to 14 hours at 22 °C before adding EDTA and PMSF to 2 mM and 0.5 mM, respectively. Cells were then harvested and lysed by sonication in lysis buffer (20 mM Tris pH 8.0, 140 mM NaCl, 2 mM EDTA, 1 mM DTT, 0.5 mM PMSF, and protease inhibitor tablets (Roche)) and then clarified by centrifugation (JA-20 rotor (Beckman), 18,000 rpm, 25 minutes, 4°C). The clarified lysate was then loaded onto a 10 mL GS4B column equilibrated in GST-binding buffer (20 mM Tris pH 8.0, 140 mM NaCl, 2 mM EDTA, 1 mM DTT) and washed with ~10 column volumes of the same buffer. Protein was eluted with ~3 column volumes of elution buffer (20 mM Tris pH 8.0, 100 mM NaCl, 1 mM DTT, 50 mM reduced L-glutathione) and fractions containing GST-SpWsp1-VCA were pooled and dialyzed overnight in 3,500 MWCO tubing against 2 L of 20 mM Tris pH 8.0, 50 mM NaCl and 1

mM DTT at 4°C in the presence of a 25:1 ratio (by mass) of TEV protease to recombinant protein. To purify the GST tagged Wsp1-VCA, the addition of TEV to the dialysis was omitted. The dialysate was loaded onto a 6 mL Source30Q column equilibrated in QA buffer (20 mM Tris pH 8.0, 50 mM NaCl, 1 mM DTT) and eluted over a 20-column volume gradient to 100 % QB buffer (20 mM Tris pH 8.0, 500 mM NaCl, 1 mM DTT). Fractions containing GST-Wsp1-VCA were concentrated to 1.5 mL and flowed over a Superdex 75 gel filtration column equilibrated in 20 mM Tris pH 8.0, 150 mM NaCl, and 1 mM DTT. Fractions containing pure protein were pooled and concentrated in a 3,500 MWCO Amicon-Ultra centrifugal filter (Millipore Sigma) in the Fiberlite F13B rotor at 2,500 rpm over several 5 to 10 minute cycles at 4°C. The concentrated, pure protein was flash frozen in liquid nitrogen. The final concentration of S. pombe Wsp1-VCA was determined by measuring the absorbance at 280 nm and dividing this by the Wsp1 extinction coefficient of 5,500 $M^{-1}cm^{-1}$.

To construct an expression plasmid for S. pombe Wsp1-CA, residues 519-574 were cloned into the pGV67 vector containing an N-terminal GST tag followed by a TEV cleavage site. The purification was carried out as described for S. pombe Wsp1-VCA above.

To purify *S. pombe* Arp2/3 complex, 10 mL of a turbid culture of S. pombe (strain TP150) cells was added to a 2.8 L flask containing 1 L of YE5S. Cultures were grown for ~12 hours at 30 °C with shaking and then EDTA was added to a final concentrations of 2 mM. All subsequent steps were carried out at 4 °C. The cultures were centrifuged to harvest cells and the pellet was resuspended in 2 mL of lysis buffer (20mM Tris pH 8.0, 50 mM NaCl, 1 mM EDTA, 1mM DTT) per gram of wet cell pellet, plus 6 protease

97

inhibitor tablets (Roche) per liter of lysis buffer. The cells were then lysed in a

microfluidizer (Microfluidics Model M-110EH-30 Microfluidizer Processor) at 23 kPSI

over 5 to 6 passes. After lysis, PMSF was added to 0.5 mM and the lysate was spun down

in a JA-10 (Beckman) rotor at 9,000 rpm for 25 minutes. The supernatant was transferred

to prechilled 70 mL polycarbonate centrifuge tubes (Beckman Coulter # 355655) and

spun at 34,000 rpm for 75 minutes in a Fiberlite F37L rotor (Thermo-Scientific). The

pellet was discarded, and the supernatant was filtered through cheesecloth into a

prechilled graduated cylinder to determine the volume. Under heavy stirring, 0.243 g of

ammonium sulfate per mL of supernatant was added over approximately 30 minutes. The

solution stirred for an additional 30 minutes, then was pelleted in a Fiberlite F37L rotor at

34,000 rpm for 90 minutes. The pellet was resuspended in 50 mL of PKME (25 mM

PIPES, 50 mM KCl, 1 mM EGTA, 3 mM MgCl2, 1 mM DTT and 0.1 mM ATP) and

dialyzed overnight in 50,000 MWCO dialysis tubing against 8 L PKME. The dialysate

was clarified by centrifugation in the Fiberlite F37L rotor at 34,000 rpm for 90 minutes.

A 10 ml column of GS4B beads was equilibrated in GST binding buffer (20 mM Tris pH

8.0, 140 mM NaCl, 1 mM EDTA, and 1 mM DTT) before it was charged with 15 mg of

GST-N-WASP-VCA to make a GST-VCA affinity column. The charged column was

washed with additional binding buffer until no protein was detectable in the flow through

by Bradford assay. The column was then equilibrated in PKME pH 7.0, the supernatant

was loaded at 1 mL per min and the column was washed with additional PKME (~45

mL). A second wash with PKME + 150 mM KCl was done until no protein was detected

in the flow through by Bradford assay (~30 mL). Protein was eluted with PKME + 1 M

NaCl into ~2 mL fractions until no protein was detected by a Bradford assay (~30mL).

Fractions containing Arp2/3 complex were pooled and dialyzed overnight in 50,000

MWCO dialysis tubing against 2 L of QA buffer (10 mM PIPES, 25 mM NaCl, 0.25 mM

EGTA, 0.25 mM MgCl2, pH 6.8 with KOH). Arp2/3 complex was further purified by ion

exchange chromatography on an FPLC using a 1mL MonoQ column with a linear

gradient of QA buffer to 100% QB buffer (10 mM PIPES, 500 mM NaCl, 0.25 mM

EGTA, 0.25 mM MgCl2, pH 6.8 with KOH) over 40 column volumes with a flow rate of

0.5 mL per minute. Fractions containing Arp2/3 complex were pooled and dialyzed

overnight in 50,000 MWCO dialysis tubing against Tris pH 8.0, 50 mM NaCl and 1 mM

DTT. The dialysate was concentrated to 1.5 mL in a 30,000 MWCO concentrator tube

(Sartorius Vivaspin Turbo 15 #VS15T21) using the Fiberlite F13B rotor at 2,500 rpm

over several 5-10 minute cycles. Between each cycle the solution was mixed by gentle

pipetting. The concentrated sample was loaded on a Superdex 200 HiLoad 16/60 gel

filtration column equilibrated in Tris pH 8.0, 50 mM NaCl, and 1 mM DTT. Fractions

containing pure Arp2/3 complex were concentrated as described above and the final

concentration was determined by measuring the absorbance at 290 nm and dividing by

139,030 $M^{-1}cm^{-1}$, the extinction coefficient (ε290) of Arp2/3 complex, before flash

freezing.

Biotin-inactivated myosin was prepared by reacting 2 mg of myosin with 5 μL of

250 mM EZ-Link-Maleimide-PEG11-Biotin dissolved in DMSO. The labeling reaction

was carried out in 500 μL reaction buffer (20 mM HEPES pH 8.0, 500 mM KCl, 5 mM

EDTA, 1 μM ATP and 1 mM MgCl2) on ice for 6 hours. The Biotin-myosin was then

dialyzed against 0.5 L of storage buffer (20 mM Imidazole pH 7.0, 500 mM KCl, 5 mM

EDTA, 1 mM DTT and 50% glycerol) using a 3500 MWCO dialysis thimble

(Thermofisher Slide-A-Lyzer MINI dialysis unit 0069550).

TIRF microscopy slide preparation

TIRF flow chambers were constructed as previously described with slight

modifications (Kuhn and Pollard 2005). All following cleaning steps were carried out at

room temperature. Coverslips (24 x 60 #1.5) were cleaned in Coplin jars by sonicating in

acetone followed by 1 M KOH for 25 min each, with a deionized water rinse between

each sonication step. Coverslips were then rinsed twice with methanol and

aminosilanized by incubating in a 1% APTES (Sigma), 5 % acetic acid in methanol

solution for 10 min before sonicating for 5 min, and then incubating for an additional 15

min. Coverslips were then rinsed with 2 volumes of methanol followed by thorough

flushing with deionized water. After air drying, TIRF chambers were created by pressing

two pieces of double-sided tape onto a cleaned coverslip with a 0.5 cm wide gap between

them. A glass microscope slide was then placed on top of the coverslip and tape

perpendicularly to create a cross-shape forming a chamber in the middle with a volume of

~14 µL. Chambers were passivated by flowing in 300 mg/mL methoxy PEG

succinimidyl succinate, MW5000 (JenKem) containing 1-3% biotin-PEG NHS ester,

MW5000 (JenKem) dissolved in 0.1 M NaHCO3 pH 8.3 and incubating for 4-5 hours.

Excess PEG was washed out with 0.1 M NaHCO3 pH 8.3 before flowing deionized water

into chambers for storage. Chambers were stored at 4 °C for less than 1 week.

Immediately prior to imaging, 1 µM NeutrAvidin (ThermoFisher) was added to chambers

and incubated for 8 minutes followed by 8 minutes with 50-150 nM biotin inactivated

myosin (Cytoskeleton, Inc), both prepared in 50 mM Tris pH 7.5, 600 mM NaCl.

Chambers were washed 2 times with 20 mg/mL BSA in 50 mM Tris pH 7.5, 600 mM

NaCl followed by 2 washes with 20 mg/mL BSA in 50 mM Tris pH 7.5, 150 mM NaCl.

Chambers were finally pre-incubated with TIRF buffer (10 mM Imidazole pH 7.0, 1 mM

MgCl2, 1 mM EGTA, 50 mM KCl, 100 mM DTT, 0.2 mM ATP, 25 mM Glucose, 0.5 %

Methylcellulose (400 cP at 2%), 0.02 mg/mL Catalase (Sigma) and 0.1 mg/mL Glucose

Oxidase (MP Biomedicals)) after which point they were ready to add reaction mixture.

Actin Polymerization Reactions in TIRF chambers

In a typical reaction, 1 µL of 2.5 mM MgCl2 and 10 mM EGTA was mixed with

5 µL of 9 µM 33% Oregon Green labeled actin and incubated for 2 minutes. Four

microliters of the actin solution were then added to 16 µL of a solution containing 1.25x

TIRF buffer and any other proteins. Reactions were imaged on a Nikon TE2000 inverted

microscope equipped with a 100x 1.49 numerical aperture TIRF objective, 50 mW 488

nm and 561 nm Sapphire continuous wave solid state laser lines (Coherent), a dual band

TIRF (zt488/561rpc) filter cube (Chroma C143315), and a 1x-1.5x intermediate

magnification module. Images were collected using an 512x512 pixel EM-CCD camera

(iXon3, Andor). For two color reactions, typical imaging conditions were 50 ms

exposures with the 488 nm laser (set to 5 mW) and 100 ms exposures with the 561 nm

laser (set to 35 mW) for 1 s intervals. The camera EM gain was set to 200. The

concentration of 568-Dip1 was kept in the low nanomolar range in all assays to prevent

high backgrounds of non-specifically adsorbed 568-Dip1 from obscuring Dip-Arp2/3

filament nucleation events.

Pyrene actin polymerization assays

In a typical reaction, 2 μL of 10X ME buffer (5 mM MgCl2, 20 mM EGTA) was added to 20 μL of 15% pyrene labeled actin and incubated for 2 minutes in 96-well flat bottom black polystyrene assay plates (Corning 3686). To initiate the reaction, 78 μL of buffer containing all other proteins was added to the actin wells using a multichannel pipette. This brought the final buffer concentration in the reaction to 10 mM Imidazole pH 7.0, 50 mM KCl, 1 mM EGTA, 1 mM MgCl2, 200 μM ATP and 1 mM DTT. Polymerization of actin was measured by exciting pyrene actin at 365 nm and monitoring the emission at 407 nm using a TECAN Safire 2 plate reader.

Quantification of the number of Dip1-Arp2/3 nucleated actin filaments

The percentage of Dip1-Arp2/3 complex nucleated actin filaments was determined by counting the number of actin filament pointed ends bound by 568-Dip1 in Oregon Green labeled actin polymerization assays imaged using TIRF microscopy. The quantification was performed on a region of interest from the movie frame that corresponded to 2 minutes and 30 seconds from the initiation of the reaction. To confirm that observed 568-Dip1-bound pointed ends represented nucleation events and to ensure that 568-Dip1 molecules that released from the pointed end or photobleached before the quantification frame were not excluded, all filaments were monitored from their appearance. To determine the percentage of Dip1-Arp2/3 nucleated filaments, the number of pointed ends bound by 568-Dip1 was divided by the total number of pointed ends in the region of interest. At least 4 replicate actin polymerization assays were quantified for each condition.

Modeling of actin polymerization assays

All modeling was carried out using the open source software application COmplex PAthway SImulator (COPASI) (Hoops et al. 2006). Fluorescence values from time courses of polymerization of 3 µM 15% pyrene-labeled actin in the presence of indicated proteins were converted to .txt files using a custom MatLab script and loaded into COPASI software. The actin filament concentrations were determined by assuming 0.1 µM actin was unpolymerized at equilibrium. Optimization of reaction parameters was carried out by simultaneously fitting all traces from a reaction set, using the Genetic algorithm method in the parameter estimation module.

Models were built by identifying interactions between the components in polymerization assays to build up a set of reactions to describe the polymerization. For many parameters included in our set of reactions, we were able to use previously measured rate constants (See Supplementary Table 2). Rate constants that had not been previously measured were allowed to float. We assumed pointed end elongation was negligible. To limit the number of floated parameters in a given simulation, we first conducted polymerization assays with actin alone at a range of concentrations (2-6 µM), and then determined a reaction pathway and rate constants that could accurately describe spontaneous nucleation and polymerization of actin alone (see Supplementary Figure 2). The on rates for actin dimerization, trimerization and tetramerization were fixed at $1.16 \times 10^7 \, M^{-1}s^{-1}$, the observed on rate for actin monomers binding to filament barbed ends. To simplify the models, steps that created a nucleus were considered irreversible and nuclei were modeled as catalysts that convert monomeric actin to filamentous actin, as previously described (Helgeson and Nolen 2013; Beltzner and Pollard 2008). We note

that the best fits for spontaneous nucleation and elongation of actin filaments were obtained using a model in which either a dimer, trimer, or tetramer could serve as the nucleus. This pathway is distinct from models we previously used to simulate spontaneous nucleation and elongation in actin alone reactions (Helgeson and Nolen 2013). To model reactions containing Dip1 and Arp2/3 complex (Fig. 3), we fixed the rate constants for the spontaneous nucleation of actin at the values determined in reactions containing actin alone, except for k_{-1}, which was re-evaluated based on an "actin alone" polymerization time course measured at the same time (in the same set) as the Dip1 and Arp2/3-containing reactions. We used the objective value, or the normalized mean square weighted sum of squares, as a measure of how well the model fit the experimental data.

BRIDGE TO CHAPTER V

In Chapter IV, we discovered that Wsp1 plays a role in endocytic actin patch initiation. In vitro work showed that Wsp1's role in initiation of actin networks is through coordinated activation of Arp2/3 complex linear actin filament nucleation with Dip1. Specifically, the V-region of Wsp1 is responsible for delivering actin monomers to Dip1-bound Arp2/3 complex to increase the rate of linear filament nucleation. In Chapter V, we will discuss the implications of these findings to actin cytoskeleton dynamics and regulation both in vitro and in vivo. We will also consider future directions to continue to elucidate the mechanism by which WASp and WDS proteins promote Arp2/3 complex activity, as well as unravel how the activities of WDS proteins are regulated in vivo.

CHAPTER V

DISCUSSION

The role of WDS proteins and preformed actin filaments in Arp2/3 complex nucleation

Despite nearly 25 years since the discovery of Arp2/3 complex, we are still realizing new features of its activity and regulation. The role of Arp2/3 complex has expanded from exclusively nucleating branched actin filaments to creating linear actin filaments as well. This finding raises many interesting questions about how these two nucleation activities are balanced to ensure that branched actin networks have the appropriate architectures. Our work has begun to address how cells solve this issue and points to some important next steps toward answering these questions.

A critical finding of this work is that WDS-mediated Arp2/3 complex linear filament nucleation does not require a preformed actin filament. While this provides a mechanism by which cells can generate the initial linear filaments required for the formation of actin networks, it also raises questions about the role of preformed filaments in Arp2/3 complex nucleation. The requirement of a preformed filament for branching nucleation indicates that it must perform some function on Arp2/3 complex that is necessary for nucleation of a new branch. The ability of WDS proteins to bypass the preformed filament requirement suggests that they must be able to perform the same function for Arp2/3 complex as actin filaments. This conclusion leads to several key questions. What is the identity of this unknown function that both WDS proteins and preformed actin filaments can provide? What are the mechanisms by which this function

is achieved by WDS proteins and preformed filaments? Is the mechanism the same in both cases or have WDS proteins evolved a new pathway to achieve the same outcome? While much work remains to answer these questions, recent studies allow us to speculate.

Structural studies have revealed an overlapping binding site on Arp2/3 complex for both WDS proteins and preformed actin filaments (Rouiller et al. 2008; Luan, Liu, et al. 2018). This suggests that interaction with similar residues on Arp2/3 complex by WDS proteins and preformed filaments may provide an identical activating feature. As to what this feature could be, a conformational change seems most likely. It was originally hypothesized that preformed actin filaments worked together with WASp to stimulate the rearrangement of the Arp2 and Arp3 subunit to the short pitch conformation. Recently, however, it was demonstrated that WASp alone is sufficient to stimulate the short pitch conformation (Rodnick-Smith et al. 2016). This suggests that preformed actin filaments might stimulate a different conformational change in Arp2/3 complex.

One potential indication for what this secondary conformational change may be comes from structural work on actin filaments. Actin monomers incorporated into an actin filament undergo a conformational change in which the two major subdomains rotate about 20 degrees leading to the overall flattening of the protein (Oda et al. 2009). It is possible that this conformational change in actin monomers is also important in the Arp2 and Arp3 subunits of Arp2/3 complex given the high degree of structural similarities between these subunits and actin monomers. Perhaps the required role of preformed actin filaments in Arp2/3 complex branching nucleation is to stimulate flattening of the Arp2 subunit, the Arp3 subunit or both. An intriguing possibility is that WDS proteins stimulate the same conformational change allowing them to bypass the

requirement for a preformed actin filament. Recent structural work showing SPIN90 bound to Arp2/3 complex indicates that the Arp3 subunit does indeed undergo a slight rotation toward the flattened conformation supporting this idea (Luan, Liu, et al. 2018).

Currently, we lack a method to directly measure the ability of WDS proteins and actin filaments to stimulate flattening of the Arp2 and Arp3 subunits. It is appealing to try to design a cysteine cross-linking assay similar to previous experiments used to measure stimulation of the conformational change from the splayed to the short pitch conformation (Rodnick-Smith et al. 2016). Unfortunately, the relatively small intra-subunit movements that occur through flattening make this challenging. Engineering cysteine residues that are close enough to cross-link only after the conformational change has occurred and not before is difficult. If this work fails to provide an adequate method for detection of Arp2/3 complex flattening, alternatives exist. Advances in structural biology techniques including cryo-electron microscopy (cryo-EM) and cross-linking mass spectrometry (XL-MS) also present intriguing possibilities to study the stimulation of Arp2 and Arp3 flattening.

Stimulating Release of WASp from Arp2/3 complex before polymerization

Our discovery that Dip1 and Wsp1 coordinate to activate Arp2/3 complex to nucleate linear actin filaments explained our observation that Wsp1 contributes to initiation of endocytic actin patches in vivo. We showed the recruitment of actin monomers by the V-region of Wsp1 is a major part of the co-activation of Arp2/3 complex with Dip1. However, the complete mechanism of this synergistic activity is not clear. Structural information shows that the Arp2/3 complex binding sites of WDS

107

proteins and WASp proteins do not overlap (Luan, Liu, et al. 2018; Luan, Zelter, et al. 2018). This suggests that simultaneous binding to Arp2/3 complex by Dip1 and Wsp1 may occur.

In preliminary work, it has proven challenging to detect evidence of a ternary complex of these NPFs and Arp2/3 complex. These results suggest that the ternary complex does not exist or is short-lived. The absence or transient nature of the ternary complex could provide important details about the mechanism of co-activation. In Arp2/3 complex branching nucleation, a critical step is the release of WASp which blocks polymerization of the new branch (Smith et al. 2013). It is likely that WASp release is also required for the nucleation of linear actin filaments given the similarities between these filaments and branches. One possibility is that WDS binding to Arp2/3 complex stimulates the release of WASp and thus, Arp2/3 complex is rarely bound by both NPFs. This would explain the inability to detect a significant population of the ternary complex. Further, the mechanism by which WDS proteins lead to the release of WASp proteins may be through stimulation of the flattening conformation of the Arp2 and Arp3 subunits. Additional efforts to capture the ternary complex are important to add support to this potential mechanism.

Balancing linear filament nucleation and branching nucleation by Arp2/3 complex

In Chapter III, we identified that actin network architecture is highly influenced by the relative activity of Arp2/3 complex linear filament nucleation compared to branching nucleation. We concluded that as linear filament nucleation progresses, high local concentration of actin filaments at endocytic sites might be the driving factor in

shifting activity towards actin branch nucleation. We also mentioned that, given the single-turnover nature of Dip1 activation of Arp2/3 complex, it is likely that the relatively small number of Dip1 molecules at endocytic sites places an upper limit on the number of linear actin filaments. While this may be true, recent work suggests that actin networks are treadmilling more rapidly than previously thought and turnover of proteins in endocytic actin networks may be on the order of 1 to 2 seconds (Lacy, Baddeley, and Berro 2019). This rapid turnover of actin filaments could recycle WDS proteins allowing for the nucleation of additional linear actin filaments. A critical next step of this work is to test this hypothesis and determine if these mechanisms contribute to balancing Arp2/3 complex activities in vivo.

Given the highly reproducible timing of endocytosis, it is reasonable to expect that the balance of Arp2/3 complex nucleation activity is controlled by more than local concentration of proteins. Perhaps in vivo, additional factors influence the binding of nucleation promoting factors like Dip1 to Arp2/3 complex. This would ensure tighter control of Arp2/3 linear filament nucleation and account for potential fluctuations in local concentration that could inhibit Wsp1-mediated branching activity. In support of this idea is preliminary work suggesting that the N-terminus of Dip1 is required in vivo, despite being dispensable for Arp2/3 complex activation in vitro (Wagner et al. 2013; Luan, Liu, et al. 2018). This indicates a role for the N-terminal region of Dip1 that is distinct from its ability to stimulate linear filament nucleation by Arp2/3 complex. It is possible that the N-terminus of WDS proteins plays a role in localization to sites of actin network assembly or potentially in regulating the activity of these proteins through interactions with other factors.

To begin to address these possibilities, it will be important to continue to visualize and quantify the behavior of WDS proteins in vivo. Construction of fluorescently labeled Dip1 mutants that lack the N-terminal residues or that ablate the interaction with Arp2/3 complex will be critical in understanding the contributions of each segment of the protein. Additionally, altering the expression levels of Dip1 in cells and specifically at sites of actin network assembly will be important. These experiments will allow us to investigate the importance of Dip1 concentration in balancing Arp2/3 complex nucleation activity. Identification of other factors that regulate Dip1 activity will be more challenging. This work highlighted an overlap in Arp2/3 complex activation by Dip1 and Wsp1. Perhaps the regulation of the Wsp1 pathway of Arp2/3 complex activation and the Dip1 activation pathway also share common features. Our current understanding of Wsp1 regulation may provide a starting point from which to begin our dissection of Dip1 regulation. The combination of these studies will open the door to new potential mechanisms of WDS protein regulation as well as elucidate how the activity of these proteins fit into the complex endocytic process.

This dissertation demonstrates the ability of dip1 to activate Arp2/3 complex to nucleate linear filaments that act as seeds for branching nucleation, identifying a potential mechanism to explain WDS protein role in endocytic actin network initiation. Additionally, it establishes that coordinated activation of Arp2/3 complex by Dip1 and Wsp1 is required for proper initiation of these branched actin networks, highlighting that the role of endocytic patch proteins is not always singular. Understanding the regulatory mechanisms that control the activities of endocytic patch proteins, both spatially and temporally, is an important future direction of this work.

APPENDIX A

SUPPLEMENTARY MATERIAL FOR CHAPTER II

Video S1: TIRF microscopy video showing an actin filament (green) growing from a Dip1 molecule (magenta) non-specifically adsorbed the coverslip surface (class I event), Related to Figure 2. Reaction contains: 500 nM Arp2/3 complex, 6 nM Alexa568-Dip1 and 1.5 µM 33% Oregon Green labeled actin. Scale bar: 2 µM. (15 fps)

Video S2: TIRF microscopy video showing an actin filament pre-bound to Dip1 landing on the coverslip surface (class II event), Related to Figure 2. Dip1 is shown in magenta and actin is shown in green. Reaction contains 500 nM Arp2/3 complex, 6 nM Alexa568-Dip1 and 1.5 µM 33% Oregon Green labeled actin. Scale bar: 2 µM. (15 fps)

Video S3: TIRF microscopy video showing Dip1 (magenta) binding to the pointed end of a surface-captured actin filament (class III event), Related to Figure 2. Reaction contains 500 nM Arp2/3 complex, 6 nM Alexa568-Dip1 and 1.5 µM 33% Oregon Green labeled actin. Scale bar: 2 µM. (15 fps)

Video S4: TIRF microscopy video showing an actin filament (green) nucleated by Dip1-bound Arp2/3 (magenta) serving as the mother filament for branching nucleation, Related to Figure 3. Reaction contains 250 nM Arp2/3 complex, 150 nM GST-Wsp1-VCA, 6 nM Alexa568-Dip1 and 1.5 µM 33% Oregon Green labeled actin. Scale bar: 2 µM.

Video S5: Same conditions as Video 4, but with a larger field of view, Related to Figure 3.

[Dip1] (µM)	Best-fit Frictional Ratio	rmsd	c(S) (% of total)	sw(20,w)	Calculated MW (Da)	Frictional coefficient
6.9	1.38	0.0049	96.7	3.3	50,300	0.64
13.7	1.22	0.0066	95.0	3.4	43,200	0.54
20.6	1.23	0.0079	94.8	3.4	43,600	0.54
			c(S) (% of total)	sw(20,w)	Calculated MW (Da)	Frictional coefficient
			1.74	5.135	95,700	0.80
			3.00	5.631	91,000	0.69
			4.54	4.742	70,900	0.64

Supplemental Table 1: Sedimentation velocity analytical ultracentrifugation analysis. The top portion of the tables corresponds to the analysis of the Dip1 monomer peak (sedimentation values of 2.7 to 3.9). The bottom portion of the table is the analysis of a putative Dip1 dimer peak (sedimentation values of 4.3 to 6.0). c(S) is the sedimentation coefficient distribution. sw(20,w) is the signal-weighted average sedimentation coefficient corrected to standard conditions of water at 20°C.

REAGENT or RESOURCE	SOURCE	IDENTIFIER
Bacterial and Virus Strains		
BL21-CodonPlus(DE3)-RIL	Agilent	Cat. #230245
Biological Samples		
Acetone powder of rabbit skeletal muscle	Pel-Freeze Biologicals	Cat. #41995-2
S. pombe Arp2/3 complex	This Study	N/A
Chemicals, Peptides, and Recombinant Proteins		
Alexa Fluor 568 C5 maleimide	ThermoFisher Scientific	Cat. # A20341
Oregon Green 488 maleimide	ThermoFisher Scientific	Cat. # O6034
N-(1-pyrene)iodoacetamide	ThermoFisher Scientific	Cat. #P29
EZ-Link-NHS-PEG12-biotin	ThermoFisher Scientific	Cat. # 21312
PEG succinimidyl succinate, MW5000	JenKem	Cat. # A3011-1
biotin-PEG NHS ester, MW5000	JenKem	A5027-1
NeutrAvidin	ThermoFisher Scientific	Cat.# 31000
cOmplete, EDTA-free Protease Inhibitor Cocktail tablets	Sigma	Cat.# 11873580001
S. pombe Dip1	This study	N/A
S. pombe Dip1(6CysAla)	This study	N/A
Catalase	Sigma	Cat.# C3515
Glucose Oxidase	MP Biomedicals	Cat.#195196
Myosin II, rabbit skeletal muscle	Cytoskeleton	Cat # MYO2
Albumin, from bovine serum	Sigma	Cat # A2153
Experimental Models: Organisms/Strains		
S. pombe TP150	[12]	N/A
Recombinant DNA		
pGV67_SpDip1	[4]	Plasmid #174
pGV67_SpDip1(6CysAla)	This study	Plasmid #180
pRK1043	[35]	N/A
pGEX-N-WASp-WA	[36]	Plasmid #222
Software and Algorithms		
Fiji/ImageJ	[37]	https://fiji.sc/
Matlab	Mathworks	N/A
Image J filament tracking plugin	Gift from Jeff Kuhn	
SEDFIT	[34]	http://www.analyticalultracentrifugation.com/default.htm

Key Resources Table: Details the reagents, organisms and resources used throughout the work outlined in Chapter II.

APPENDIX B

SUPPLEMENTARY MATERIAL FOR CHAPTER III

Video S1. TIRF microscopy video taken under low exposure conditions showing signal for Alexa568-Dip1 (magenta) bound to the end of an elongating Oregon Green-labeled actin filament (green) for 8 minutes. Related to Figure 2. Conditions: 1.5 µM 33% Oregon Green-labeled actin in the presence of 6 nM Alexa568-Dip1, 250 nM GST-Wsp1-VCA and 500 nM SpArp2/3 complex collected with 50 ms exposure times at 5 second intervals.

Video S2. Spinning disk microscopy video showing *end4Δ S. pombe* cells expressing Dip1-mNeonGreen (green) and Fim1-mCherry (magenta). Related to Figure 3. White arrows show examples of Dip1 treadmilling with the Fim1-marked actin network. Scale bar: 2 µm.

Video S3. Spinning disk microscopy video showing wildtype *S. pombe* cells expressing Dip1-mNeonGreen (green) and mCherry-Wsp1 (magenta). Related to Figure 3. White arrows show an example of an endocytic site at which Dip1 is further into the cytoplasm than Wsp1. Scale bar: 1 µm.

Video S4. Spinning disk microscopy video showing *end4Δ S. pombe* cells expressing GFP-Wsp1 (green) and Fim1-mCherry (magenta). Related to Figure 3. White arrows show an example of Wsp1 signal remaining predominately at the cortex with only a small portion treadmilling with the Fim1-marked actin network. Scale bar: 2 µm.

Figure S1: Visualization of TIRF images for reactions with or without Dip1 at equivalent timepoints. Related to Figure 1. Actin polymerization assays contained 150 nM GST-Wsp1-VCA, 1.5 µM 33% Oregon Green-labeled actin and 50 nM SpArp2/3 complex in the presence or absence of 75 nM Dip1. The reaction time is indicated above each pair of images. Frames used for quantification from Figure 1A are shown above or below the corresponding time series. Because polymer accumulates rapidly to fill the field of view in the presence of Dip1, we could not compare branching densities for reactions with or without Dip1 at identical timepoints. Scale Bars: 5 µm.
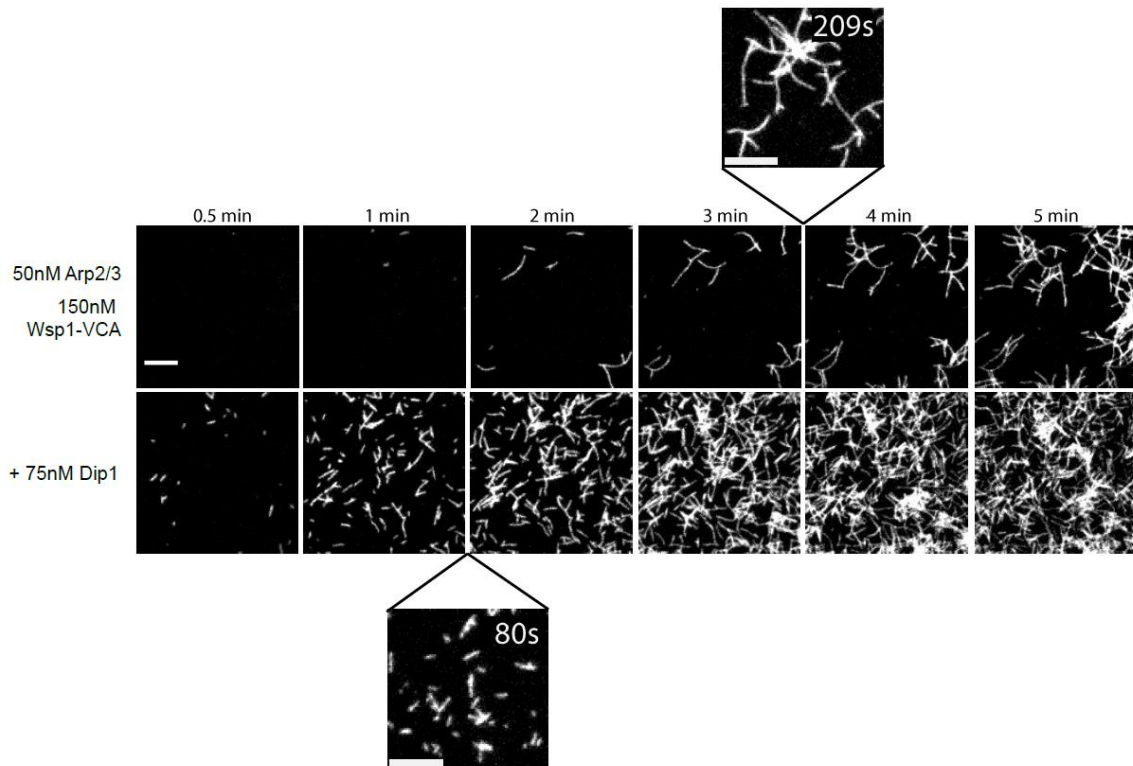
Figure S2: Dip1 decreases branching density and branch to linear filament ratio in reactions containing Wsp1. Related to Figure 1. A. TIRF images showing reactions containing 150 nM GST-Wsp1-VCA, 1.5 µM 33% Oregon Green-labeled actin, 50 nM SpArp2/3 complex and either 3.75 nM or 75 nM Dip1, 80 seconds after initiating the reaction. Scale bar: 5 µm. **B.** Bar plot showing the branch density of actin filaments in TIRF reactions in panel A. **C.** Bar plot comparing the ratio of the total number of branches to the total number of actin seed filaments in the same reactions as in panel B. Error Bars for panel B and C: SE from 4 regions of interest containing at least 45 µm of total actin filaments from a single reaction for each condition. The reported p-values are the result of two-tailed t-tests assuming unequal variances. **D.** Plot showing the branch density over time in reactions containing 150 nM GST-Wsp1-VCA, 1.5 µM 33% Oregon Green-labeled actin and 50 nM SpArp2/3 complex with or without 75 nM Dip1. The four plotted time points for each condition represent the average time at which the reactions hit 250, 500, 750 and 1500 µm of total actin filament. The best fit line for each condition is plotted over the data. **E.** Plot showing the ratio of the total number of branches to linear filaments in the same reactions as in panel D. Error Bars for panel D and E: y-axis; SE from 4 regions of interest from 2 reactions for each condition, x-axis; SE of the average times for the equivalent reactions for each condition to reach the total actin filament lengths reported for panel D.

116
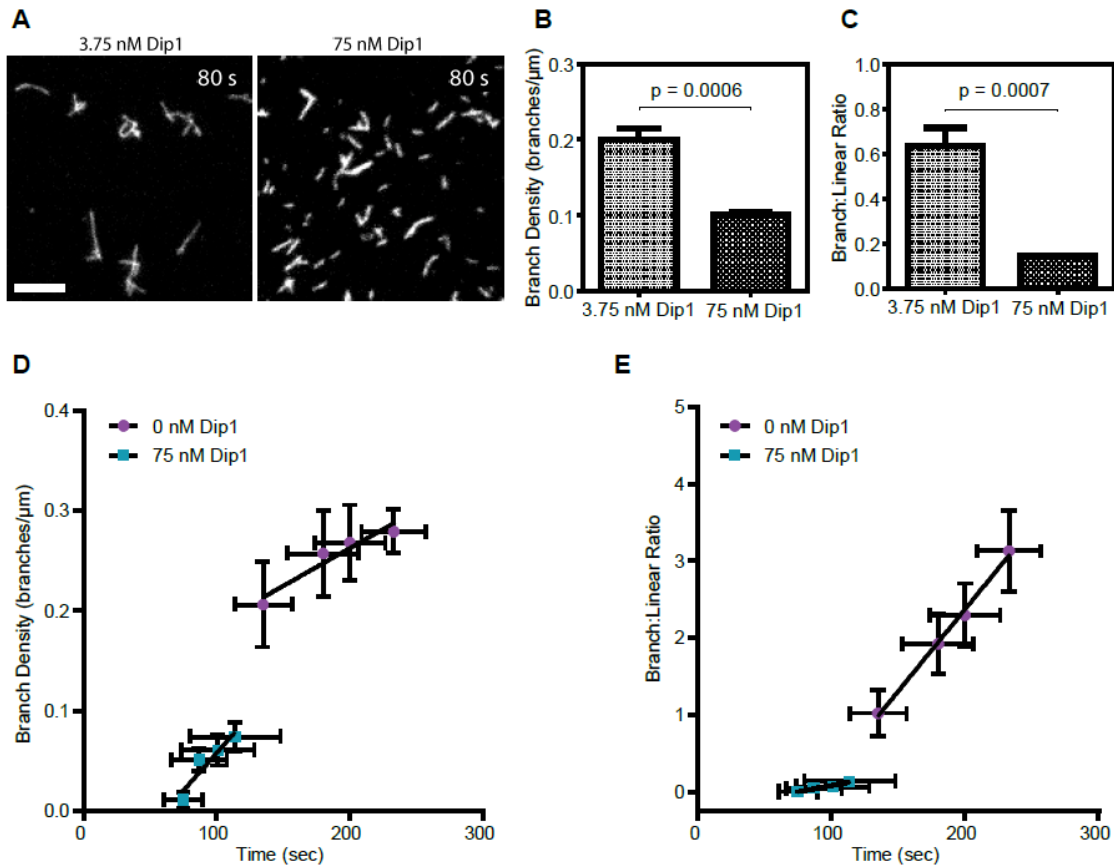
Figure S3: Wsp1 remains predominantly cortical, while Dip1 often moves inward with treadmilling actin comet tails. Related to Figure 3. A. Bar plot showing the percentage of time (# of frames) that the peak signal of Dip1-mNeonGreen and GFP-Wsp1 is cortical. Error Bars: SE from 20 comet tails measured from 6 or 8 cells for Wsp1 and Dip1, respectively. The reported p-value is the result of a two tailed t-test assuming unequal variances. **B.** Histogram of the data from panel A showing the number of comet tails in which Dip1-mNeonGreen or GFP-Wsp1 was cortical for the specified percentage of the lifetime of the comet tail.
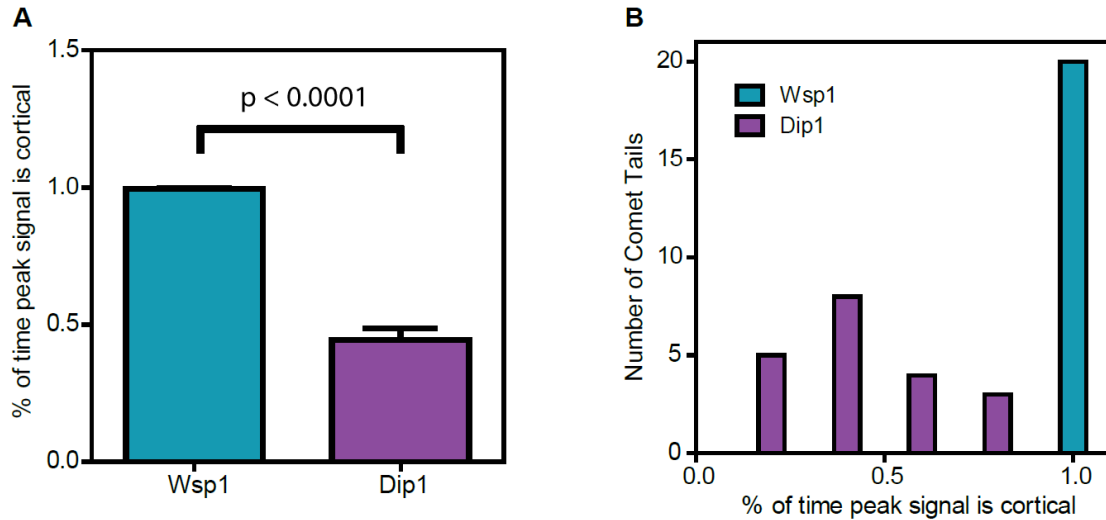
Figure S4: Under conditions required to visualize Dip1-mNeonGreen, autofluorescent structures were observed in some cells. Related to Figure 3. Spinning disk microscope image of S. pombe cells expressing mCherry-Wsp1 and Dip1-mNeonGreen (left) or unlabeled Dip1 (right) after 15 seconds of 300 ms exposures of 25 mW 488 laser at 1 second intervals. White arrows point out examples of large autofluorescent structures present after passing through a 525 nm (50 nm bandwidth) emission filter, even in the absence of an mNeonGreen label. The Dip1 signal is distinguishable from the autofluorescent structures because it is dynamic, small, punctate and partially colocalizes with Wsp1 (VideoS2). Blue arrows show examples of Dip1-mNeonGreen signal at endocytic sites. Scale Bar: 2 μm.

Dip1-mNeonGreen   Autofluorescence
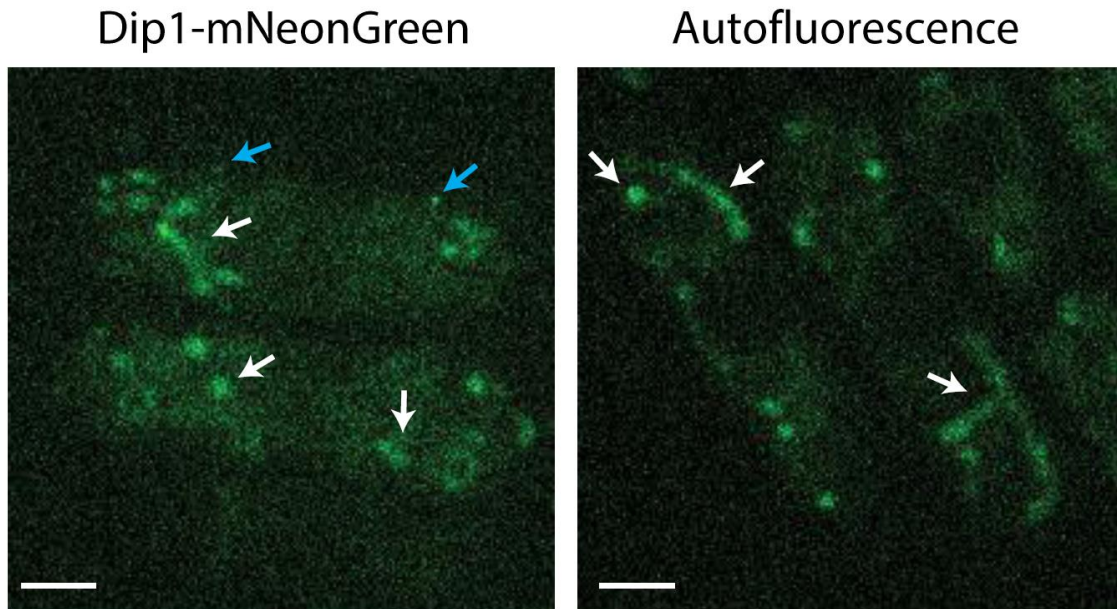
P-value	0.002			
Number of Groups	5			
F	6.52			
R-squared	0.58			
Tukey's Multiple Comparison Test	Mean Difference	q	Significance	95% CI of difference
0 nM vs 3.75 nM Dip1	0.049	1.48	ns	-0.092 to 0.19
0 nM vs 7.5 nM Dip1	0.031	1.03	ns	-0.097 to 0.16
0 nM vs 15 nM Dip1	0.12	3.86	ns	-0.012 to 0.25
0 nM vs 75 nM Dip1	0.20	6.19	**	0.064 to 0.35
3.75 nM vs 7.5 nM Dip1	-0.018	0.59	ns	-0.15 to 0.11
3.75 nM vs 15 nM Dip1	0.068	2.24	ns	-0.061 to 0.20
3.75 nM vs 75 nM Dip1	0.16	4.71	*	0.015 to 0.30
7.5 nM vs 15 nM Dip1	0.086	3.17	ns	-0.029 to 0.20
7.5 nM vs 75 nM Dip1	0.17	5.75	**	0.045 to 0.30
15 nM vs 75 nM Dip1	0.088	2.92	ns	-0.040 to 0.22

Supplemental Table 1: One-way ANOVA and Tukey's Multiple Comparison test results for the data in Figure 1 panel B. For significance, "ns", "*" and "**" corresponds to a p-values of > 0.05, ≤ 0.05 and ≤ 0.01, respectively.

P-value	0.719			
Number of Groups	3			
F	0.34			
R-squared	0.06			
Tukey's Multiple Comparison Test	Mean Difference	q	Significance	95% CI of difference
150 nM vs 300 nM Wsp1	0.015	0.60	ns	-0.081 to 0.11
150 nM vs 600 nM Wsp1	0.029	1.16	ns	-0.067 to 0.12
300 nM vs 600 nM Wsp1	0.014	0.50	ns	-0.091 to 0.12

Supplemental Table 2: One-way ANOVA and Tukey's Multiple Comparison test results for the data in Figure 1 panel D.

P-value	0.851			
Number of Groups	5			
F	0.33			
R-squared	0.07			
Tukey's Multiple Comparison Test	Mean Difference	q	Significance	95% CI of difference
0 nM vs 3.75 nM Dip1	0.00043	0.46	ns	-0.0036 to 0.0044
0 nM vs 7.5 nM Dip1	0.00025	0.29	ns	-0.0034 to 0.0039
0 nM vs 15 nM Dip1	-0.0000077	0.01	ns	-0.0037 to 0.0036
0 nM vs 75 nM Dip1	0.0013	1.35	ns	-0.0027 to 0.0053
3.75 nM vs 7.5 nM Dip1	-0.00018	0.21	ns	-0.0038 to 0.0035
3.75 nM vs 15 nM Dip1	-0.00044	0.51	ns	-0.0041 to 0.0032
3.75 nM vs 75 nM Dip1	0.00084	0.89	ns	-0.0032 to 0.0048
7.5 nM vs 15 nM Dip1	-0.00026	0.34	ns	-0.0035 to 0.0030
7.5 nM vs 75 nM Dip1	0.0010	1.19	ns	-0.0026 to 0.0047
15 nM vs 75 nM Dip1	0.0013	1.49	ns	-0.0024 to 0.0049

Supplemental Table 3: One-way ANOVA and Tukey's Multiple Comparison test results for the data in Figure 1 panel F.

Key Resources Table: Details the reagents, organisms and resources used throughout the work outlined in Chapter III.

| REAGENT or RESOURCE	SOURCE	IDENTIFIER
Bacterial and Virus Strains		
BL21-CodonPlus(DE3)-RIL	Agilent	Cat. #230245
Biological Samples		
Rabbit Muscle Acetone Powder	Pel-Freeze Biologicals	Cat. #41995-2
S. pombe Arp2/3 complex	This study	N/A
Chemicals, Peptides, and Recombinant Proteins		
Alexa Fluor 568 C5 maleimide	ThermoFisher Scientific	Cat. # A20341
Oregon Green 488 maleimide	ThermoFisher Scientific	Cat. # O6034
(3-Aminopropyl)triethoxysilane (APTES)	MilliporeSigma	Cat. # 440140
EZ-Link-NHS-PEG12-biotin	ThermoFisher Scientific	Cat. # 21312
Methoxy PEG succinimidyl succinate, MW5000	JenKem	Cat. # A3011-1
Biotin-PEG NHS ester, MW5000	JenKem	Cat. # A5027-1
NeutrAvidin	ThermoFisher Scientific	Cat. # 31000
Catalase	Sigma	Cat. # C3515
Glucose Oxidase	MP Biomedicals	Cat. # 195196
Myosin II, rabbit skeletal muscle	Cytoskeleton	Cat. # MYO2
Albumin, from bovine serum	Sigma	Cat. # A2153
cOmplete, Mini, EDTA-free Protease Inhibitor Cocktail tablets	Sigma	Cat. # 11836170001
Zymolyase-100T	Nacalai tesque	Cat. # 07665-55
Salmon Sperm DNA, sheared (10 mg/mL)	Invitrogen	CAS # 7732-18-5
S. pombe Dip1	This study	N/A
S. pombe Dip1(6CysAla)	This study	N/A
S. pombe Wsp1-VCA	This study	N/A
Critical Commercial Assays		
In-Fusion HD Cloning Plus CE	Takara	Cat. # 638916
Experimental Models: Organisms/Strains		
S. pombe TP150 (protease deficient**,** h- leu1)	Vladimir Sirotkin	SpBN110
S. pombe VS872 (h- end4::ura4+ ade6-M216, his3-D1, leu1-32 , ura4-D18)	Vladimir Sirotkin	SpBN109
S. pombe VS1124a (h+ kanMX6-Pwsp1-mGFP-wsp1, fim1-mCherry-natMX6, ade6-M210, his3-D1, leu1-32, ura4-D18)	Vladimir Sirotkin	SpBN282
S. pombe VS1025-7 (h- kanMX6-Pwsp1-mCherry-wsp1, ade6-M216, his3-D1, leu1-32, ura4-D18)	Vladimir Sirotkin	SpBN259
S. pombe SpBN157-6 (end4::ura4+, kanMX6-Pwsp1-mGFP-wsp1, fim1-mCherry-natMX6, his3-D1, leu1-32 , ura4-D18)	This study	SpBN157-6
S. pombe SpBN165-1 (end4::ura4+, dip1-mGFP-kanMX6, fim1-mCherry-natMX6, his3-D1, leu1-32 , ura4-D18)	This study	SpBN165-1

Key Resources Table (continued).

REAGENT or RESOURCE	SOURCE	IDENTIFIER
S. pombe SpBN278-3 (end4::ura4+, dip1-mNeonGreen-hphMX6, fim1-mCherry-natMX6, his3-D1, leu1-32 , ura4-D18)	This study	SpBN278-3
S. pombe SpBN280-1 (h- kanMX6-Pwsp1-mCherry-wsp1, dip1-mNeonGreen-hphMX6, ade6-M216, his3-D1, leu1-32 , ura4-D18)	This study	SpBN280-1
Recombinant DNA		
pGV67_SpDip1	[7]	Plasmid #174
pGV67_SpDip1(6cysAla)	[8]	Plasmid #180
pGV67_SpWsp1(VCA)-497	[44]	Plasmid #4
pGEX6_NWASP-WA	[45]	Plasmid #222
pRK1043	[46]	N/A
pJK148_SpDip1-mNeonGreen-hphMX6	This study	Pombe vector #181
Software and Algorithms		
Fiji/ImageJ	[41]	https://fiji.sc/
MATLAB	MathWorks	N/A
ImageJ filament tracking plugin	Gift from Jeff Kuhn	N/A
ImageJ StackProfileData macro	Michael Schmid	https://imagej.nih.gov/ij/macros/StackProfileData.txt
Other		
Amicon Ultra-4 Centrifugal Filters 10,000 MWCO	MilliporeSigma	Cat. # UFC9010
Vivaspin Turbo 15 30,000 MWCO	Sartorius	Cat. # VS15T21
Vivaspin Turbo 15 3,500 MWCO	Sartorius	Cat. # VS15T91
Richard-Allan Scientific Slip-Rite Cover Glass (24 x 60 #1.5 coverslips)	ThermoFisher Scientific	Cat. # 152460

Supplementary Figure 1: Simulated and measured time courses of actin polymerization reactions containing Dip1 and Arp2/3 complex. **A.** Time courses of polymerization of 3 µM 15% pyrene-labeled actin in the presence of 50 nM SpArp2/3 complex and a range of Dip1 from 0 to 15 µM (solid lines). Dashed lines indicate the best fits from the no monomer binding kinetic model. **B.** Time courses of actin polymerization assays as described in A. Dashed lines over each trace indicate the best fits from the one monomer collision COPASI model.
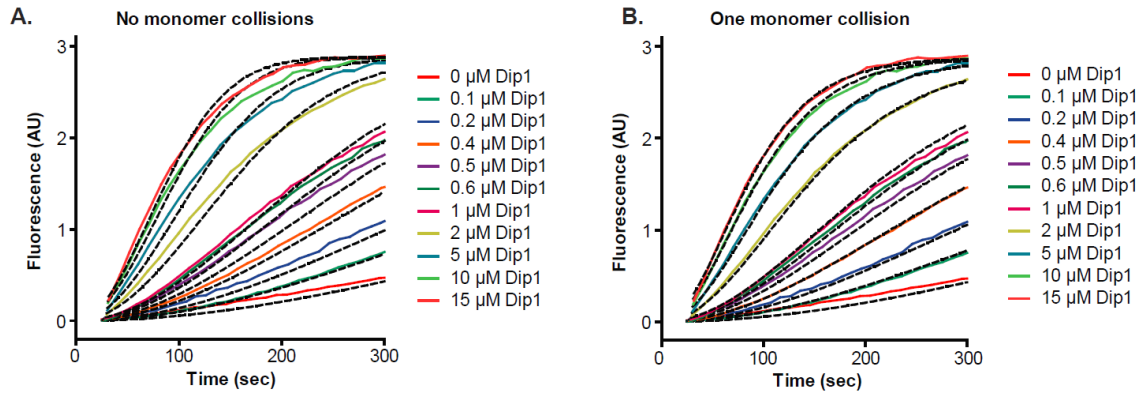
Supplementary Figure 2: Full models used to fit actin polymerization time courses in reactions containing Dip1 and Arp2/3 complex with sensitivity analysis of floated parameters. A. Kinetic pathways for the spontaneous nucleation of actin filaments (top) and for the activation of Arp2/3 complex by Dip1 via the single monomer binding pathway (bottom). Rate constants that were floated in the actin alone simulations (see panel B and methods) are boxed in cyan. Rate constants that we floated in the Dip1-mediated Arp2/3 complex activation simulations are boxed in green. See methods for more information and Supplementary Table 2 for the values used for each reaction parameter in the simulations. **B.** Time courses of polymerization of 15% pyrene labeled actin at the indicated concentrations (solid lines). Dashed lines show simulated polymerization time courses based on the spontaneous nucleation and elongation model depicted in panel A. **C.** Plot of the quality of fit (objective value) versus k_{-9} for simulations of the time courses of actin polymerization in the presence of Dip1 and Arp2/3 complex. The rate constants k_{-10} and k_{11} were allowed to float in these simulations. Dashed red line shows the value for the best fit. **D.** Plot of the quality of fit (objective value) versus k_{11} for simulations of the time courses of actin polymerization in the presence of Dip1 and Arp2/3 complex. The rate constants k_{-9} and k_{-10} were allowed to float in these simulations. Note that a range of values of k_{11} fit the data. **E.** Plot of the objective value of the fit versus k_{-10} for simulations of the time courses of actin polymerization in the presence of Dip1 and Arp2/3 complex. The rate constants k_{-9} and k_{11} were allowed to float in these simulations. Note that a range of values of k_{-10} fit the data.

124
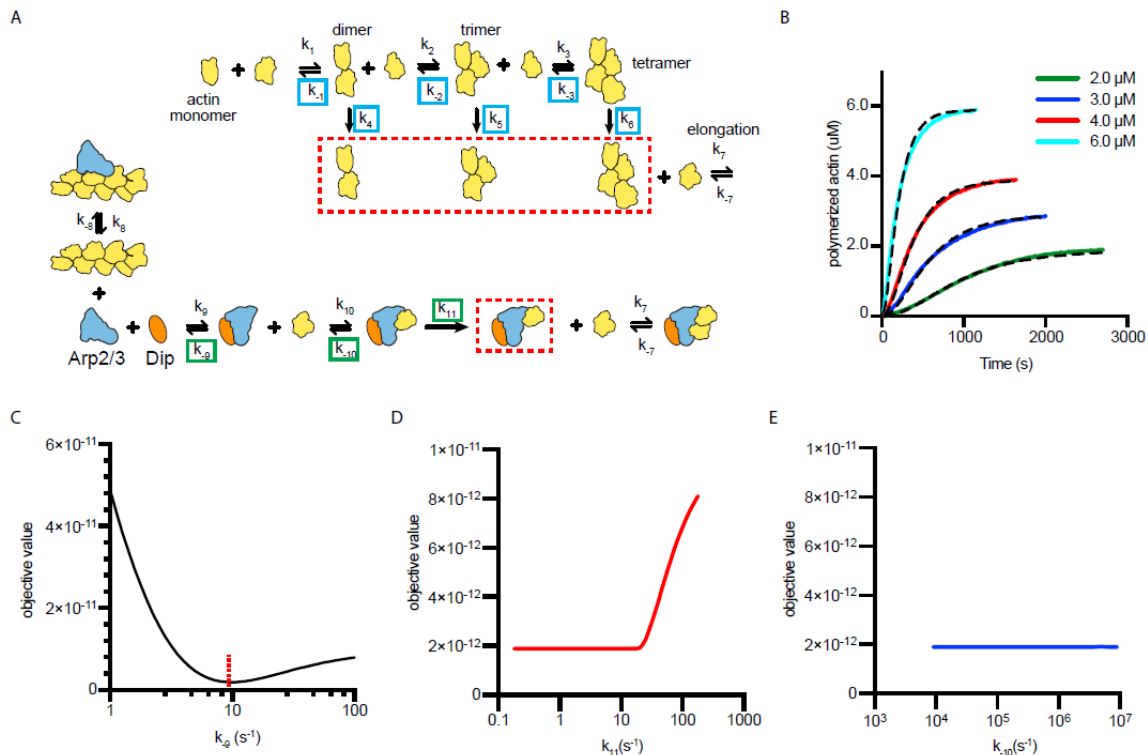
	Dip1 Alone	**Dip1 + Wsp1-VCA**	**Dip1 + GST-VCA**	**Dip1 + Wsp1-CA**
Best-fit values				
Max. Poly. Rate$_{max}$	19.77	28.61	11.75	17.12
$K_{1/2}$	4.222	0.4718	0.5706	2.894
Std. Error				
Max. Poly. Rate$_{max}$	0.4248	0.8862	0.3265	0.6942
$K_{1/2}$	0.3755	0.07717	0.08303	0.5443
95% Confidence Intervals				
Max. Poly. Rate$_{max}$	18.81 to 20.73	26.61 to 30.62	11.01 to 12.49	15.55 to 18.69
$K_{1/2}$	3.372 to 5.071	0.2972 to 0.6464	0.3828 to 0.7584	1.663 to 4.125
Goodness of Fit				
Degrees of Freedom	9	9	9	9
R²	0.9971	0.9766	0.9836	0.9852

Supplementary Table 1: Summary of the fits of maximum polymerization rate data in Figure 2 panel B,H and Figure 3 panel F. The best-fit values for the maximum maximum polymerization rate (Max. Poly. Rate$_{max}$) and the concentration of Dip1 (µM) needed to get half-maximum max polymerization rate for Dip1 alone or in the presence of Wsp1-VCA, GST-Wsp1-VCA or Wsp1-CA. Data points were fit to the following equation: Max poly rate = (max poly rate$_{max}$ x [Dip1])/($K_{1/2}$ + [Dip1]) + y-intercept. The y-intercept was set as the maximum polymerization rate in the absence of Dip1 for each condition.

Reaction #	Description	K_{on} (M^{-1}s^{-1})	K_{off} (s^{-1})	K_D (µM)	Reference
1	Actin dimerization	1.16×10^7	5.88×10^4	5.07×10^3	This Study
2	Actin trimerization	1.16×10^7	9.81×10^3	846	This Study
3	Actin tetramerization	1.16×10^7	96.9	8.36	This Study
4	Actin dimer nucleation	1.13×10^{-4}			This Study
5	Actin trimer nucleation	1.41×10^{-3}			This Study
6	Actin tetramer nucleation	5.86×10^{-2}			This Study
7	Barbed end elongation	1.16×10^7	1.4		Pollard 1986
8	Arp2/3 binds actin filament	150	0.001	6.67	Beltzner 2007
9	Dip1 binds Arp2/3	1×10^6	4.37*	4.37	
10	Dip-bound Arp2/3 nucleation	91034*			
11	Elongation from Dip1-bound Arp2/3	1.16×10^7	1.4		Pollard 1986
12	First actin monomer collides with Dip1-Arp2/3 nucleus	1.16×10^7	2.22×10^{6}*		
13	Second actin monomer collides with Dip1-Arp2/3-actin nucleus	1.16×10^7	12.2*		
14	Third actin monomer collides with Dip1-Arp2/3 -actin-actin nucleus	1.16×10^7	2.3*		

Supplementary Table 2: Summary of the numerical values used for each reaction parameter in COPASI modeling of actin polymerization traces. * indicates that a range of values for this parameter fit the model equally well. The * values reported represent one set of parameter values for the model that provided the best fit to the experimental data.

REFERENCES CITED

CHAPTER I

Allwood, Ellen G., Joe J. Tyler, Agnieszka N. Urbanek, Iwona I. Smaczynska-de Rooij, and Kathryn R. Ayscough. 2016. "Elucidating Key Motifs Required for Arp2/3-Dependent and Independent Actin Nucleation by Las17/WASP." Edited by Robert Alan Arkowitz. *PLOS ONE* 11 (9): e0163177. https://doi.org/10.1371/journal.pone.0163177.

Amann, Kurt J., and Thomas D. Pollard. 2001. "The Arp2/3 Complex Nucleates Actin Filament Branches from the Sides of Pre-Existing Filaments." *Nature Cell Biology* 3 (3): 306–10. https://doi.org/10.1038/35060104.

Arasada, Rajesh, and Thomas D. Pollard. 2011. "Distinct Roles for F-BAR Proteins Cdc15p and Bzz1p in Actin Polymerization at Sites of Endocytosis in Fission Yeast." *Current Biology* 21 (17): 1450–59. https://doi.org/10.1016/j.cub.2011.07.046.

Arasada, Rajesh, Wasim A. Sayyad, Julien Berro, and Thomas D. Pollard. 2018. "High-Speed Superresolution Imaging of the Proteins in Fission Yeast Clathrin-Mediated Endocytic Actin Patches." *Molecular Biology of the Cell* 29 (3): 295–303. https://doi.org/10.1091/mbc.E17-06-0415.

Ayala, Inmaculada, Massimiliano Baldassarre, Giada Giacchetti, Giusi Caldieri, Stefano Tetè, Alberto Luini, and Roberto Buccione. 2008. "Multiple Regulatory Inputs Converge on Cortactin to Control Invadopodia Biogenesis and Extracellular Matrix Degradation." *Journal of Cell Science* 121 (3): 369–78. https://doi.org/10.1242/jcs.008037.

Basu, Roshni, and Fred Chang. 2011. "Characterization of Dip1p Reveals a Switch in Arp2/3-Dependent Actin Assembly for Fission Yeast Endocytosis." *Current Biology : CB* 21 (11): 905–16. https://doi.org/10.1016/j.cub.2011.04.047.

Bernard, Marina de, Monica Moschioni, Giorgio Napolitani, Rino Rappuoli, and Cesare Montecucco. 2000. "The VacA Toxin of Helicobacter Pylori Identifies a New Intermediate Filament-Interacting Protein." *The EMBO Journal* 19 (1): 48–56. https://doi.org/10.1093/emboj/19.1.48.

Berro, Julien, Vladimir Sirotkin, and Thomas D. Pollard. 2010. "Mathematical Modeling of Endocytic Actin Patch Kinetics in Fission Yeast: Disassembly Requires Release of Actin Filament Fragments." *Molecular Biology of the Cell* 21 (16): 2905–15. https://doi.org/10.1091/mbc.e10-06-0494.

Bitsikas, Vassilis, Ivan R Corrêa Jr, and Benjamin J Nichols. 2014. "Clathrin-Independent Pathways Do Not Contribute Significantly to Endocytic Flux." Edited by Suzanne R Pfeffer. *ELife* 3 (September): e03970. https://doi.org/10.7554/eLife.03970.

Blanchoin, Laurent, Thomas D Pollard, and Sarah E Hitchcock-DeGregori. 2001. "Inhibition of the Arp2/3 Complex-Nucleated Actin Polymerization and Branch Formation by Tropomyosin." *Current Biology* 11 (16): 1300–1304. https://doi.org/10.1016/S0960-9822(01)00395-5.

Burston, Helen E., Lymarie Maldonado-Báez, Michael Davey, Benjamen Montpetit, Cayetana Schluter, Beverly Wendland, and Elizabeth Conibear. 2009. "Regulators of Yeast Endocytosis Identified by Systematic Quantitative Analysis." *The Journal of Cell Biology* 185 (6): 1097–1110. https://doi.org/10.1083/jcb.200811116.

Campellone, Kenneth G., and Matthew D. Welch. 2010. "A Nucleator Arms Race: Cellular Control of Actin Assembly." *Nature Reviews Molecular Cell Biology* 11 (4): 237–51. https://doi.org/10.1038/nrm2867.

Ceresa, Brian P., Aimee W. Kao, Scott R. Santeler, and Jeffrey E. Pessin. 1998. "Inhibition of Clathrin-Mediated Endocytosis Selectively Attenuates Specific Insulin Receptor Signal Transduction Pathways." *Molecular and Cellular Biology* 18 (7): 3862–70. https://doi.org/10.1128/MCB.18.7.3862.

Chen, Qian, and Thomas Pollard. 2013. "Actin Filament Severing by Cofilin Dismantles Actin Patches and Produces Mother Filaments for New Patches." *Current Biology : CB* 23 (13): 1154–62. https://doi.org/10.1016/j.cub.2013.05.005.

Collins, Agnieszka, Anthony Warrington, Kenneth A. Taylor, and Tatyana Svitkina. 2011. "Structural Organization of the Actin Cytoskeleton at Sites of Clathrin-Mediated Endocytosis." *Current Biology* 21 (14): 1167–75. https://doi.org/10.1016/j.cub.2011.05.048.

Conibear, Elizabeth. 2010. "Converging Views of Endocytosis in Yeast and Mammals." *Current Opinion in Cell Biology*, Membranes and organelles, 22 (4): 513–18. https://doi.org/10.1016/j.ceb.2010.05.009.

Cooper, John A., E. Loren Buhle, Simon B. Walker, Tian Y. Tsong, and Thomas D. Pollard. 1983. "Kinetic Evidence for a Monomer Activation Step in Actin Polymerization." *Biochemistry* 22 (9): 2193–2202. https://doi.org/10.1021/bi00278a021.

Dawson, John C., John A. Legg, and Laura M. Machesky. 2006. "Bar Domain Proteins: A Role in Tubulation, Scission and Actin Assembly in Clathrin-Mediated Endocytosis." *Trends in Cell Biology*, Membrane Dynamics, 16 (10): 493–98. https://doi.org/10.1016/j.tcb.2006.08.004.

Dayel, Mark J., and R. Dyche Mullins. 2004. "Activation of Arp2/3 Complex: Addition of the First Subunit of the New Filament by a WASP Protein Triggers Rapid ATP Hydrolysis on Arp2." *PLOS Biology* 2 (4): e91. https://doi.org/10.1371/journal.pbio.0020091.

Dergai, Mykola, Anton Iershov, Olga Novokhatska, Serhii Pankivskyi, and Alla Rynditch. 2016. "Evolutionary Changes on the Way to Clathrin-Mediated Endocytosis in Animals." *Genome Biology and Evolution* 8 (3): 588–606. https://doi.org/10.1093/gbe/evw028.

Dominguez, Roberto. 2009. "Actin Filament Nucleation and Elongation Factors – Structure-Function Relationships." *Critical Reviews in Biochemistry and Molecular Biology* 44 (6): 351–66. https://doi.org/10.3109/10409230903277340.

Dyche Mullins, R, and Thomas D Pollard. 1999. "Structure and Function of the Arp2/3 Complex." *Current Opinion in Structural Biology* 9 (2): 244–49. https://doi.org/10.1016/S0959-440X(99)80034-7.

Efimova, Nadia, and Tatyana M. Svitkina. 2018. "Branched Actin Networks Push against Each Other at Adherens Junctions to Maintain Cell–Cell Adhesion." *The Journal of Cell Biology* 217 (5): 1827–45. https://doi.org/10.1083/jcb.201708103.

Egile, Coumaran, Isabelle Rouiller, Xiao-Ping Xu, Niels Volkmann, Rong Li, and Dorit Hanein. 2005. "Mechanism of Filament Nucleation and Branch Stability Revealed by the Structure of the Arp2/3 Complex at Actin Branch Junctions." *PLoS Biology* 3 (11). https://doi.org/10.1371/journal.pbio.0030383.

Espinoza-Sanchez, Sofia, Lauren Ann Metskas, Steven Z. Chou, Elizabeth Rhoades, and Thomas D. Pollard. 2018. "Conformational Changes in Arp2/3 Complex Induced by ATP, WASp-VCA, and Actin Filaments." *Proceedings of the National Academy of Sciences* 115 (37): E8642–51. https://doi.org/10.1073/pnas.1717594115.

Esue, Osigwe, Yiider Tseng, and Denis Wirtz. 2009. "α-Actinin and Filamin Cooperatively Enhance the Stiffness of Actin Filament Networks." *PLOS ONE* 4 (2): e4411. https://doi.org/10.1371/journal.pone.0004411.

Firat-Karalar, Elif Nur, and Matthew D. Welch. 2011. "New Mechanisms and Functions of Actin Nucleation." *Current Opinion in Cell Biology* 23 (1): 4–13. https://doi.org/10.1016/j.ceb.2010.10.007.

Fletcher, Daniel A., and R. Dyche Mullins. 2010. "Cell Mechanics and the Cytoskeleton." *Nature* 463 (7280): 485–92. https://doi.org/10.1038/nature08908.

Fukuoka, Maiko, Shiro Suetsugu, Hiroaki Miki, Kiyoko Fukami, Takeshi Endo, and Tadaomi Takenawa. 2001. "A Novel Neural Wiskott-Aldrich Syndrome Protein (N-Wasp) Binding Protein, Wish, Induces Arp2/3 Complex Activation Independent of Cdc42." *The Journal of Cell Biology* 152 (3): 471–82.

Galletta, Brian J., and John A. Cooper. 2009. "Actin and Endocytosis: Mechanisms and Phylogeny." *Current Opinion in Cell Biology* 21 (1): 20–27. https://doi.org/10.1016/j.ceb.2009.01.006.

Galletta, Brian J., Anders E. Carlsson, and John A. Cooper. 2012. "Molecular Analysis of Arp2/3 Complex Activation in Cells." *Biophysical Journal* 103 (10): 2145–56. https://doi.org/10.1016/j.bpj.2012.10.009.

Goley, Erin D., Stacia E. Rodenbusch, Adam C. Martin, and Matthew D. Welch. 2004. "Critical Conformational Changes in the Arp2/3 Complex Are Induced by Nucleotide and Nucleation Promoting Factor." *Molecular Cell* 16 (2): 269–79. https://doi.org/10.1016/j.molcel.2004.09.018.

Goley, Erin D., and Matthew D. Welch. 2006. "The ARP2/3 Complex: An Actin Nucleator Comes of Age." *Nature Reviews Molecular Cell Biology* 7 (10): 713–26. https://doi.org/10.1038/nrm2026.

Goode, Bruce L., Julian A. Eskin, and Beverly Wendland. 2015. "Actin and Endocytosis in Budding Yeast." *Genetics* 199 (2): 315–58. https://doi.org/10.1534/genetics.112.145540.

Gunning, Peter W., Edna C. Hardeman, Pekka Lappalainen, and Daniel P. Mulvihill. 2015. "Tropomyosin – Master Regulator of Actin Filament Function in the Cytoskeleton." *Journal of Cell Science* 128 (16): 2965–74. https://doi.org/10.1242/jcs.172502.

Helgeson, Luke A, and Brad J Nolen. 2013. "Mechanism of Synergistic Activation of Arp2/3 Complex by Cortactin and N-WASP." Edited by Wesley Sundquist. *ELife* 2 (September): e00884. https://doi.org/10.7554/eLife.00884.

Hetrick, Byron, Min Suk Han, Luke A. Helgeson, and Brad J. Nolen. 2013. "Small Molecules CK-666 and CK-869 Inhibit Actin-Related Protein 2/3 Complex by Blocking an Activating Conformational Change." *Chemistry & Biology* 20 (5): 701–12. https://doi.org/10.1016/j.chembiol.2013.03.019.

Higgs, Henry N., and Thomas D. Pollard. 1999. "Regulation of Actin Polymerization by Arp2/3 Complex and WASp/Scar Proteins." *Journal of Biological Chemistry* 274 (46): 32531–34. https://doi.org/10.1074/jbc.274.46.32531.

Hudson, Andrew M., and Lynn Cooley. 2002. "A Subset of Dynamic Actin Rearrangements in Drosophila Requires the Arp2/3 Complex." *The Journal of Cell Biology* 156 (4): 677–87. https://doi.org/10.1083/jcb.200109065.

Huxley, H. E. 1963. "Electron Microscope Studies on the Structure of Natural and Synthetic Protein Filaments from Striated Muscle." *Journal of Molecular Biology* 7 (3): 281-IN30. https://doi.org/10.1016/S0022-2836(63)80008-X.

Innocenti, Metello. 2018. "New Insights into the Formation and the Function of Lamellipodia and Ruffles in Mesenchymal Cell Migration." *Cell Adhesion & Migration* 12 (5): 401–16. https://doi.org/10.1080/19336918.2018.1448352.

Kaksonen, Marko, and Aurélien Roux. 2018. "Mechanisms of Clathrin-Mediated Endocytosis." *Nature Reviews Molecular Cell Biology* 19 (5): 313–26. https://doi.org/10.1038/nrm.2017.132.

Khurana, Seema, and Sudeep P George. 2011. "The Role of Actin Bundling Proteins in the Assembly of Filopodia in Epithelial Cells." *Cell Adhesion & Migration* 5 (5): 409–20. https://doi.org/10.4161/cam.5.5.17644.

Kim, Dae Joong, Sung Hyun Kim, Chol Seung Lim, Kyu Yeong Choi, Chun Shik Park, Bong Hwan Sung, Myeong Gu Yeo, Sunghoe Chang, Jin-Kyu Kim, and Woo Keun Song. 2006. "Interaction of SPIN90 with the Arp2/3 Complex Mediates Lamellipodia and Actin Comet Tail Formation." *Journal of Biological Chemistry* 281 (1): 617–25. https://doi.org/10.1074/jbc.M504450200.

Kim, Hwan, Hyejin Oh, Young Soo Oh, Jeomil Bae, Nan Hyung Hong, Su Jung Park, Suyeon Ahn, et al. 2019. "SPIN90, an Adaptor Protein, Alters the Proximity between Rab5 and Gapex5 and Facilitates Rab5 Activation during EGF Endocytosis." *Experimental & Molecular Medicine* 51 (7): 1–14. https://doi.org/10.1038/s12276-019-0284-5.

Kim, Seon-Myung, Jeomil Bae, In Ha Cho, Kyu Yeong Choi, Yeon Jung Park, Jin Hee Ryu, Jang-Soo Chun, and Woo Keun Song. 2011. "Control of Growth Cone Motility and Neurite Outgrowth by SPIN90." *Experimental Cell Research* 317 (16): 2276–87. https://doi.org/10.1016/j.yexcr.2011.06.018.

Kim, Sung Hyun, Hyun Jin Choi, Kyoung Woo Lee, Nan Hyung Hong, Bong Hwan Sung, Kyu Yeong Choi, Seon-Myung Kim, Sunghoe Chang, Soo Hyun Eom, and Woo Keun Song. 2006. "Interaction of SPIN90 with Syndapin Is Implicated in Clathrin-Mediated Endocytic Pathway in Fibroblasts." *Genes to Cells* 11 (10): 1197–1211. https://doi.org/10.1111/j.1365-2443.2006.01008.x.

Kim, Yujin, Sunyun Kim, Suho Lee, Sung Hyun Kim, Yoonju Kim, Zee Yong Park, Woo Keun Song, and Sunghoe Chang. 2005. "Interaction of SPIN90 with Dynamin I and Its Participation in Synaptic Vesicle Endocytosis." *Journal of Neuroscience* 25 (41): 9515–23. https://doi.org/10.1523/JNEUROSCI.1643-05.2005.

Kovar, David R., Vladimir Sirotkin, and Matthew Lord. 2011. "Three's Company: The Fission Yeast Actin Cytoskeleton." *Trends in Cell Biology* 21 (3): 177–87. https://doi.org/10.1016/j.tcb.2010.11.001.

Kurisu, Shusaku, and Tadaomi Takenawa. 2009. "The WASP and WAVE Family Proteins." *Genome Biology* 10 (6): 226. https://doi.org/10.1186/gb-2009-10-6-226.

Lamason, Rebecca L., and Matthew D. Welch. 2017. "Actin-Based Motility and Cell-to-Cell Spread of Bacterial Pathogens." *Current Opinion in Microbiology* 35 (February): 48–57. https://doi.org/10.1016/j.mib.2016.11.007.

Lee, Suho, Kyoungwoo Lee, Suha Hwang, Sung Hyun Kim, Woo Keun Song, Zee Yong Park, and Sunghoe Chang. 2006. "SPIN90/WISH Interacts with PSD-95 and Regulates Dendritic Spinogenesis via an N-WASP-Independent Mechanism." *The EMBO Journal* 25 (20): 4983–95. https://doi.org/10.1038/sj.emboj.7601349.

Lim, Chol Seung, Eui Sun Park, Dae Joong Kim, Young Hwa Song, Soo Hyun Eom, Jang-Soo Chun, Jae Hong Kim, Jin-Kyu Kim, Dongeun Park, and Woo Keun Song. 2001. "SPIN90 (SH3 ProteinInteracting with Nck, 90 KDa), an Adaptor Protein That Is Developmentally Regulated during Cardiac Myocyte Differentiation." *Journal of Biological Chemistry* 276 (16): 12871–78. https://doi.org/10.1074/jbc.M009411200.

Lodish, Harvey, Arnold Berk, S. Lawrence Zipursky, Paul Matsudaira, David Baltimore, and James Darnell. 2000. "The Actin Cytoskeleton." *Molecular Cell Biology. 4th Edition*. https://www.ncbi.nlm.nih.gov/books/NBK21493/.

Lu, Rebecca, David G. Drubin, and Yidi Sun. 2016. "Clathrin-Mediated Endocytosis in Budding Yeast at a Glance." *Journal of Cell Science* 129 (8): 1531–36. https://doi.org/10.1242/jcs.182303.

Luan, Qing, Su-Ling Liu, Luke A. Helgeson, and Brad J. Nolen. 2018. "Structure of the Nucleation-promoting Factor SPIN90 Bound to the Actin Filament Nucleator Arp2/3 Complex." *The EMBO Journal* 37 (22): e100005. https://doi.org/10.15252/embj.2018100005.

Machesky, L. M., S. J. Atkinson, C. Ampe, J. Vandekerckhove, and T. D. Pollard. 1994. "Purification of a Cortical Complex Containing Two Unconventional Actins from Acanthamoeba by Affinity Chromatography on Profilin-Agarose." *The Journal of Cell Biology* 127 (1): 107–15.

Machesky, Laura M., and Robert H. Insall. 1998. "Scar1 and the Related Wiskott–Aldrich Syndrome Protein, WASP, Regulate the Actin Cytoskeleton through the Arp2/3 Complex." *Current Biology* 8 (25): 1347–56. https://doi.org/10.1016/S0960-9822(98)00015-3.

Machesky, Laura M., R. Dyche Mullins, Henry N. Higgs, Donald A. Kaiser, Laurent Blanchoin, Robin C. May, Margaret E. Hall, and Thomas D. Pollard. 1999. "Scar, a WASp-Related Protein, Activates Nucleation of Actin Filaments by the Arp2/3 Complex." *Proceedings of the National Academy of Sciences* 96 (7): 3739–44. https://doi.org/10.1073/pnas.96.7.3739.

Manenschijn, Hetty E, Andrea Picco, Markus Mund, Anne-Sophie Rivier-Cordey, Jonas Ries, and Marko Kaksonen. 2019. "Type-I Myosins Promote Actin Polymerization to Drive Membrane Bending in Endocytosis." *ELife* 8 (August): 44215. https://doi.org/10.7554/eLife.44215.

Marchand, Jean-Baptiste, Donald A. Kaiser, Thomas D. Pollard, and Henry N. Higgs. 2001. "Interaction of WASP/Scar Proteins with Actin and Vertebrate Arp2/3 Complex." *Nature Cell Biology* 3 (1): 76–82. https://doi.org/10.1038/35050590.

Matsudalra, Paul. 1991. "Modular Organization of Actin Crosslinking Proteins." *Trends in Biochemical Sciences* 16 (January): 87–92. https://doi.org/10.1016/0968-0004(91)90039-X.

Matsuyama, Akihisa, Ritsuko Arai, Yoko Yashiroda, Atsuko Shirai, Ayako Kamata, Shigeko Sekido, Yumiko Kobayashi, et al. 2006. "ORFeome Cloning and Global Analysis of Protein Localization in the Fission Yeast Schizosaccharomyces Pombe." *Nature Biotechnology* 24 (7): 841–47. https://doi.org/10.1038/nbt1222.

McCollum, D., A. Feoktistova, M. Morphew, M. Balasubramanian, and K. L. Gould. 1996. "The Schizosaccharomyces Pombe Actin-Related Protein, Arp3, Is a Component of the Cortical Actin Cytoskeleton and Interacts with Profilin." *The EMBO Journal* 15 (23): 6438–46. https://doi.org/10.1002/j.1460-2075.1996.tb01035.x.

Medalia, Ohad, Martin Beck, Mary Ecke, Igor Weber, Ralph Neujahr, Wolfgang Baumeister, and Günther Gerisch. 2007. "Organization of Actin Networks in Intact Filopodia." *Current Biology* 17 (1): 79–84. https://doi.org/10.1016/j.cub.2006.11.022.

Miki, Hiroaki, and Tadaomi Takenawa. 1998. "Direct Binding of the Verprolin-Homology Domain in N-WASP to Actin Is Essential for Cytoskeletal Reorganization." *Biochemical and Biophysical Research Communications* 243 (1): 73–78. https://doi.org/10.1006/bbrc.1997.8064.

Mogilner, A, and G Oster. 1996. "Cell Motility Driven by Actin Polymerization." *Biophysical Journal* 71 (6): 3030–45.

Morel, Etienne, Robert G. Parton, and Jean Gruenberg. 2009. "Annexin A2-Dependent Polymerization of Actin Mediates Endosome Biogenesis." *Developmental Cell* 16 (3): 445–57. https://doi.org/10.1016/j.devcel.2009.01.007.

Morrell, Jennifer L., Mary Morphew, and Kathleen L. Gould. 1999. "A Mutant of Arp2p Causes Partial Disassembly of the Arp2/3 Complex and Loss of Cortical Actin Function in Fission Yeast." *Molecular Biology of the Cell* 10 (12): 4201–15. https://doi.org/10.1091/mbc.10.12.4201.

Mullins, R. Dyche, John A. Heuser, and Thomas D. Pollard. 1998. "The Interaction of Arp2/3 Complex with Actin: Nucleation, High Affinity Pointed End Capping, and Formation of Branching Networks of Filaments." *Proceedings of the National Academy of Sciences* 95 (11): 6181–86. https://doi.org/10.1073/pnas.95.11.6181.

Mund, Markus, Johannes Albertus van der Beek, Joran Deschamps, Serge Dmitrieff, Philipp Hoess, Jooske Louise Monster, Andrea Picco, François Nédélec, Marko Kaksonen, and Jonas Ries. 2018. "Systematic Nanoscale Analysis of Endocytosis Links Efficient Vesicle Formation to Patterned Actin Nucleation." *Cell* 174 (4): 884-896.e17. https://doi.org/10.1016/j.cell.2018.06.032.

Neuhaus, Jean-Marc, Michael Wanger, Thomas Keiser, and Albrecht Wegner. 1983. "Treadmilling of Actin." *Journal of Muscle Research & Cell Motility* 4 (5): 507–27. https://doi.org/10.1007/BF00712112.

Nolen, Brad J., and Thomas D. Pollard. 2008. "Structure and Biochemical Properties of Fission Yeast Arp2/3 Complex Lacking the Arp2 Subunit." *Journal of Biological Chemistry* 283 (39): 26490–98. https://doi.org/10.1074/jbc.M802607200.

Oh, Hyejin, Hwan Kim, Kyung-Hwun Chung, Nan Hyung Hong, Baehyun Shin, Woo Jin Park, Youngsoo Jun, Sangmyung Rhee, and Woo Keun Song. 2013. "SPIN90 Knockdown Attenuates the Formation and Movement of Endosomal Vesicles in the Early Stages of Epidermal Growth Factor Receptor Endocytosis." *PLoS ONE* 8 (12). https://doi.org/10.1371/journal.pone.0082610.

Ono, Shoichiro. 2007. "Mechanism of Depolymerization and Severing of Actin Filaments and Its Significance in Cytoskeletal Dynamics." In *International Review of Cytology*, 258:1–82. Academic Press. https://doi.org/10.1016/S0074-7696(07)58001-0.

Padrick, Shae B., Lynda K. Doolittle, Chad A. Brautigam, David S. King, and Michael K. Rosen. 2011. "Arp2/3 Complex Is Bound and Activated by Two WASP Proteins." *Proceedings of the National Academy of Sciences* 108 (33): E472–79. https://doi.org/10.1073/pnas.1100236108.

Palmer, Sarah E., Iwona I. Smaczynska-de Rooij, Christopher J. Marklew, Ellen G. Allwood, Ritu Mishra, Simeon Johnson, Martin W. Goldberg, and Kathryn R. Ayscough. 2015. "A Dynamin-Actin Interaction Is Required for Vesicle Scission during Endocytosis in Yeast." *Current Biology* 25 (7): 868–78. https://doi.org/10.1016/j.cub.2015.01.061.

Picco, Andrea, Markus Mund, Jonas Ries, François Nédélec, and Marko Kaksonen. 2015. "Visualizing the Functional Architecture of the Endocytic Machinery." Edited by Suzanne R Pfeffer. *ELife* 4 (February): e04535. https://doi.org/10.7554/eLife.04535.

Pollard, T. D. 1986. "Rate Constants for the Reactions of ATP- and ADP-Actin with the Ends of Actin Filaments." *The Journal of Cell Biology* 103 (6): 2747–54. https://doi.org/10.1083/jcb.103.6.2747.

Pollard, T. D. 1990. "Actin." *Current Opinion in Cell Biology* 2 (1): 33–40. https://doi.org/10.1016/S0955-0674(05)80028-6.

Pollard, Thomas D. 1986. "Mechanism of Actin Filament Self-Assembly and Regulation of the Process by Actin-Binding Proteins." *Biophysical Journal* 49 (1): 149–51.

Pollard, Thomas D., Laurent Blanchoin, and R. Dyche Mullins. 2000. "Molecular Mechanisms Controlling Actin Filament Dynamics in Nonmuscle Cells." *Annual Review of Biophysics and Biomolecular Structure* 29 (1): 545–76. https://doi.org/10.1146/annurev.biophys.29.1.545.

Pollard, Thomas D, and Gary G Borisy. 2003. "Cellular Motility Driven by Assembly and Disassembly of Actin Filaments." *Cell* 112 (4): 453–65. https://doi.org/10.1016/S0092-8674(03)00120-X.

Pollard, Thomas D., and John A. Cooper. 1984. "Quantitative Analysis of the Effect of Acanthamoeba Profilin on Actin Filament Nucleation and Elongation." *Biochemistry* 23 (26): 6631–41. https://doi.org/10.1021/bi00321a054.

Pollard, Thomas D., and John A. Cooper. 1986. "Actin and Actin-Binding Proteins. a Critical Evaluation of Mechanisms and Functions." *Annual Review of Biochemistry* 55 (1): 987–1035. https://doi.org/10.1146/annurev.bi.55.070186.005011.

Pratap Sahi, Vaidurya, Petra Cifrová, Judith García-González, Innu Kotannal Baby, Gregory Mouillé, Emilie Gineau, Karel Müller, et al. 2018. "Arabidopsis Thaliana Plants Lacking the ARP2/3 Complex Show Defects in Cell Wall Assembly and Auxin Distribution." *Annals of Botany* 122 (5): 777–89. https://doi.org/10.1093/aob/mcx178.

Pujol, Thomas, Olivia du Roure, Marc Fermigier, and Julien Heuvingh. 2012. "Impact of Branching on the Elasticity of Actin Networks." *Proceedings of the National Academy of Sciences* 109 (26): 10364–69. https://doi.org/10.1073/pnas.1121238109.

Quinlan, Margot E., John E. Heuser, Eugen Kerkhoff, and R. Dyche Mullins. 2005. "Drosophila Spire Is an Actin Nucleation Factor." *Nature* 433 (7024): 382–88. https://doi.org/10.1038/nature03241.

Robinson, Robert C., Kirsi Turbedsky, Donald A. Kaiser, Jean-Baptiste Marchand, Henry N. Higgs, Senyon Choe, and Thomas D. Pollard. 2001. "Crystal Structure of Arp2/3 Complex." *Science* 294 (5547): 1679–84. https://doi.org/10.1126/science.1066333.

Rodnick-Smith, Max, Qing Luan, Su-Ling Liu, and Brad J. Nolen. 2016. "Role and Structural Mechanism of WASP-Triggered Conformational Changes in Branched Actin Filament Nucleation by Arp2/3 Complex." *Proceedings of the National Academy of Sciences* 113 (27): E3834–43. https://doi.org/10.1073/pnas.1517798113.

Royle, Stephen J., and Leon Lagnado. 2003. "Endocytosis at the Synaptic Terminal." *The Journal of Physiology* 553 (2): 345–55. https://doi.org/10.1113/jphysiol.2003.049221.

Sano, Kimihiko, Akira Hayakawa, Jin-Hua Piao, Yoshiyuki Kosaka, and Hajime Nakamura. 2000. "Novel SH3 Protein Encoded by the AF3p21 Gene Is Fused to the Mixed Lineage Leukemia Protein in a Therapy-Related Leukemia with t(3;11) (P21;Q23)." *Blood* 95 (3): 1066–68. https://doi.org/10.1182/blood.V95.3.1066.003k11_1066_1068.

Satoh, Sachie, and Tomoko Tominaga. 2001. "MDia-Interacting Protein Acts Downstream of Rho-MDia and Modifies Src Activation and Stress Fiber Formation." *Journal of Biological Chemistry* 276 (42): 39290–94. https://doi.org/10.1074/jbc.M107026200.

Sawa, Mariko, Shiro Suetsugu, Asako Sugimoto, Hiroaki Miki, Masayuki Yamamoto, and Tadaomi Takenawa. 2003. "Essential Role of the C. Elegans Arp2/3 Complex in Cell Migration during Ventral Enclosure." *Journal of Cell Science* 116 (8): 1505–18. https://doi.org/10.1242/jcs.00362.

Schaub, Sébastien, Jean-Jacques Meister, and Alexander B. Verkhovsky. 2007. "Analysis of Actin Filament Network Organization in Lamellipodia by Comparing Experimental and Simulated Images." *Journal of Cell Science* 120 (8): 1491–1500. https://doi.org/10.1242/jcs.03379.

Schrank, Benjamin R., Tomas Aparicio, Yinyin Li, Wakam Chang, Brian T. Chait, Gregg G. Gundersen, Max E. Gottesman, and Jean Gautier. 2018. "Nuclear Arp2/3 Drives DNA Break Clustering for Homology-Directed Repair." *Nature* 559 (7712): 61–66. https://doi.org/10.1038/s41586-018-0237-5.

Sirotkin, Vladimir, Christopher C. Beltzner, Jean-Baptiste Marchand, and Thomas D. Pollard. 2005. "Interactions of WASp, Myosin-I, and Verprolin with Arp2/3 Complex during Actin Patch Assembly in Fission Yeast." *The Journal of Cell Biology* 170 (4): 637–48. https://doi.org/10.1083/jcb.200502053.

Sirotkin, Vladimir, Julien Berro, Keely Macmillan, Lindsey Zhao, and Thomas D. Pollard. 2010. "Quantitative Analysis of the Mechanism of Endocytic Actin Patch Assembly and Disassembly in Fission Yeast." *Molecular Biology of the Cell* 21 (16): 2894–2904. https://doi.org/10.1091/mbc.E10-02-0157.

Smith, Benjamin A., Karen Daugherty-Clarke, Bruce L. Goode, and Jeff Gelles. 2013. "Pathway of Actin Filament Branch Formation by Arp2/3 Complex Revealed by Single-Molecule Imaging." *Proceedings of the National Academy of Sciences of the United States of America* 110 (4): 1285–90. https://doi.org/10.1073/pnas.1211164110.

Smith, Benjamin A, Shae B Padrick, Lynda K Doolittle, Karen Daugherty-Clarke, Ivan R Corrêa Jr, Ming-Qun Xu, Bruce L Goode, Michael K Rosen, and Jeff Gelles. 2013. "Three-Color Single Molecule Imaging Shows WASP Detachment from Arp2/3 Complex Triggers Actin Filament Branch Formation." Edited by Wesley Sundquist. *ELife* 2 (September): e01008. https://doi.org/10.7554/eLife.01008.

Stossel, T. P., C. Chaponnier, R. M. Ezzell, J. H. Hartwig, P. A. Janmey, D. J. Kwiatkowski, S. E. Lind, et al. 1985. "Nonmuscle Actin-Binding Proteins." *Annual Review of Cell Biology* 1 (1): 353–402. https://doi.org/10.1146/annurev.cb.01.110185.002033.

Sun, Yidi, Johannes Schöneberg, Xuyan Chen, Tommy Jiang, Charlotte Kaplan, Ke Xu, Thomas D Pollard, and David G Drubin. 2019. "Direct Comparison of Clathrin-Mediated Endocytosis in Budding and Fission Yeast Reveals Conserved and Evolvable Features." Edited by Suzanne R Pfeffer and Vladimir Sirotkin. *ELife* 8 (December): e50749. https://doi.org/10.7554/eLife.50749.

Suraneni, Praveen, Boris Rubinstein, Jay R. Unruh, Michael Durnin, Dorit Hanein, and Rong Li. 2012. "The Arp2/3 Complex Is Required for Lamellipodia Extension and Directional Fibroblast Cell Migration." *The Journal of Cell Biology* 197 (2): 239–51. https://doi.org/10.1083/jcb.201112113.

Svitkina, Tatyana. 2018. "The Actin Cytoskeleton and Actin-Based Motility." *Cold Spring Harbor Perspectives in Biology* 10 (1). https://doi.org/10.1101/cshperspect.a018267.

Svitkina, Tatyana M., Alexander B. Verkhovsky, Kyle M. McQuade, and Gary G. Borisy. 1997. "Analysis of the Actin–Myosin II System in Fish Epidermal Keratocytes: Mechanism of Cell Body Translocation." *The Journal of Cell Biology* 139 (2): 397–415. https://doi.org/10.1083/jcb.139.2.397.

Szymanski, Daniel B., and Daniel J. Cosgrove. 2009. "Dynamic Coordination of Cytoskeletal and Cell Wall Systems during Plant Cell Morphogenesis." *Current Biology* 19 (17): R800–811. https://doi.org/10.1016/j.cub.2009.07.056.

Teodorof, Carmen, Jeom Il Bae, Seon-Myung Kim, Hye Jin Oh, Yong Seok Kang, Jeonghoon Choi, Jang-Soo Chun, and Woo Keun Song. 2009. "SPIN90-IRSp53 Complex Participates in Rac-Induced Membrane Ruffling." *Experimental Cell Research* 315 (14): 2410–19. https://doi.org/10.1016/j.yexcr.2009.05.010.

Tyler, Joe J., Ellen G. Allwood, and Kathryn R. Ayscough. 2016. "WASP Family Proteins, More than Arp2/3 Activators." *Biochemical Society Transactions* 44 (5): 1339–45. https://doi.org/10.1042/BST20160176.

Ujfalusi, Zoltán, Andrea Vig, Gábor Hild, and Miklós Nyitrai. 2009. "Effect of Tropomyosin on Formin-Bound Actin Filaments." *Biophysical Journal* 96 (1): 162–68. https://doi.org/10.1529/biophysj.108.138420.

Urbanek, Agnieszka N., Adam P. Smith, Ellen G. Allwood, Wesley I. Booth, and Kathryn R. Ayscough. 2013. "A Novel Actin-Binding Motif in Las17/WASP Nucleates Actin Filaments Independently of Arp2/3." *Current Biology* 23 (3): 196–203. https://doi.org/10.1016/j.cub.2012.12.024.

Volkmann, N. 2001. "Structure of Arp2/3 Complex in Its Activated State and in Actin Filament Branch Junctions." *Science* 293 (5539): 2456–59. https://doi.org/10.1126/science.1063025.

Wagner, Andrew R., Qing Luan, Su-Ling Liu, and Brad J. Nolen. 2013. "WISH/DIP/SPIN90 Proteins Form a Class of Arp2/3 Complex Activators That Function without Preformed Actin Filaments." *Current Biology : CB* 23 (20): 1990–98. https://doi.org/10.1016/j.cub.2013.08.029.

Wallar, Bradley J, and Arthur S Alberts. 2003. "The Formins: Active Scaffolds That Remodel the Cytoskeleton." *Trends in Cell Biology* 13 (8): 435–46. https://doi.org/10.1016/S0962-8924(03)00153-3.

Wang, Yu-Li. 1985. "Exchange of Actin Subunits at the Leading Edge of Living Fibroblasts: Possible Role of Treadmilling." *The Journal of Cell Biology* 101 (2): 597–602.

Weaver, Alissa M., Andrei V. Karginov, Andrew W. Kinley, Scott A. Weed, Yan Li, J. Thomas Parsons, and John A. Cooper. 2001. "Cortactin Promotes and Stabilizes Arp2/3-Induced Actin Filament Network Formation." *Current Biology* 11 (5): 370–74. https://doi.org/10.1016/S0960-9822(01)00098-7.

Wei, Zhongya, Wenfeng Su, Huifang Lou, Shumin Duan, and Gang Chen. 2018. "Trafficking Pathway between Plasma Membrane and Mitochondria via Clathrin-Mediated Endocytosis." *Journal of Molecular Cell Biology* 10 (6): 539–48. https://doi.org/10.1093/jmcb/mjy060.

Welch, Matthew D., and R. Dyche Mullins. 2002. "Cellular Control of Actin Nucleation." *Annual Review of Cell and Developmental Biology* 18 (1): 247–88. https://doi.org/10.1146/annurev.cellbio.18.040202.112133.

Welch, Matthew D., and Michael Way. 2013. "Arp2/3-Mediated Actin-Based Motility: A Tail of Pathogen Abuse." *Cell Host & Microbe* 14 (3): 242–55. https://doi.org/10.1016/j.chom.2013.08.011.

Winter, Dirk C., Elizabeth Y. Choe, and Rong Li. 1999. "Genetic Dissection of the Budding Yeast Arp2/3 Complex: A Comparison of the in Vivo and Structural Roles of Individual Subunits." *Proceedings of the National Academy of Sciences* 96 (13): 7288–93. https://doi.org/10.1073/pnas.96.13.7288.

Winter, Dirk, Alexandre V. Podtelejnikov, Matthias Mann, and Rong Li. 1997. "The Complex Containing Actin-Related Proteins Arp2 and Arp3 Is Required for the Motility and Integrity of Yeast Actin Patches." *Current Biology* 7 (7): 519–29. https://doi.org/10.1016/S0960-9822(06)00223-5.

Ydenberg, Casey A., Benjamin A. Smith, Dennis Breitsprecher, Jeff Gelles, and Bruce L. Goode. 2011. "Cease-Fire at the Leading Edge: New Perspectives on Actin Filament Branching, Debranching and Cross-Linking." *Cytoskeleton (Hoboken, N.J.)* 68 (11): 596–602. https://doi.org/10.1002/cm.20543.

You, Eunae, Yun Hyun Huh, Ahreum Kwon, So Hee Kim, In Hee Chae, Ok-Jun Lee, Je-Hwang Ryu, et al. 2017. "SPIN90 Depletion and Microtubule Acetylation Mediate Stromal Fibroblast Activation in Breast Cancer Progression." *Cancer Research* 77 (17): 4710–22. https://doi.org/10.1158/0008-5472.CAN-17-0657.

Young, Michael E., John A. Cooper, and Paul C. Bridgman. 2004. "Yeast Actin Patches Are Networks of Branched Actin Filaments." *The Journal of Cell Biology* 166 (5): 629–35. https://doi.org/10.1083/jcb.200404159.

Zhou, Kang, Kaelyn D. Sumigray, and Terry Lechler. 2015. "The Arp2/3 Complex Has Essential Roles in Vesicle Trafficking and Transcytosis in the Mammalian Small Intestine." *Molecular Biology of the Cell* 26 (11): 1995–2004. https://doi.org/10.1091/mbc.E14-10-1481.

CHAPTER II

1.   Rotty, J.D., Wu, C., and Bear, J.E. (2013). New insights into the regulation and cellular functions of the ARP2/3 complex. Nat. Rev. Mol. Cell Biol. 14, 7–12.

2.   Achard, V., Martiel, J.-L., Michelot, A., Guérin, C., Reymann, A.-C., Blanchoin, L., and Boujemaa-Paterski, R. (2010). A "Primer"-Based Mechanism Underlies Branched Actin Filament Network Formation and Motility. Current Biology 20, 423–428.

3.   Machesky, L.M., Mullins, R.D., Higgs, H.N., Kaiser, D.A., Blanchoin, L., May, R.C., Hall, M.E., and Pollard, T.D. (1999). Scar, a WASp-related protein, activates nucleation of actin filaments by the Arp2/3 complex. Proc. Natl. Acad. Sci. U.S.A. 96, 3739–3744.

4.   Wagner, A.R., Luan, Q., Liu, S.-L., and Nolen, B.J. (2013). Dip1 defines a class of Arp2/3 complex activators that function without preformed actin filaments. Curr. Biol. 23, 1990–1998.

5.   Basu, R., and Chang, F. (2011). Characterization of dip1p reveals a switch in Arp2/3-dependent actin assembly for fission yeast endocytosis. Curr Biol 21, 905–916.

6.   Luan, Q., Liu, S.-L., Luke A. Helgeson, and Nolen, B.J. Structure of the nucleation promoting factor SPIN90 bound to the actin filament nucleator Arp2/3 complex. EMBO J. in press.

7.   Marchand, J.-B., Kaiser, D.A., Pollard, T.D., and Higgs, H.N. (2001). Interaction of WASP/Scar proteins with actin and vertebrate Arp2/3 complex. Nature Cell Biology 3, 76–82.

8. Rohatgi, R., Ma, L., Miki, H., Lopez, M., Kirchhausen, T., Takenawa, T., and Kirschner, M.W. (1999). The Interaction between N-WASP and the Arp2/3 Complex Links Cdc42-Dependent Signals to Actin Assembly. Cell 97, 221–231.

9. Luan, Q., Zelter, A., MacCoss, M.J., Davis, T.N., and Nolen, B.J. (2018). Identification of Wiskott-Aldrich syndrome protein (WASP) binding sites on the branched actin filament nucleator Arp2/3 complex. Proc. Natl. Acad. Sci. U.S.A. 115, E1409–E1418.

10. Ti, S.-C., Jurgenson, C.T., Nolen, B.J., and Pollard, T.D. (2011). Structural and biochemical characterization of two binding sites for nucleation-promoting factor WASp-VCA on Arp2/3 complex. Proc. Natl. Acad. Sci. U.S.A. 108, E463-471.

11. Padrick, S.B., Doolittle, L.K., Brautigam, C.A., King, D.S., and Rosen, M.K. (2011). Arp2/3 complex is bound and activated by two WASP proteins. Proc. Natl. Acad. Sci. U.S.A. 108, E472-479.

12. Rodnick-Smith, M., Liu, S.-L., Balzer, C.J., Luan, Q., and Nolen, B.J. (2016). Identification of an ATP-controlled allosteric switch that controls actin filament nucleation by Arp2/3 complex. Nat Commun 7, 12226.

13. Boczkowska, M., Rebowski, G., Kast, D.J., and Dominguez, R. (2014). Structural analysis of the transitional state of Arp2/3 complex activation by two actin-bound WCAs. Nat Commun 5, 3308.

14. Rodnick-Smith, M., Luan, Q., Liu, S.-L., and Nolen, B.J. (2016). Role and structural mechanism of WASP-triggered conformational changes in branched actin filament nucleation by Arp2/3 complex. PNAS 113, E3834–E3843.

15. Xu, X.-P., Rouiller, I., Slaughter, B.D., Egile, C., Kim, E., Unruh, J.R., Fan, X., Pollard, T.D., Li, R., Hanein, D., et al. (2012). Three-dimensional reconstructions of Arp2/3 complex with bound nucleation promoting factors. EMBO J. 31, 236–247.

16. Espinoza Sanchez, Sofia, Metskas, Lauren Ann, Chou, Steven Z., Rhoades, Elizabeth, and Pollard, Thomas D. (2018). Conformational changes in Arp2/3 complex induced by ATP, WASp-VCA and actin filaments. PNAS.

17. Hetrick, B., Han, M.S., Helgeson, L.A., and Nolen, B.J. (2013). Small molecules CK-666 and CK-869 inhibit actin-related protein 2/3 complex by blocking an activating conformational change. Chem. Biol. 20, 701–712.

18. Rouiller, I., Xu, X.-P., Amann, K.J., Egile, C., Nickell, S., Nicastro, D., Li, R., Pollard, T.D., Volkmann, N., and Hanein, D. (2008). The structural basis of actin filament branching by the Arp2/3 complex. J. Cell Biol. 180, 887–895.

19.   Kuhn, J.R., and Pollard, T.D. (2005). Real-time measurements of actin filament polymerization by total internal reflection fluorescence microscopy. Biophys. J. 88, 1387–1402.

20.   Skau, C.T., Neidt, E.M., and Kovar, D.R. (2009). Role of Tropomyosin in Formin-mediated Contractile Ring Assembly in Fission Yeast. Mol Biol Cell 20, 2160–2173.

21.   Hsiao, J.Y., Goins, L.M., Petek, N.A., and Mullins, R.D. (2015). Arp2/3 complex and cofilin modulate binding of tropomyosin to branched actin networks. Curr. Biol. 25, 1573–1582.

22.   Papp, G., Bugyi, B., Ujfalusi, Z., Barkó, S., Hild, G., Somogyi, B., and Nyitrai, M. (2006). Conformational changes in actin filaments induced by formin binding to the barbed end. Biophys. J. 91, 2564–2572.

23.   Luan, Q., and Nolen, B.J. (2013). Structural basis for regulation of Arp2/3 complex by GMF. Nat Struct Mol Biol 20, 1062–1068.

24.   Ydenberg, C.A., Padrick, S.B., Sweeney, M.O., Gandhi, M., Sokolova, O., and Goode, B.L. (2013). GMF severs actin-Arp2/3 complex branch junctions by a cofilin-like mechanism. Curr Biol 23, 1037–1045.

25.   Gandhi, M., Smith, B.A., Bovellan, M., Paavilainen, V., Daugherty-Clarke, K., Gelles, J., Lappalainen, P., and Goode, B.L. (2010). GMF is a cofilin homolog that binds Arp2/3 complex to stimulate filament debranching and inhibit actin nucleation. Curr. Biol. 20, 861–867.

26.   Sirotkin, V., Beltzner, C.C., Marchand, J.-B., and Pollard, T.D. (2005). Interactions of WASp, myosin-I, and verprolin with Arp2/3 complex during actin patch assembly in fission yeast. The Journal of Cell Biology 170, 637–648.

27.   Kovar, D.R., Sirotkin, V., and Lord, M. (2011). Three's company: The fission yeast actin cytoskeleton. Trends Cell Biol 21, 177–187.

28.   Burston, H.E., Maldonado-Báez, L., Davey, M., Montpetit, B., Schluter, C., Wendland, B., and Conibear, E. (2009). Regulators of yeast endocytosis identified by systematic quantitative analysis. J Cell Biol 185, 1097–1110.

29.   Oh, H., Kim, H., Chung, K.-H., Hong, N.H., Shin, B., Park, W.J., Jun, Y., Rhee, S., and Song, W.K. (2013). SPIN90 Knockdown Attenuates the Formation and Movement of Endosomal Vesicles in the Early Stages of Epidermal Growth Factor Receptor Endocytosis. PLoS One 8. Available at: https://www.ncbi.nlm.nih.gov/pmc/articles/PMC3858329/ [Accessed August 7, 2018].

30.   Kim, D.J., Kim, S.H., Lim, C.S., Choi, K.Y., Park, C.S., Sung, B.H., Yeo, M.G., Chang, S., Kim, J.-K., and Song, W.K. (2006). Interaction of SPIN90 with the Arp2/3 Complex Mediates Lamellipodia and Actin Comet Tail Formation. J. Biol. Chem. 281, 617–625.

31.   Isogai, T., van der Kammen, R., Leyton-Puig, D., Kedziora, K.M., Jalink, K., and Innocenti, M. (2015). Initiation of lamellipodia and ruffles involves cooperation between mDia1 and the Arp2/3 complex. J. Cell. Sci. 128, 3796–3810.

32.   Urbanek, A.N., Smith, A.P., Allwood, E.G., Booth, W.I., and Ayscough, K.R. (2013). A Novel Actin-Binding Motif in Las17/WASP Nucleates Actin Filaments Independently of Arp2/3. Current Biology 23, 196–203.

33.   Chen, Q., and Pollard, T. (2013). Actin filament severing by cofilin dismantles actin patches and produces mother filaments for new patches. Curr Biol 23, 1154–1162.

34.   Schuck, P. (2000). Size-distribution analysis of macromolecules by sedimentation velocity ultracentrifugation and lamm equation modeling. Biophys J 78, 1606–1619.

35.   Kapust, R.B., Tözsér, J., Fox, J.D., Anderson, D.E., Cherry, S., Copeland, T.D., and Waugh, D.S. (2001). Tobacco etch virus protease: mechanism of autolysis and rational design of stable mutants with wild-type catalytic proficiency. Protein Eng. 14, 993–1000.

36.   Liu, S.-L., May, J.R., Helgeson, L.A., and Nolen, B.J. (2013). Insertions within the actin core of actin-related protein 3 (Arp3) modulate branching nucleation by Arp2/3 complex. J. Biol. Chem. 288, 487–497.

37.   Schneider, C.A., Rasband, W.S., and Eliceiri, K.W. (2012). NIH Image to ImageJ: 25 years of Image Analysis. Nat Methods 9, 671–675.

CHAPTER III

1.   Mooren, O.L., Galletta, B.J., and Cooper, J.A. (2012). Roles for Actin Assembly in Endocytosis. Annual Review of Biochemistry 81, 661–686.

2.   Yi, K., Unruh, J.R., Deng, M., Slaughter, B.D., Rubinstein, B., and Li, R. (2011). Dynamic maintenance of asymmetric meiotic spindle position through Arp2/3-complex-driven cytoplasmic streaming in mouse oocytes. Nat. Cell Biol. 13, 1252–1258.

3.   Wang, P.-S., Chou, F.-S., Ramachandran, S., Xia, S., Chen, H.-Y., Guo, F., Suraneni, P., Maher, B.J., and Li, R. (2016). Crucial roles of the Arp2/3 complex during mammalian corticogenesis. Development 143, 2741–2752.

4.	Wu, C., Asokan, S.B., Berginski, M.E., Haynes, E.M., Sharpless, N.E., Griffith, J.D., Gomez, S.M., and Bear, J.E. (2012). Arp2/3 is critical for lamellipodia and response to extracellular matrix cues but is dispensable for chemotaxis. Cell 148, 973–987.

5.	Achard, V., Martiel, J.-L., Michelot, A., Guérin, C., Reymann, A.-C., Blanchoin, L., and Boujemaa-Paterski, R. (2010). A "Primer"-Based Mechanism Underlies Branched Actin Filament Network Formation and Motility. Current Biology 20, 423–428.

6.	Machesky, L.M., Mullins, R.D., Higgs, H.N., Kaiser, D.A., Blanchoin, L., May, R.C., Hall, M.E., and Pollard, T.D. (1999). Scar, a WASp-related protein, activates nucleation of actin filaments by the Arp2/3 complex. Proc. Natl. Acad. Sci. U.S.A. 96, 3739–3744.

7.	Wagner, A.R., Luan, Q., Liu, S.-L., and Nolen, B.J. (2013). WISH/DIP/SPIN90 proteins form a class of Arp2/3 complex activators that function without preformed actin filaments. Curr Biol 23, 1990–1998.

8.	Balzer, C.J., Wagner, A.R., Helgeson, L.A., and Nolen, B.J. (2018). Dip1 Co-opts Features of Branching Nucleation to Create Linear Actin Filaments that Activate WASP-Bound Arp2/3 Complex. Current Biology 28, 3886-3891.e4.

9.	Pollard, T.D., and Borisy, G.G. (2003). Cellular Motility Driven by Assembly and Disassembly of Actin Filaments. Cell 112, 453–465.

10.	Berro, J., Michelot, A., Blanchoin, L., Kovar, D.R., and Martiel, J.-L. (2007). Attachment Conditions Control Actin Filament Buckling and the Production of Forces. Biophys J 92, 2546–2558.

11.	Sirotkin, V., Beltzner, C.C., Marchand, J.-B., and Pollard, T.D. (2005). Interactions of WASp, myosin-I, and verprolin with Arp2/3 complex during actin patch assembly in fission yeast. The Journal of Cell Biology 170, 637–648.

12.	Basu, R., and Chang, F. (2011). Characterization of dip1p reveals a switch in Arp2/3-dependent actin assembly for fission yeast endocytosis. Curr Biol 21, 905–916.

13.	Rodnick-Smith, M., Luan, Q., Liu, S.-L., and Nolen, B.J. (2016). Role and structural mechanism of WASP-triggered conformational changes in branched actin filament nucleation by Arp2/3 complex. PNAS 113, E3834–E3843.

14.	Padrick, S.B., Doolittle, L.K., Brautigam, C.A., King, D.S., and Rosen, M.K. (2011). Arp2/3 complex is bound and activated by two WASP proteins. PNAS 108, E472–E479.

15. Ti, S.-C., Jurgenson, C.T., Nolen, B.J., and Pollard, T.D. (2011). Structural and biochemical characterization of two binding sites for nucleation-promoting factor WASp-VCA on Arp2/3 complex. Proc Natl Acad Sci U S A 108, E463–E471.

16. Luan, Q., Liu, S.-L., Helgeson, L.A., and Nolen, B.J. (2018). Structure of the nucleation-promoting factor SPIN90 bound to the actin filament nucleator Arp2/3 complex. The EMBO Journal 37, e100005.

17. Luan, Q., Zelter, A., MacCoss, M.J., Davis, T.N., and Nolen, B.J. (2018). Identification of Wiskott-Aldrich syndrome protein (WASP) binding sites on the branched actin filament nucleator Arp2/3 complex. PNAS 115, E1409–E1418.

18. Boczkowska, M., Rebowski, G., Kast, D.J., and Dominguez, R. (2014). Structural analysis of the transitional state of Arp2/3 complex activation by two actin-bound WCAs. Nat Commun 5, 3308.

19. Jurgenson, C.T., and Pollard, T.D. (2015). Crystals of the Arp2/3 complex in two new space groups with structural information about actin-related protein 2 and potential WASP binding sites. Acta Crystallogr F Struct Biol Commun 71, 1161–1168.

20. Rodnick-Smith, M., Liu, S.-L., Balzer, C.J., Luan, Q., and Nolen, B.J. (2016). Identification of an ATP-controlled allosteric switch that controls actin filament nucleation by Arp2/3 complex. Nat Commun 7, 12226.

21. Martin, A.C., Welch, M.D., and Drubin, D.G. (2006). Arp2/3 ATP hydrolysis-catalysed branch dissociation is critical for endocytic force generation. Nature Cell Biology 8, 826–833.

22. Smith, B.A., Padrick, S.B., Doolittle, L.K., Daugherty-Clarke, K., Corrêa, I.R., Jr, Xu, M.-Q., Goode, B.L., Rosen, M.K., and Gelles, J. (2013). Three-color single molecule imaging shows WASP detachment from Arp2/3 complex triggers actin filament branch formation. eLife 2, e01008.

23. Akin, O., and Mullins, R.D. (2008). Capping Protein Increases the Rate of Actin-based Motility by Promoting Filament Nucleation by the Arp2/3 Complex. Cell 133, 841–851.

24. Millius, A., Watanabe, N., and Weiner, O.D. (2012). Diffusion, capture and recycling of SCAR/WAVE and Arp2/3 complexes observed in cells by single-molecule imaging. J Cell Sci 125, 1165–1176.

25. Iwasa, J.H., and Mullins, R.D. (2007). Spatial and temporal relationships between actin-filament nucleation, capping, and disassembly. Curr. Biol. 17, 395–406.

26. Smith, B.A., Daugherty-Clarke, K., Goode, B.L., and Gelles, J. (2013). Pathway of actin filament branch formation by Arp2/3 complex revealed by single-molecule imaging. Proc. Natl. Acad. Sci. U.S.A. 110, 1285–1290.

27. Mullins, R.D., Heuser, J.A., and Pollard, T.D. (1998). The interaction of Arp2/3 complex with actin: nucleation, high affinity pointed end capping, and formation of branching networks of filaments. Proc. Natl. Acad. Sci. U.S.A. 95, 6181–6186.

28. Idrissi, F.-Z., Blasco, A., Espinal, A., and Geli, M.I. (2012). Ultrastructural dynamics of proteins involved in endocytic budding. Proc. Natl. Acad. Sci. U.S.A. 109, E2587-2594.

29. Arasada, R., Sayyad, W.A., Berro, J., and Pollard, T.D. (2018). High-speed superresolution imaging of the proteins in fission yeast clathrin-mediated endocytic actin patches. Mol. Biol. Cell 29, 295–303.

30. Kaksonen, M., Sun, Y., and Drubin, D.G. (2003). A pathway for association of receptors, adaptors, and actin during endocytic internalization. Cell 115, 475–487.

31. Sirotkin, V., Berro, J., Macmillan, K., Zhao, L., and Pollard, T.D. (2010). Quantitative Analysis of the Mechanism of Endocytic Actin Patch Assembly and Disassembly in Fission Yeast. Mol Biol Cell 21, 2894–2904.

32. Reymann, A.-C., Martiel, J.-L., Cambier, T., Blanchoin, L., Boujemaa-Paterski, R., and Théry, M. (2010). Nucleation geometry governs ordered actin networks structures. Nature Materials 9, 827–832.

33. Bieling, P., Hansen, S.D., Akin, O., Li, T.-D., Hayden, C.C., Fletcher, D.A., and Mullins, R.D. (2018). WH2 and proline-rich domains of WASP-family proteins collaborate to accelerate actin filament elongation. EMBO J. 37, 102–121.

34. Kaksonen, M., Toret, C.P., and Drubin, D.G. (2006). Harnessing actin dynamics for clathrin-mediated endocytosis. Nature Reviews Molecular Cell Biology 7, 404–414.

35. Lacy, M.M., Ma, R., Ravindra, N.G., and Berro, J. (2018). Molecular mechanisms of force production in clathrin-mediated endocytosis. FEBS Lett. 592, 3586–3605.

36. Mund, M., van der Beek, J.A., Deschamps, J., Dmitrieff, S., Hoess, P., Monster, J.L., Picco, A., Nédélec, F., Kaksonen, M., and Ries, J. (2018). Systematic Nanoscale Analysis of Endocytosis Links Efficient Vesicle Formation to Patterned Actin Nucleation. Cell 174, 884-896.e17.

37. Picco, A., Mund, M., Ries, J., Nédélec, F., and Kaksonen, M. (2015). Visualizing the functional architecture of the endocytic machinery. Elife 4.

38. Campellone, K.G., and Welch, M.D. (2010). A nucleator arms race: cellular control of actin assembly. Nat. Rev. Mol. Cell Biol. 11, 237–251.

39. Forsburg, S.L., and Rhind, N. (2006). Basic methods for fission yeast. Yeast 23, 173–183.

40. Hagan, Iain, Carr, Antony M., and Nurse, Paul (2016). Fission Yeast: A Laboratory Manual (Cold Spring Harbor Laboratory Press) Available at: https://cshlpress.com/default.tpl?cart=1558030115142488353&fromlink=T&link action=full&linksortby=oop_title&--eqSKUdatarq=1106 [Accessed May 16, 2019].

41. Rueden, C.T., Schindelin, J., Hiner, M.C., DeZonia, B.E., Walter, A.E., Arena, E.T., and Eliceiri, K.W. (2017). ImageJ2: ImageJ for the next generation of scientific image data. BMC Bioinformatics 18, 529.

42. Kuhn, J.R., and Pollard, T.D. (2005). Real-time measurements of actin filament polymerization by total internal reflection fluorescence microscopy. Biophys. J. 88, 1387–1402.

43. Pollard, T.D. (1986). Rate constants for the reactions of ATP- and ADP-actin with the ends of actin filaments. J. Cell Biol. 103, 2747–2754.

44. Nolen, B.J., and Pollard, T.D. (2008). Structure and biochemical properties of fission yeast Arp2/3 complex lacking the Arp2 subunit. J. Biol. Chem. 283, 26490–26498.

45. Liu, S.-L., May, J.R., Helgeson, L.A., and Nolen, B.J. (2013). Insertions within the actin core of actin-related protein 3 (Arp3) modulate branching nucleation by Arp2/3 complex. J. Biol. Chem. 288, 487–497.

46. Kapust, R.B., Tözsér, J., Fox, J.D., Anderson, D.E., Cherry, S., Copeland, T.D., and Waugh, D.S. (2001). Tobacco etch virus protease: mechanism of autolysis and rational design of stable mutants with wild-type catalytic proficiency. Protein Eng. 14, 993–1000.

CHAPTER IV

Achard V, Martiel J-L, Michelot A, Guérin C, Reymann A-C, Blanchoin L, Boujemaa-Paterski R. 2010. A "Primer"-Based Mechanism Underlies Branched Actin Filament Network Formation and Motility. *Current Biology* **20**:423–428. doi:10.1016/j.cub.2009.12.056

Arasada R, Pollard TD. 2011. Distinct roles for F-BAR proteins Cdc15p and Bzz1p in actin polymerization at sites of endocytosis in fission yeast. *Curr Biol* **21**:1450–1459. doi:10.1016/j.cub.2011.07.046

Balzer CJ, Wagner AR, Helgeson LA, Nolen BJ. 2019. Single-Turnover Activation of Arp2/3 Complex by Dip1 May Balance Nucleation of Linear versus Branched Actin Filaments. *Current Biology* **29**:3331-3338.e7. doi:10.1016/j.cub.2019.08.023

Balzer CJ, Wagner AR, Helgeson LA, Nolen BJ. 2018. Dip1 Co-opts Features of Branching Nucleation to Create Linear Actin Filaments that Activate WASP-Bound Arp2/3 Complex. *Current Biology* **28**:3886-3891.e4. doi:10.1016/j.cub.2018.10.045

Banjade S, Rosen MK. 2014. Phase transitions of multivalent proteins can promote clustering of membrane receptors. *eLife* **3**. doi:10.7554/eLife.04123

Basu R, Chang F. 2011. Characterization of dip1p reveals a switch in Arp2/3-dependent actin assembly for fission yeast endocytosis. *Curr Biol* **21**:905–916. doi:10.1016/j.cub.2011.04.047

Beltzner CC, Pollard TD. 2008. Pathway of actin filament branch formation by Arp2/3 complex. *J Biol Chem* **283**:7135–7144. doi:10.1074/jbc.M705894200

Berro J, Pollard TD. 2014a. Local and global analysis of endocytic patch dynamics in fission yeast using a new "temporal superresolution" realignment method. *Mol Biol Cell* **25**:3501–3514. doi:10.1091/mbc.E13-01-0004

Berro J, Pollard TD. 2014b. Local and global analysis of endocytic patch dynamics in fission yeast using a new "temporal superresolution" realignment method. *Mol Biol Cell* **25**:3501–3514. doi:10.1091/mbc.E13-01-0004

Boczkowska M, Rebowski G, Kast DJ, Dominguez R. 2014. Structural analysis of the transitional state of Arp2/3 complex activation by two actin-bound WCAs. *Nat Commun* **5**:3308. doi:10.1038/ncomms4308

Galletta BJ, Chuang DY, Cooper JA. 2008. Distinct Roles for Arp2/3 Regulators in Actin Assembly and Endocytosis. *PLOS Biology* **6**:e1. doi:10.1371/journal.pbio.0060001

Goley ED, Welch MD. 2006. The ARP2/3 complex: an actin nucleator comes of age. *Nat Rev Mol Cell Biol* **7**:713–726. doi:10.1038/nrm2026

Goode BL, Eskin JA, Wendland B. 2015. Actin and Endocytosis in Budding Yeast. *Genetics* **199**:315–358. doi:10.1534/genetics.112.145540

Helgeson LA, Nolen BJ. 2013. Mechanism of synergistic activation of Arp2/3 complex by cortactin and N-WASP. *Elife* **2**:e00884. doi:10.7554/eLife.00884

Hetrick B, Han MS, Helgeson LA, Nolen BJ. 2013. Small molecules CK-666 and CK-869 inhibit actin-related protein 2/3 complex by blocking an activating conformational change. *Chem Biol* **20**:701–712. doi:10.1016/j.chembiol.2013.03.019

Higgs HN, Pollard TD. 2001. Regulation of Actin Filament Network Formation Through ARP2/3 Complex: Activation by a Diverse Array of Proteins. *Annual Review of Biochemistry* **70**:649–676. doi:10.1146/annurev.biochem.70.1.649

Hurst V, Shimada K, Gasser SM. 2019. Nuclear Actin and Actin-Binding Proteins in DNA Repair. *Trends Cell Biol* **29**:462–476. doi:10.1016/j.tcb.2019.02.010

Lacy MM, Baddeley D, Berro J. 2019. Single-molecule turnover dynamics of actin and membrane coat proteins in clathrin-mediated endocytosis. *Elife* **8**. doi:10.7554/eLife.52355

Lacy MM, Ma R, Ravindra NG, Berro J. 2018. Molecular mechanisms of force production in clathrin-mediated endocytosis. *FEBS Lett* **592**:3586–3605. doi:10.1002/1873-3468.13192

Li P, Banjade S, Cheng H-C, Kim S, Chen B, Guo L, Llaguno M, Hollingsworth JV, King DS, Banani SF, Russo PS, Jiang Q-X, Nixon BT, Rosen MK. 2012. Phase transitions in the assembly of multivalent signalling proteins. *Nature* **483**:336–340. doi:10.1038/nature10879

Luan Q, Liu S-L, Helgeson LA, Nolen BJ. 2018a. Structure of the nucleation-promoting factor SPIN90 bound to the actin filament nucleator Arp2/3 complex. *The EMBO Journal* **37**:e100005. doi:10.15252/embj.2018100005

Luan Q, Zelter A, MacCoss MJ, Davis TN, Nolen BJ. 2018b. Identification of Wiskott-Aldrich syndrome protein (WASP) binding sites on the branched actin filament nucleator Arp2/3 complex. *Proc Natl Acad Sci USA* **115**:E1409–E1418. doi:10.1073/pnas.1716622115

Machesky LM, Mullins RD, Higgs HN, Kaiser DA, Blanchoin L, May RC, Hall ME, Pollard TD. 1999. Scar, a WASp-related protein, activates nucleation of actin filaments by the Arp2/3 complex. *Proc Natl Acad Sci USA* **96**:3739–3744.

MacQuarrie CD, Mangione MC, Carroll R, James M, Gould KL, Sirotkin V. 2019. The S. pombe adaptor protein Bbc1 regulates localization of Wsp1 and Vrp1 during endocytic actin patch assembly. *J Cell Sci* **132**. doi:10.1242/jcs.233502

Marchand J-B, Kaiser DA, Pollard TD, Higgs HN. 2001. Interaction of WASP/Scar proteins with actin and vertebrate Arp2/3 complex. *Nature Cell Biology* **3**:76–82. doi:10.1038/35050590

Murphy DA, Courtneidge SA. 2011. The "ins" and "outs" of podosomes and invadopodia: characteristics, formation and function. *Nat Rev Mol Cell Biol* **12**:413–426. doi:10.1038/nrm3141

Padrick SB, Cheng H-C, Ismail AM, Panchal SC, Doolittle LK, Kim S, Skehan BM, Umetani J, Brautigam CA, Leong JM, Rosen MK. 2008. Hierarchical regulation of WASP/WAVE proteins. *Mol Cell* **32**:426–438. doi:10.1016/j.molcel.2008.10.012

Padrick SB, Doolittle LK, Brautigam CA, King DS, Rosen MK. 2011. Arp2/3 complex is bound and activated by two WASP proteins. *Proc Natl Acad Sci USA* **108**:E472-479. doi:10.1073/pnas.1100236108

Rodnick-Smith M, Luan Q, Liu S-L, Nolen BJ. 2016. Role and structural mechanism of WASP-triggered conformational changes in branched actin filament nucleation by Arp2/3 complex. *Proc Natl Acad Sci USA* **113**:E3834-3843. doi:10.1073/pnas.1517798113

Rohatgi R, Ma L, Miki H, Lopez M, Kirchhausen T, Takenawa T, Kirschner MW. 1999. The interaction between N-WASP and the Arp2/3 complex links Cdc42-dependent signals to actin assembly. *Cell* **97**:221–231.

Rotty JD, Wu C, Bear JE. 2013. New insights into the regulation and cellular functions of the ARP2/3 complex. *Nat Rev Mol Cell Biol* **14**:7–12. doi:10.1038/nrm3492

Sirotkin V, Beltzner CC, Marchand J-B, Pollard TD. 2005. Interactions of WASp, myosin-I, and verprolin with Arp2/3 complex during actin patch assembly in fission yeast. *The Journal of Cell Biology* **170**:637–648. doi:10.1083/jcb.200502053

Sirotkin V, Berro J, Macmillan K, Zhao L, Pollard TD. 2010. Quantitative Analysis of the Mechanism of Endocytic Actin Patch Assembly and Disassembly in Fission Yeast. *Mol Biol Cell* **21**:2894–2904. doi:10.1091/mbc.E10-02-0157

Smith BA, Daugherty-Clarke K, Goode BL, Gelles J. 2013a. Pathway of actin filament branch formation by Arp2/3 complex revealed by single-molecule imaging. *Proc Natl Acad Sci USA* **110**:1285–1290. doi:10.1073/pnas.1211164110

Smith BA, Padrick SB, Doolittle LK, Daugherty-Clarke K, Corrêa IR, Xu M-Q, Goode BL, Rosen MK, Gelles J. 2013b. Three-color single molecule imaging shows WASP detachment from Arp2/3 complex triggers actin filament branch formation. *Elife* **2**:e01008. doi:10.7554/eLife.01008

Sun Y, Leong NT, Jiang T, Tangara A, Darzacq X, Drubin DG. 2017. Switch-like Arp2/3 activation upon WASP and WIP recruitment to an apparent threshold level by multivalent linker proteins in vivo. *Elife* **6**. doi:10.7554/eLife.29140

Sun Y, Schöneberg J, Chen X, Jiang T, Kaplan C, Xu K, Pollard TD, Drubin DG. 2019. Direct comparison of clathrin-mediated endocytosis in budding and fission yeast reveals conserved and evolvable features. *eLife* **8**:e50749. doi:10.7554/eLife.50749

Ti S-C, Jurgenson CT, Nolen BJ, Pollard TD. 2011. Structural and biochemical characterization of two binding sites for nucleation-promoting factor WASp-VCA on Arp2/3 complex. *Proc Natl Acad Sci USA* **108**:E463-471. doi:10.1073/pnas.1100125108

Wagner AR, Luan Q, Liu S-L, Nolen BJ. 2013. WISH/DIP/SPIN90 proteins form a class of Arp2/3 complex activators that function without preformed actin filaments. *Curr Biol* **23**:1990–1998. doi:10.1016/j.cub.2013.08.029

Yi K, Unruh JR, Deng M, Slaughter BD, Rubinstein B, Li R. 2011. Dynamic maintenance of asymmetric meiotic spindle position through Arp2/3-complex-driven cytoplasmic streaming in mouse oocytes. *Nat Cell Biol* **13**:1252–1258. doi:10.1038/ncb2320

Young ME, Cooper JA, Bridgman PC. 2004. Yeast actin patches are networks of branched actin filaments. *J Cell Biol* **166**:629–635. doi:10.1083/jcb.200404159

CHAPTER V

Lacy, Michael M, David Baddeley, and Julien Berro. 2019. "Single-Molecule Turnover Dynamics of Actin and Membrane Coat Proteins in Clathrin-Mediated Endocytosis." Edited by Pekka Lappalainen and Vivek Malhotra. *ELife* 8 (December): e52355. https://doi.org/10.7554/eLife.52355.

Luan, Qing, Su-Ling Liu, Luke A. Helgeson, and Brad J. Nolen. 2018. "Structure of the Nucleation-promoting Factor SPIN90 Bound to the Actin Filament Nucleator Arp2/3 Complex." *The EMBO Journal* 37 (22): e100005. https://doi.org/10.15252/embj.2018100005.

Luan, Qing, Alex Zelter, Michael J. MacCoss, Trisha N. Davis, and Brad J. Nolen. 2018. "Identification of Wiskott-Aldrich Syndrome Protein (WASP) Binding Sites on the Branched Actin Filament Nucleator Arp2/3 Complex." *Proceedings of the National Academy of Sciences* 115 (7): E1409–18. https://doi.org/10.1073/pnas.1716622115.

Oda, Toshiro, Mitsusada Iwasa, Tomoki Aihara, Yuichiro Maéda, and Akihiro Narita. 2009. "The Nature of the Globular- to Fibrous-Actin Transition." *Nature* 457 (7228): 441–45. https://doi.org/10.1038/nature07685.

Rodnick-Smith, Max, Qing Luan, Su-Ling Liu, and Brad J. Nolen. 2016. "Role and Structural Mechanism of WASP-Triggered Conformational Changes in Branched Actin Filament Nucleation by Arp2/3 Complex." *Proceedings of the National Academy of Sciences* 113 (27): E3834–43. https://doi.org/10.1073/pnas.1517798113.

Rouiller, Isabelle, Xiao-Ping Xu, Kurt J. Amann, Coumaran Egile, Stephan Nickell, Daniela Nicastro, Rong Li, Thomas D. Pollard, Niels Volkmann, and Dorit Hanein. 2008. "The Structural Basis of Actin Filament Branching by the Arp2/3 Complex." *The Journal of Cell Biology* 180 (5): 887–95. https://doi.org/10.1083/jcb.200709092.

Smith, Benjamin A, Shae B Padrick, Lynda K Doolittle, Karen Daugherty-Clarke, Ivan R Corrêa Jr, Ming-Qun Xu, Bruce L Goode, Michael K Rosen, and Jeff Gelles. 2013. "Three-Color Single Molecule Imaging Shows WASP Detachment from Arp2/3 Complex Triggers Actin Filament Branch Formation." Edited by Wesley Sundquist. *ELife* 2 (September): e01008. https://doi.org/10.7554/eLife.01008.

Wagner, Andrew R., Qing Luan, Su-Ling Liu, and Brad J. Nolen. 2013.
"WISH/DIP/SPIN90 Proteins Form a Class of Arp2/3 Complex Activators That Function
without Preformed Actin Filaments." *Current Biology : CB* 23 (20): 1990–98.
https://doi.org/10.1016/j.cub.2013.08.029.